Master Thesis, Department of Geosciences

Late Cretaceous Sedimentation (Mavuji Group) in Mandawa Basin, Tanzania.

Guanqun Hou

UNIVERSITY OF OSLO
FACULTY OF MATHEMATICS AND NATURAL SCIENCES

Late Cretaceous Sedimentation (Mavuji Group) in Mandawa Basin, Tanzania.

Guanqun Hou

Master Thesis in Geosciences

Discipline: Geology

Department of Geosciences

Faculty of Mathematics and Natural Sciences

University of Oslo

June 1st, 2015

Acknowledgments

Abstract

Sedimentary successions of Early Cretaceous have been studied in the Mandawa Basin, with the focus on describing facies and facies associations to supply information about the depositional environments. The petrographical studies comprise XRD and thin section analysis, providing information about the diagenetic history.

In this studied field outcrops composes of claystones, limestones and sandstones from the Kihuluhulu, Kiturika, and Makonde formations, display depositional environments from marine to fluvial settings. These three formations represent time-equivalent units developed in Early Cretaceous. The outcrops of Kihuluhulu Fm. display the most characteristic developments of stratigraphy, and have been the focus in this thesis. Kihuluhulu Fm. displays a marine depositional setting of outer shelf setting. The dominant lithology is clay/siltstones interbedded with turbiditic sandstones, with sparitic calcite cement. Kiturika and Makonde formations are also present, but relative briefly, in order to compare the petrographic and diagenesic characters of the Kihuluhulu, Kiturika and Makonde formations. The Kiturika Fm. was deposited in a shallow wave agitated marine environment, dominated by reef limestone. Makonde Fm. was deposited in mouth bar associated with terminal distributary channel environments. The typical lithology of Makonde Fm. is cross-bedded sandstone.

In addition, the petrographic data from Gundersveen (2014) will be used with respect to the core samples from well site 24 and 21, in order to give comparison between the surface samples and the core ones. The core samples from well site 24 and 21 are time equivalent as Kihuluhulu Fm.

Contents

1. Introduction

This master thesis utilizes field observations and petrographical studies to give a sedimentological description of the Lower Cretaceous contemporaneous Makonde, Kiturika and Kihuluhulu formations (Aptian-Mid Turonian) of the Mandawa Basin in the coastal Tanzania. The main goal of this study is to address questions of the depositional environment and compare the north with the south of the Kihuluhulu, Kiturika and Makonde Formations.

This thesis is a part of a the Mandawa Basin Project (MBP) which is an interdisciplinary international research project established by University of Oslo (UiO),University of Dar Es Salaam (UDSM), and Tanzania Petroleum Development Corporation (TPDC) as participating institutions in 2013. The project will run for four years and is financially supported by Statoil Tanzania. The aim of the project is to disclose sedimentary and structural history of the Mandawa Basin in order to better understand the stratigraphical developments, sediment formation and transportation as well as sediment provenance. The final goal of the project is to compare onshore studies with available material from offshore sites (Statoil), to tie land and offshore geology together. Scientists from UDSM, UiO, TPDC and Statoil along with PhD students and master students from both universities are involved in this project.

During the three weeks' field campaign (from 22nd October to 4th November), several outcrops of the Makonde, Kiturika and Kihuluhulu formations (Figure 1.2) were studied and sampled. Two detailed logs were produced from the Kihuluhulu Fm., while sketch logging was used for Makonde and Kiturika outcrops (Fig.1.1). In addition, several Kihuluhulu outcrops were sampled along the road (N5-22, N5-26 and N5-27). Key sandstone samples from the outcrops were selected and studied in detail in order to give a description of sedimentology, petrology and diagenesis process in the North and South/ Central Mandawa Basin, while key claystone samples

were selected and used XRD to provide the qualitative and quantitative analysis.

Nine samples from Hudson's Dublin collection were studied in thin section, where from Makonde, Kiturika and Kihuluhulu Fm. respectively, in order to compare the characteristics of sedimentology, petrology and diagenetic history with the samples taken from the outcrops. The Dublin samples were picked by Hudson (2010) with Nicholas, and all the samples from Mandawa Basin were stored in Dublin.

In addition, the samples of 2013 (Gundersveen, 2014) from both outcrops and cores have been used in comparison. Gundersveen has described these samples in her master thesis, from sedimentological and petrological aspects (Gundersveen, 2014).

1.1 Study area

The Mandawa Basin is located at the southern coast of Tanzania, a prospective onshore hydrocarbon basin in Tanzania (Fig. 1.1) (Hudson, 2011). The Mandawa Basin is bounded by the Rufuji trough to the north, and separated from the Ruvuma Basin by the Ruvuma Saddle to the south. In addition, it is bounded by the metamorphic basement in the west, and offshore basins in the east (Hudson & Nicholas, 2014). The Mandawa Basin evolved from the Permian (Nicholas et al., 2007) and contains sediments of various depositional environments from alluvial, fluvial, deltaic, restricted marine, shallow marine to a shelf environment (Hudson, 2011).

Table 1.1 *Samples overview from Kihuluhulu, Kiturika and Makonde formations.*

Locality	Formation
2014 field outcrops	
WP-92	**Kihuluhulu Fm.**
WP-223	
WP-222	
N5-22	
N5-26	
N5-27	
WP-71	**Kiturika Fm.**
WP-62	**Makonde Fm.**
Hudson's Dublin Collection	
M29-3	**Kihuluhulu Fm.**
M31-20	
M31-17	
M6-6	**Kiturika Fm.**
M5-7	
M6-3	
WP-63	**Makonde Fm.**
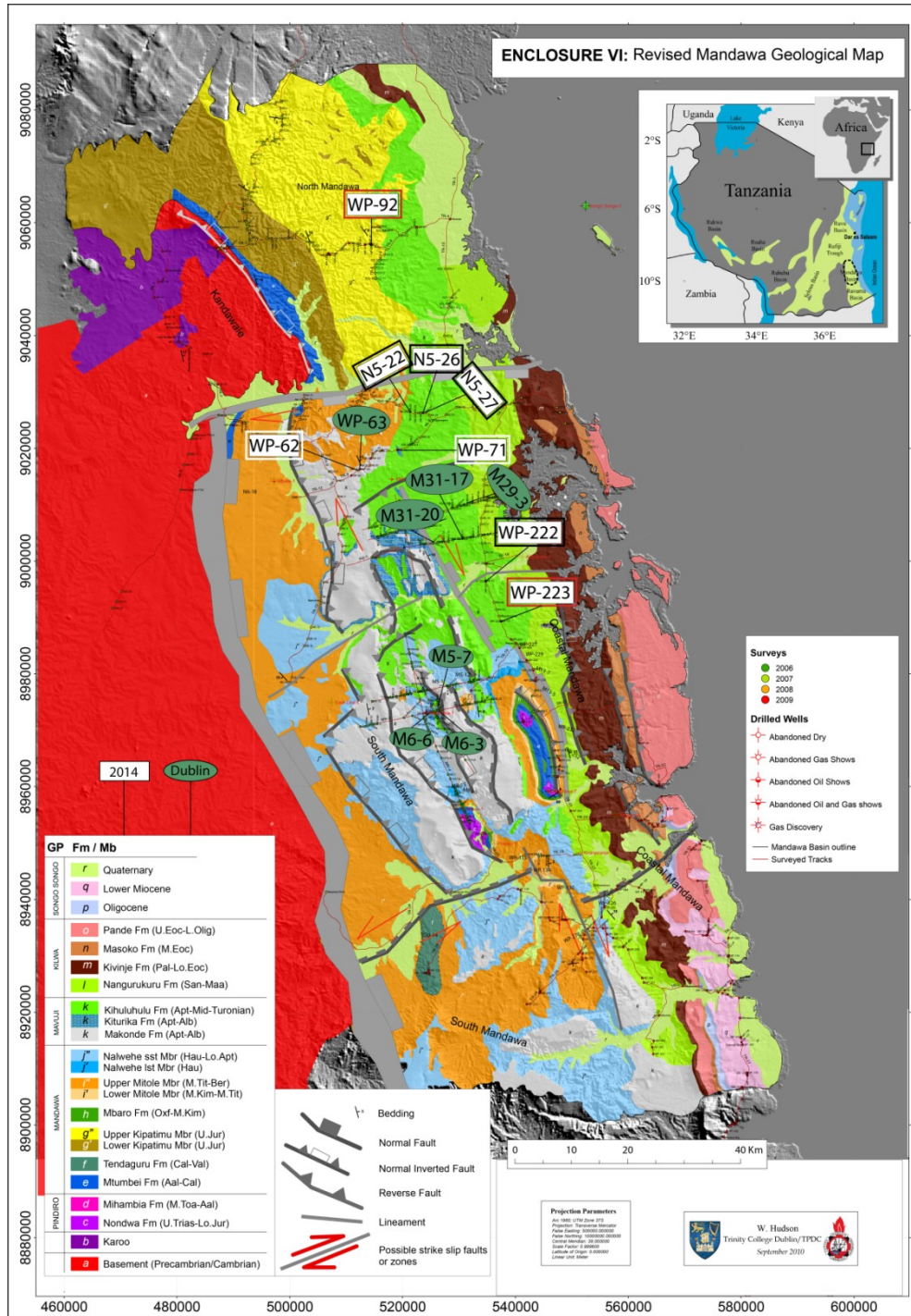
Figure 1.1 *GeologicalMap of the Mandawa Basin (Hudson, 2011). All the sampled localities are displayed on this map, which were sampled in the fieldwork of 2014 and Dublin collections by Hudson. Two localities (WP-92 & WP-223) with red boxes were worked with detailed sedimentary logs and sampling, the white boxes with two localities (WP-71 & WP-62) were worked with sketch map and logs, the rest four localities with black boxes were only sampled. The Hudson's Dublin collections were studied in thin section and SEM analysis.*

1.2 **Geological development of the Mandawa Basin**

Mandawa Basin is a rift basin within the Tanzania coastal belt stretching from Kenyan border in the north to the Mozambiquan border in south (Mbede, 1991). The development of the Mandawa Basin was controlled by the rifting of Madagascar away from the mainland East Africa and the break-up of Gondwana (Salman &Abdula, 1995, Kapilima, 2003, Hudson, 2011). The depositional history of the Mandawa Basin is strongly affected by the break-up of Gondwana (Berrocoso & Macleod, 2010). The Mandawa Basin can be divided into five different groups: Pindiro, Mandawa, Mavuji, Kilwa and Songosongo respectively (Figure 1.2) (Hudson, 2011).Prior to the break-up of the Gondwana continent, the depositional environment was continental and dominated by fluvial and deltaic deposits (Hudson, 2011, Salman & Abdula, 1995). As the rifting and drifting continued (Early to Middle Jurassic), the palaeo-Tethys transgression formed restricted marine embayments with barrier reefs separating a number of saline lagoons (Salman & Abdula, 1995, Hankel, 1994). In the Late Jurassic to the Early Cretaceous, the basin was subsiding at a higher rate and clasticsediments were deposited. This gave rise to the deposition of alluvial and fluvial deposits of the prograding Mandawa and Mavuji groups (Hudson, 2011). The coastal Mandawa Basin which was under mid- to outer shelf environment subsided at a constant rate from Aptian to Paleogene. This resulted in the deposition of the Kilwa Group (Hudson, 2011). This thesis pays majority attention to the Mavuji Group, which consists of three time-equivalent formations (Makonde, Kitiruca and Kihuluhulu Fm.) (Figure 1.2). Further, the Kihuluhulu Fm. would be given most attention among these three formations due to more available and better exposed outcrops. The Kihuluhulu Fm. unconfomably overlay the fluvio-deltaic Upper Jurassic Kipatimu Formation, and underlay the Nangurukuru Formation of the Kilwa Group separated by the Turonian-Santonian unconformity (Figure. 1.2) (Hudson, 2011).
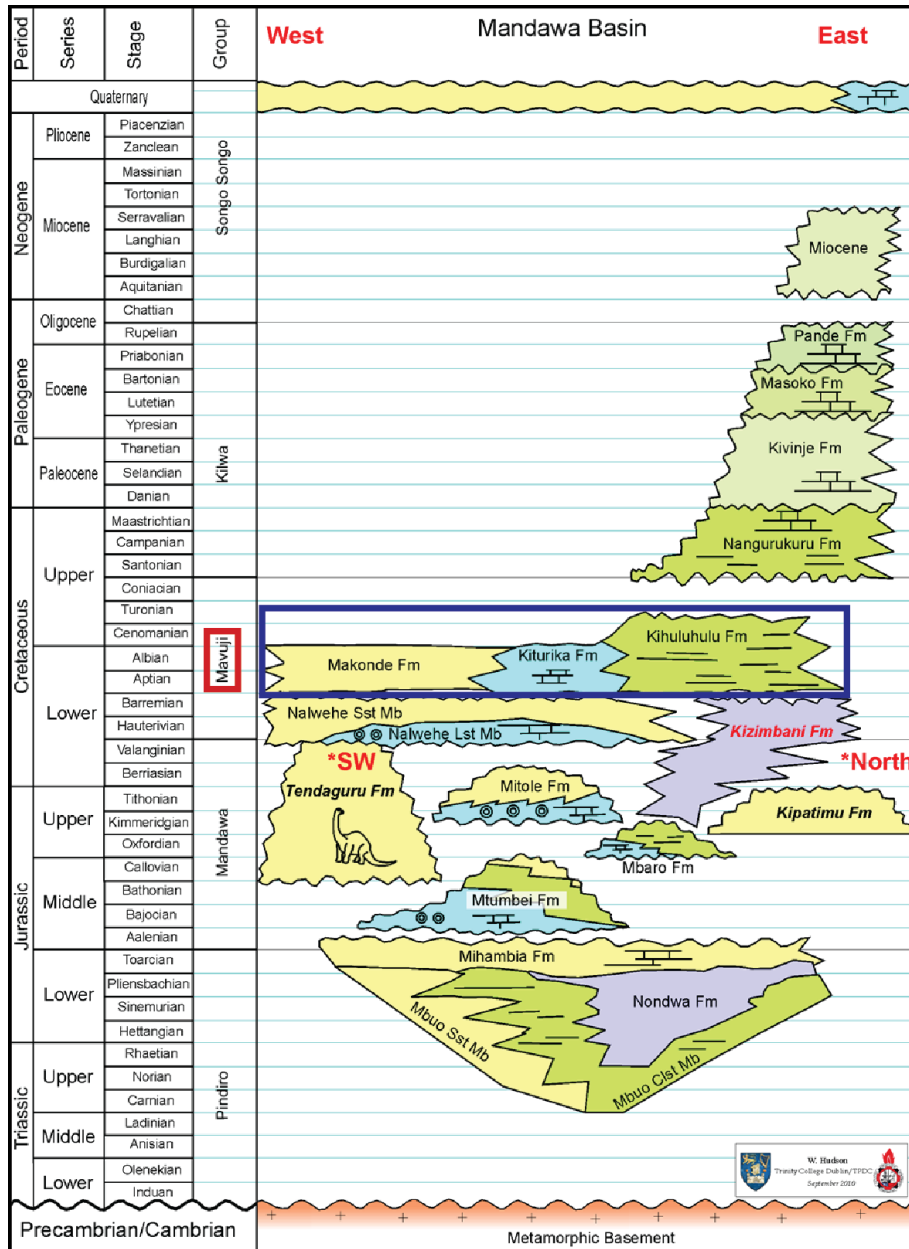
Figure 1.2 *Stratigraphical development of Mandawa Basin from Precambrian to*
Quaternary. The blue block presents the studied formations of this thesis (Mavuji Gp.).
Modified from Hudson (2010).

1.2.1 Permian to Early Jurassic

The Permian to Early Jurassic was the major rifting stage for the Gondwana
supercontinent (Hudson, 2011). The Karoo rifts developed from Permian, and became
weakly activity during Cretaceous and Tertiary (Mbede, 1991). The rifting phase
initiated as a result of a thermal dome upwelling, activated the extensional tectonics.

1. Introduction

This tectonic activity gave rise to faults, grabens and basinal structures where triggered the initial opening of the Indian Ocean and the deposition of sediments within the Gondwana (Mpanda, 1997, Kapilima, 2003). During the Gondwana rifting phase (300-205 Ma), a broad platform depression was created due to the block faults (Salman & Abdula, 1995, Mpanda, 1997). The Karoo is used as a term to describe the sediments that during the depositional events ranging from Late Carbonniferous to Early Jurassic period (Balduzzt et al., 1992). Within the Mandawa Basin, the Pindiro Group, composing of Mbuo, Nondwa, and Mihambia Formations, make out the Karoo (Hudson & Nicholas, 2014). The Pindiro Group is the basal stratigraphy of the Mandawa Basin (Figure 1.2). The Mbuo Fm. occurs as the first sediments within the Pindiro Group, overlain by the Nondwa Formation with a clearly boundary surface (Figure 1.2). The Mbuo Fm. consists of two sedimentary members. At the base of the Mbuo sandstone Member, a shift from metamorphic rocks to clastic sediments occurred, whereas evaporates (Nondwa Fm.) represent the top of the Mbuo claystone Member (Figure 1.3) (Hudson & Nicholas, 2014). The Mbuo Fm. was deposited in laucustrine, alluvial and fluvial environments (Hudson & Nicholas, 2014).
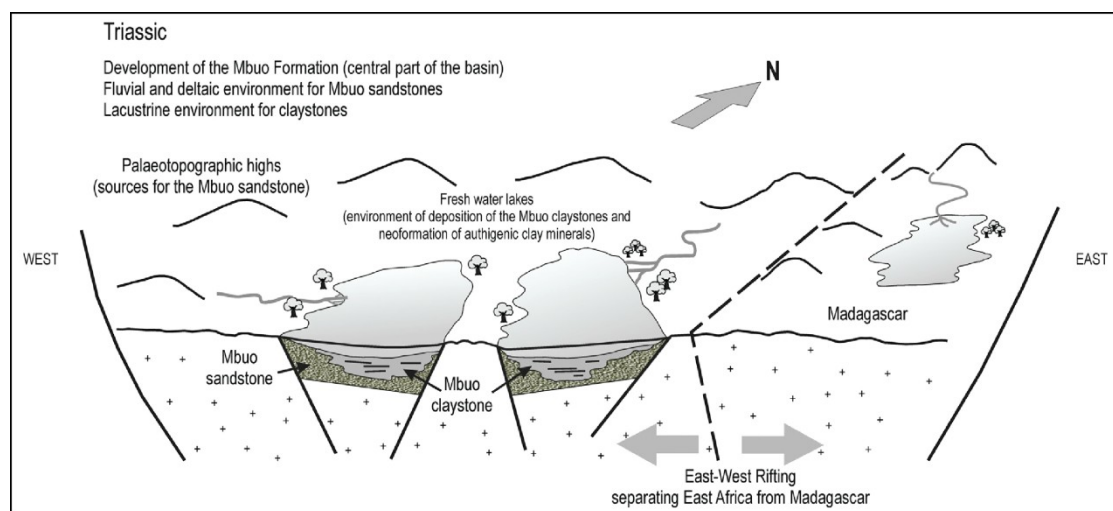
Figure 1.3 *Triassic palaeogeography models for deposition of the Mbuo Fm. (Hudson & Nicholas, 2014).*

During Late Triassic period for the Gondwana fragmentation, only cyclical marine

invasions and fluxionary regional uplift operated, which gave rise to the restricted marine deposits. These sediments are identified as Nondwa evaporates (Figures 1.2 and 1.4) (Kapilima, 2003, Hudson & Nicholas, 2014). The Mihambia Fm. deposited above the Nondawa evaporites, consists of clastic sediments with minor limestones depositing range from Toarcian to Aalenian (Figure 1.2).
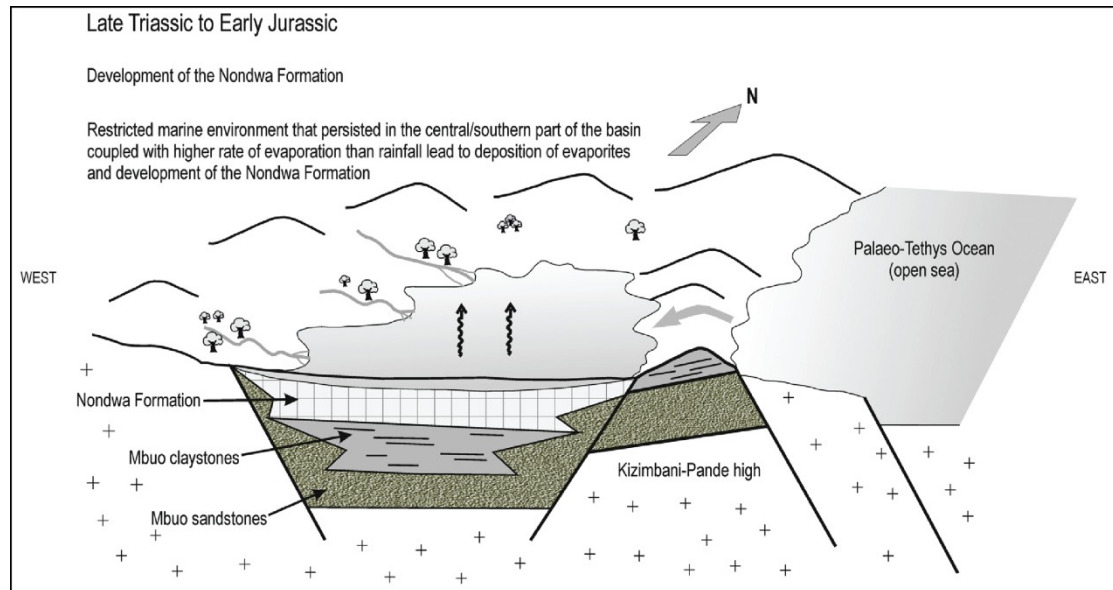
Figure 1.4 *Paleogeographic models for the deposition of Nondwa Fm., from Late Triassic to Early Jurassic times. The Kizimbani-Pande high provided a barrier for a restricted marine environment and the deposition of the Nondwa evaporates in the central part of the basin. The Mbuo Fm. deposited below the Nondwa Fm. From Hudson & Nicholas (2014).*

1.2.2 Middle Jurassic to Late Cretaceous

This period was mainly affected by the post-Gondwana stage (157-118 Ma). The post-Gondwana stage is a period of an active break-up of Gondwana and formation of Inidan Ocean continental margins (Salman & Abdula, 1995). The Karoo rifting episode created a zone of weakness, which gave rise to the break-up of the Gondwana eastern margin. Further, active sea-floor spreading separated Gondwana into West Gondwana (Africa-South America landmass to the west) and East Gondwana

(Madagascar, India and Sri Lanka, Seychelles, Australia and Antarctica landmass to the east) (Salman & Abdula, 1995, Pearson et al., 2004, Hudson, 2011). Madagascar was separated from East Africa due to the east-west extension. As a result, the break-up created the opening of the East Africa coastal basins, including Mandawa Basin. Coinstantaneously the dextral strike-slip movement of Madagascar began from east to west, along the Davie Fracture Ridge transform zone (Figure 1.5) (Mpanda, 1997, Hudson, 2011).
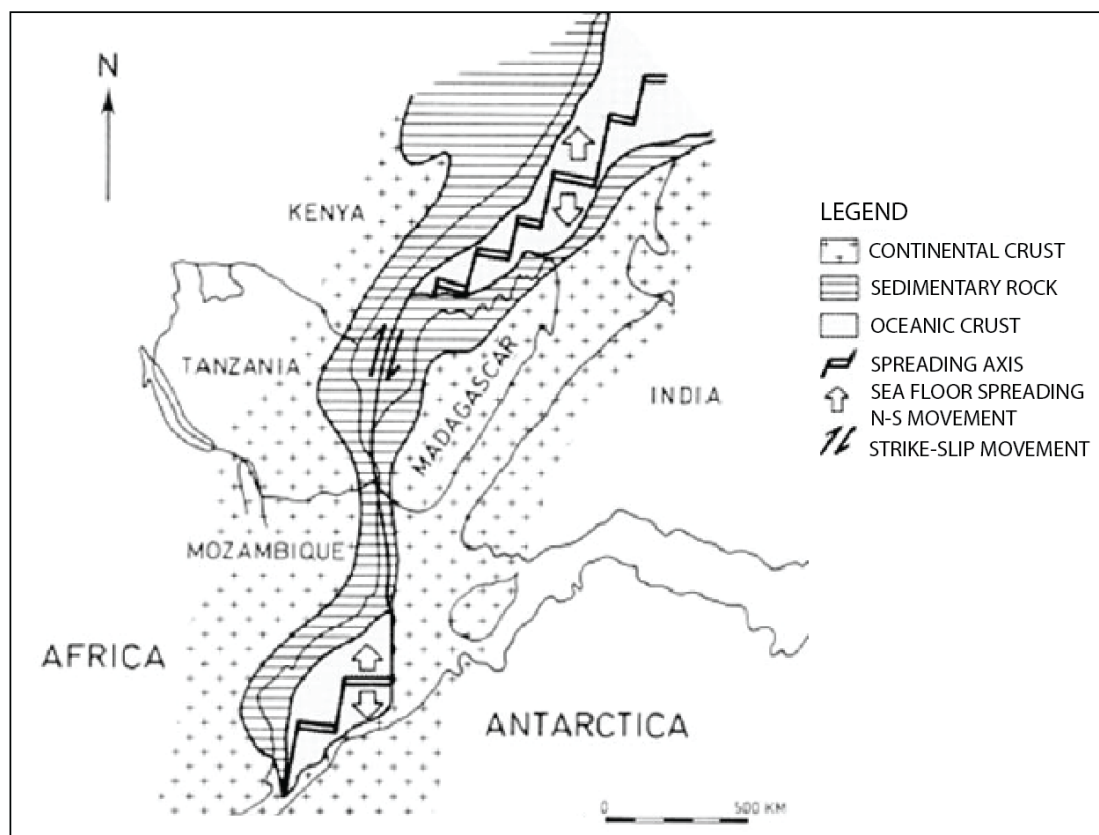
Figure 1.5 *The opening of the Indian Ocean during an early stage of Gondwana breakup and the positions of continental plates during Late to Mid Jurassic. The drifting of the continents happened along spreading axis and the rifting happened along a strike-slip movement (Davie Fracture Zone) (Mpanda, 1997).*

During Jurassic to Cenozoic, the Mandawa Basin experienced several cycles of transgressive and regressive periods, and as a result, thick Mesozoic and Cenozoic

depositional sequences accumulated (Kapilima, 2003). In the Middle Jurassic period, the first widespread marine transgression covered across the entire Tanzanian coastal basin. As a result, the continental shelf was established with deposition of shallow to deep marine sediments (Mpanda, 1997, Kapilima, 2003). The marine sediments are identified as Mtumbei Fm. of the Mandawa Group (Figure 1.2) (Hudson, 2011). The marine transgression continued into the Late Jurassic and possibly into the Early Cretaceous (Mpanda, 1997). Moreover, the basin experienced a higher rate of subsidence which resulted in the clastic sedimentary. This gave rise to the fluvial sandstones of and oolitic limestone beds. The sandstones consist of Kipatimu, Mbaro and Mitole Formations (Mandawa Group) and the Nalwehe Fm. sandstone Member (Mavuji Group) while the limestone beds comprise Lower Mitole Member and Nalwehe limestone Member (Figures 1.2 and 1.6) (Hudson, 2011). Figure 1.6 displays the paleogeographic model of the deposition for the Mitole Fm. in the central part of the Mandawa basin.
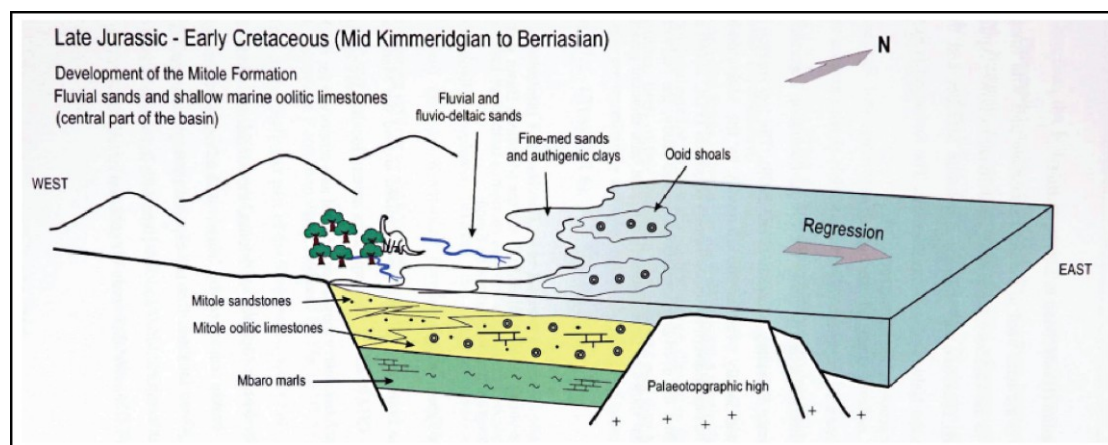
Figure 1.6 *Paleogeographic model for the deposition from Late Jurassic to Early Cretaceous within the central part of the Mandawa Basin. The Lower Mitole Member is dominated by shallow marine environment. In addition, the prograding Upper Mitole Member sandstones deposited over the oolitic limestones as the sea regressed (Hudson, 2011).*

The rate of sea-floor spreading ceased between East Africa and Madagascar around

123 Ma in the Late Cretaceous, which characterized as the stabilization phase of the post-Gondwana stage (Figure 1.7) (Salman & Abdula, 1995, Gaina et al., 2013). This phase resulted in the Mandawa Basin subsided at a constant rate. Based on the stable tectonic events, the deposition of the Kihuluhulu Fm. of the Mavuji Group and later the Kilwa Group (Nangurukuru, Kivinje, Masoko and Pande Formations) were under the mid- to outer shelf marine environment (Figure 1.2) (Hudson, 2011). The rest formations of the Mavuji Group consist of Makonde, Kiturika Formations (Figure 1.2). The deltaic sandstones of Makonde Fm. dominate the western part of the Mandawa Basin, the reefal limestones of Kiturika Fm. are present in a small central area, and the Kihuluhulu Fm. occupied a large area in the eastern part of the Basin, dominated by shelf marine clays interbedded with turbiditic sandstones (Hudson, 2011). The Kihuluhulu Fm. comprises several fossil types, such as foraminifera, cephalopod, and gastropod. The recovery of foraminifera suggest a possible Coniacian boundary (probably an unconformity) separating the Kihuluhulu Fm. from the Nangurukuru Fm (Hudson, 2011).

1.2.3 Late Cretaceous to Late Paleogene

The Kilwa Group was deposited during late Cretaceous and Paleogene, which was deposited unconformable above the Mavuji Group (Figure 1.2). The drifting ended in Santonian (85 Ma) which led to the East African coast underwent weakly extensional tectonics. Hence, this period experienced low energy environment where large successions of marine clays and reef limestones were deposits (Kilwa Group) (Hudson, 2011, Mpanda, 1997). The Kilwa Group consists of a homogeneous sedimentary package which is dominated by clays and claystones to marls (Nicholas et al., 2006). Four formations are established within the Kilwa Group at present: the Nangurukuru Fm., Kivinje Fm., Masoko Fm. and Pande Fm. (Figure 1.2). Abundant fossils are presented in the Kilwa Group (e.g. benthic foraminifera, gastropods, nummulites, et al.) (Nicholas et al., 2006).
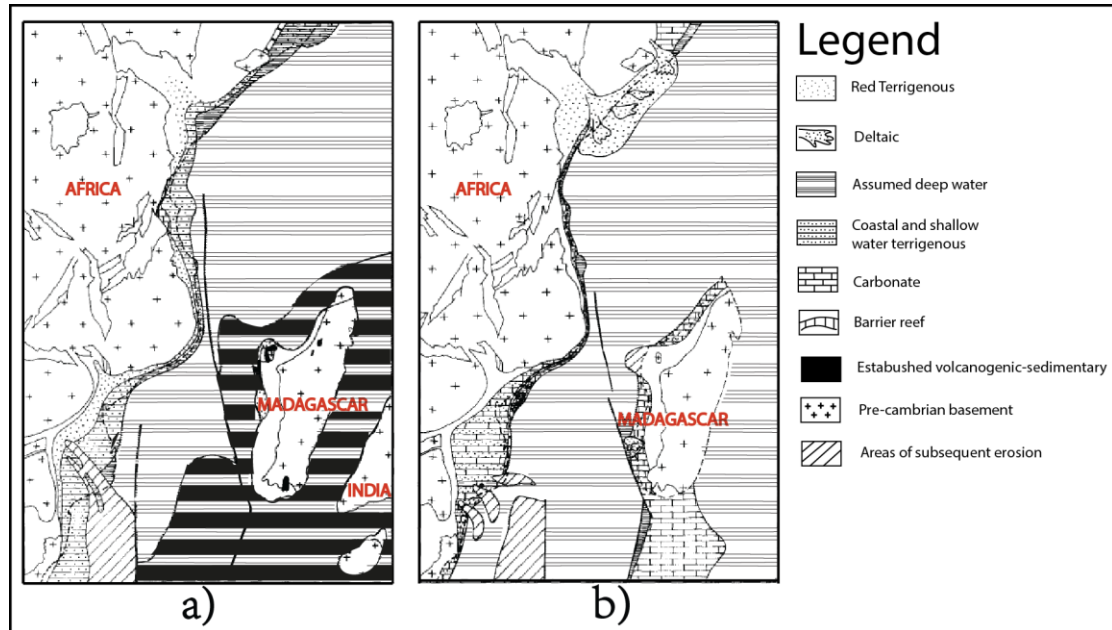
Figure 1.7 *The second phase of post-Gondwana stage that was named as stabilization phase. a) The first part of the phase of stabilization, 97-65 Ma (Late Cretaceous), the start of India / Seychelles block drifting from Africa /Madagascar block relatively; b) The end of this phase, 65-35 Ma (Paleocene - Eocene), together with carbonate sediment deposited, a broad shallow marine transgressive process was generated in the African continent (Modified from Salman & Abdula, 1995)*

1.2.4 Late Paleogene to Recent

The Late Paleogene to resent represents a calm environment as a result to the drifting and spreading tectonics between East Africa and Madagascar. In general, the last marine regression phase dominated in this period. The Songo songo Group marks the topmost part of the infill sequence in the Mandawa Basin (Hudson, 2011).

2. Method

2.1 Field work and sampling

The field work was undertaken from 22.10.14-04.11.14, in the northern and southern parts of the Mandawa Basin (Figure). Key localities of the Kihuluhulu, Makonde and Kiturika formations were logged and sampled. The sample name refers to the sampled locality - section number - sample number - year of collection. For example, a sample of the Kihuluhulu Fm. at locality WP223couldbe WP223-1-14 (WP = Way Point). (WP is named by Hudson, 2011).

Two detailed logs were measured from the outcrops of Kihuluhulu Fm. (Figures 3.2 and 3.4), whilst the other two formations (Makone and Kiturika) were sketch logged, due to the poor quality of exposures (WP62 and WP71). The scale of the logs varies from 1:20 to 1:100, owing to the outcrops' differentiation. Each logged section was measured radiation from the base to the top. All the logs were measured the gamma radiation by using a Thermo Scientific RadEye B20. The instrument measures natural gamma radiation emitted from U, Th and K. Radiation is given in counts per second (cps).

Gundersveen (2014) has given descriptions for the Makonde Fm. and the core samples from Kihuluhulu Fm. in her thesis, some data will be used in this thesis in order to compare the characteristics for the corresponding formations.

2.2 Facies description and facies associations

Field observations, sedimentary logs, photos and thin sections analysis were used to identify lithofacies. A facies is defined as a rock body, distinguished from the adjacent rock bodies based on the significant characteristics, such as lithological, physical and biological features (Dalrymple & James, 2010). Facies association is the combination

of group facies which can be combined with each another. The facies association composes large bodies of rocks that may result in an interpretation of the depositional environment (Dalrymple & James, 2010). The classification of the grain size was applied by the Wentworth grain-size scale (Table 3.1) (Wentworth, 1992).

Table 2.1 *The Wentworth grain size classification with varies millimeters and phi units (Wentworth, 1992).*

Millimeters	Phi (φ) units	Wentworth size class
>256	-8	Boulder
16 – 64	-6	Cobble
4 – 16	-4	Pebble
2 – 4	-2	Granule
1 – 2	-1	Very coarse sand
0.50 – 1	0	Coarse sand
0.25 – 0.50	1	Medium sand
0.125 – 0.25	2	Fine sand
0.0625 – 0.125	3	Very fine sand
0.004 – 0.0625	4	Silt
< 0.004	8	Clay

According to the mineralogical composition, the sandstones were further classified into different categories (Fig. 2.2). The sand and sandstone classification diagram describe the continuous nature of textural variation from mudstone to arenite and from stable to unstable grain composition. Quartz, feldspar and rock fragment occupies each corner of the three front apices, representing relative physical and chemical durability. The horizontal axis represents the most important of the three parameters of textural maturity (Dott, 1964).
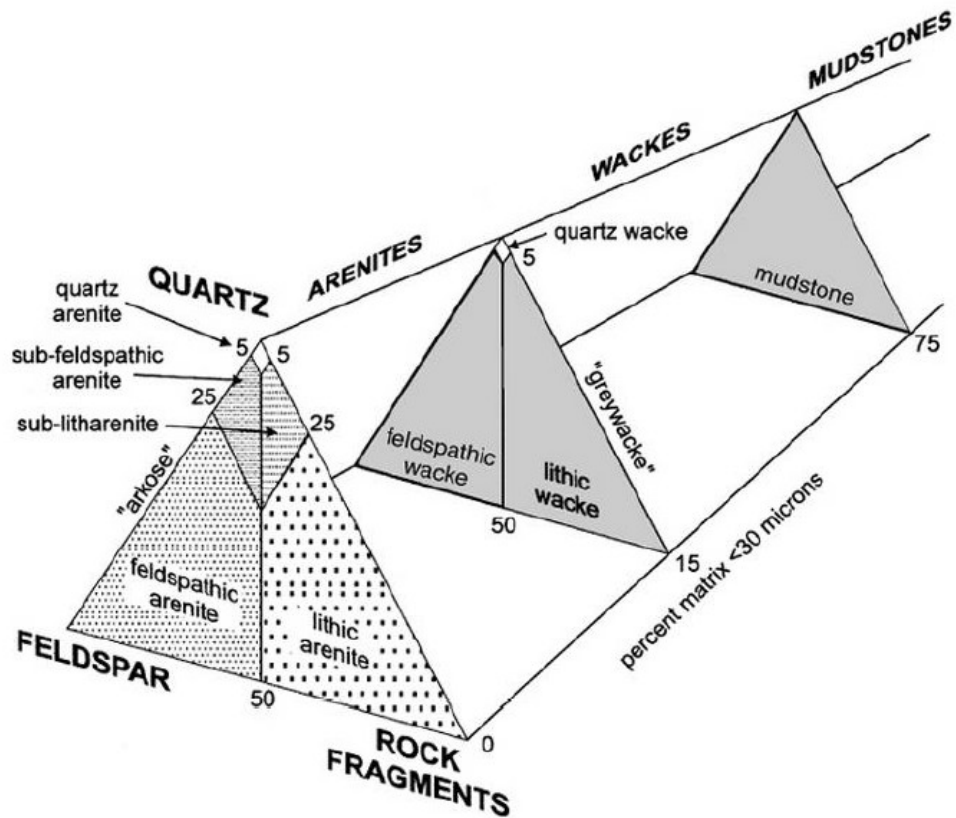
Figure 2.2 *Sand and sandstone classification according to the composition. The*
classification diagram is modified by Miall (2003) after Dott (1964)

Among the studied formations, the Kiturika Fm. is dominated by reefal limestones,
and the limestones was used the classification by Dunham (1962)(Figure 2.3). This
classification is based on the depositional texture of the limestone, and the
fundamental criterion is the nature of the framework (Figure 2.3). The carbonate
particles with a grain size <20μm are termed as mud. Mud-supported deposits consist
of mudstones (limestones with very few grains (<10%) floating in a mud matrix) and
wackestones (contains >10% grains). Grain-supported limestones can be divided into
packestones (limestones have a mud matrix) and grainstones (limestones with a
greater or lesser amount of calcite cement in the intergranular pores). The boundstone
is defined as the original components are bound together during deposition (Dunham,
1962, Hanken et al., 2010). However, some of the carbonate samples contain
silsiciclastic sediments, these samples were firstly classified with respect to the size of

the dominant mechanically deposited grains: Calcilutite (grains<63µm), calcarenite (grains between 63µm and 2mm) and calcirudite (grains >2mm) (Hanken et al., 2010).

Original components not bound together during deposition				Original components bound together	Depositional texture not recognizable
Contains lime mud			Lacks mud and is grain-supported		
Mud-supported		Grain-supported			
Less than 10% grains	More than 10% grains				Crystalline carbonate
Mudstone	Wackestone	Packstone	Grainstone	Boundstone	Crystalline
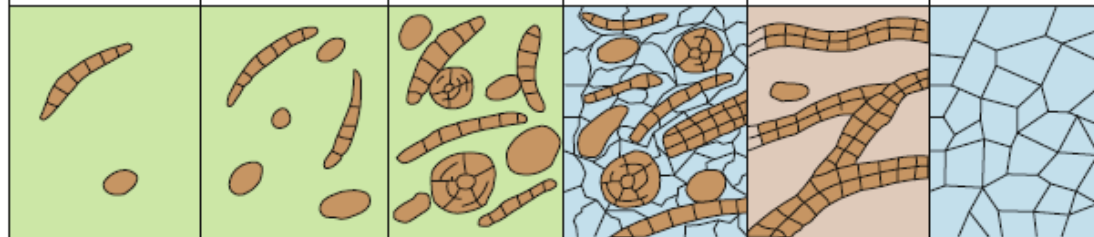
Figure 2.3 *Classification of carbonate rocks by Dunham (1962), according to depositional texture (Hanken et al., 2010)*

2.3 Digitalizing of sedimentary logs

Detailed sedimentary logs from WP-223, WP-92 (Kihuluhulu Fm.) and the sketch logs from WP-62 and WP-71 localities were digitalized by the author in Adobe Illustrator (Figure 2.4). The legend of Figure 2.3 has been applied in all the sedimentary logs.
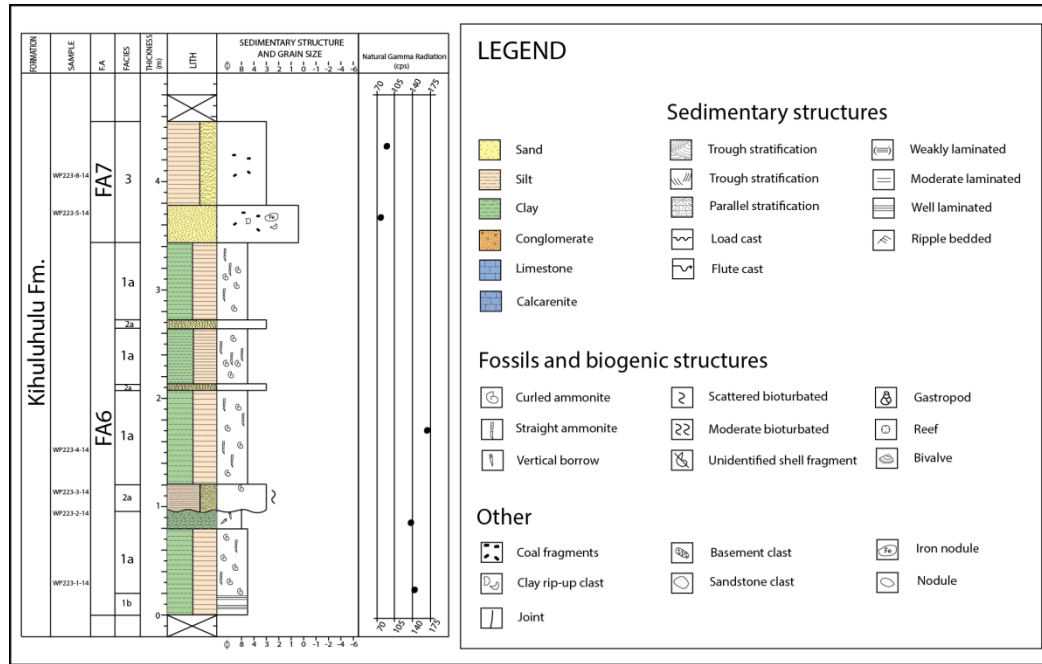
Figure 2.4 *A sedimentary log from WP-223 outcrop of the Kihuluhulu Fm., and the legend used in this thesis on logs for all the outcrops.*

2.4 Petrographical and mineralogical analysis

Petrographical analysis of sandstone samples was performed by optical thin-section observations, scanning electron microscope (SEM) on the selected samples of thin sections and stubs, X-ray diffraction (XRD) on both bulk rock assemblages and clay minerals. Remaining pieces of the studied samples were stored at the Department of Geosciences for future work.

Table 2.2 All samples studied in XRD and thin section.

Location	Formation	Sample	Bulk XRD	Clay Fraction	Thin Section
2014 Field Outcrops					
WP-92		WP92-11-14	X		X
		WP92-12-14	X		X
		WP92-13-14	X		X
		WP92-14-14	X	X	
		WP92-15-14	X		X
		WP92-16-14	X		X
		WP92-17-14	X	X	
		WP92-18-14	X	X	
		WP92-19-14	X		X
		WP92-20-14	X	X	
		WP92-21-14	X		X
WP-223	**Kihuluhulu Fm.**	WP223-1-14	X		X
		WP223-2-14	X	X	
		WP223-3-14	X		X
		WP223-4-14	X	X	X
		WP223-5-14	X		X
		WP223-8-14	X		X
WP-222		WP222-1-14	X	X	
		WP222-2-14	X		X
N5-22		N5-22-1-14	X		
N5-26		N5-26-1-14	X		
		N5-26-2-14	X		X
		N5-26-3-14	X	X	
N5-27		N5-27-1-14	X		X
		N5-27-2-14	X	X	
WP-71	**Kiturika Fm.**	WP71-1-14	X		X
		WP71-2-14	X		X
		WP71-3-14	X		X
WP-62	**Makonde Fm.**	WP62-1-14	X	X	X
		WP62-2-14	X		X
Hudson's Dublin Collection					
M29-3	**Kihuluhulu Fm.**	MDW 10			X
M31-20		MDW 62			X
M31-17		MDW 57			X
M6-6	**Kiturika Fm.**	MDW 135			X
M7-21		MDW 152			X
M5-7		MDW 118			X
M6-3		MDW 131			X
M30-13		MDW 43			X
WP-63	**Makonde Fm.**	MDW 09-08			X

2.4.1 Thin section

Twenty samples from the Kihuluhulu, Makonde and Kiturika formations of the outcrops were selected for thin section analysis and nine samples from Hudson's Dublin Collection (2010). Samples were impregnated in blue epoxy and glued on 2.5cm x 4.5cm glass slides, then polished down to a thickness of 30μm. For the twenty outcrops' samples, ten of them were produced at the Petrological Section Service (IFE Petrosec) and Salahalladin Akhavan, Department of Geology, UiO, prepared ten thin sections.
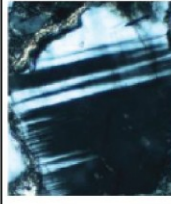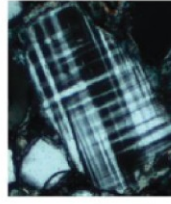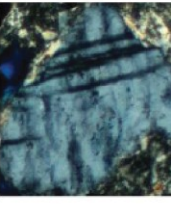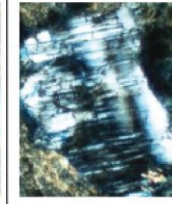
The thin sections were studied under a Nikon LABOPHOT-POL petrographic microscope. The optical analysis was used to identify the rock texture and minerals. All the thin sections were studied both under plane polarized light (ppl) and cross polarized light (xpl) to distinguish mineral characteristics, such as relief, plechroism, zoning and twinning.

2.4.2 Petrographic analysis and point counting

Point counting was accomplished using a Swift Model F automatic point counter mounted on the petrographic microscope. For each of the nineteen thin sections four-hundred points was counted. There are 10 main categories were divided in order to give detailed petrographical descriptions: 1) quartz, 2) feldspar, 3) rock fragment,4) porosity, 5) cement/matrix, 6) fossils,7) heavy mineral,8) iron oxide, 9) kaolinite, 10) coating. Quartz grains were divided into monocrystalline and polycrystalline grains and the type of extinction was noted. Extinction angles above five degrees were noted as undulatory extinction. Feldspar grains were divided in to K-feldspar and plagioclase, which were represented the degree of preservation (Table 3.3) (Fossum, 2012). Other visible features counted as well, such as chert, mica, pellet and so on.

Table 2.3 *Classification of feldspar preservation varies from category 1 to 5 in thin section, under cross polarized light (Fossum, 2012).*

Category	1	2	3	4	5
Description	Fresh, has not been subjected to weathering	Show some evidence of weathering, but twins are almost fully preserved	Intermediate. Twins start to look blurry and grain surfaces show roughness	Very rough surface. Twinning might be hard to recognize	Twins are absent or bearly identified. Hard to identify plagiocalse from microcline. Grain surfaces show extensive dissolution and has extreme rough surface.
Example					

The nineteen thin sections were point counted, and all the textural features were described; consist of grain shape, sorting, grain size, porosity, permeability, preservation of grains and grain contacts (Table 2.2). The grain shape was judged according to Powers' (1953) terminology (Figure 2.5) and the classification of sorting was determined by Compton (1962) (Figure 2.6).
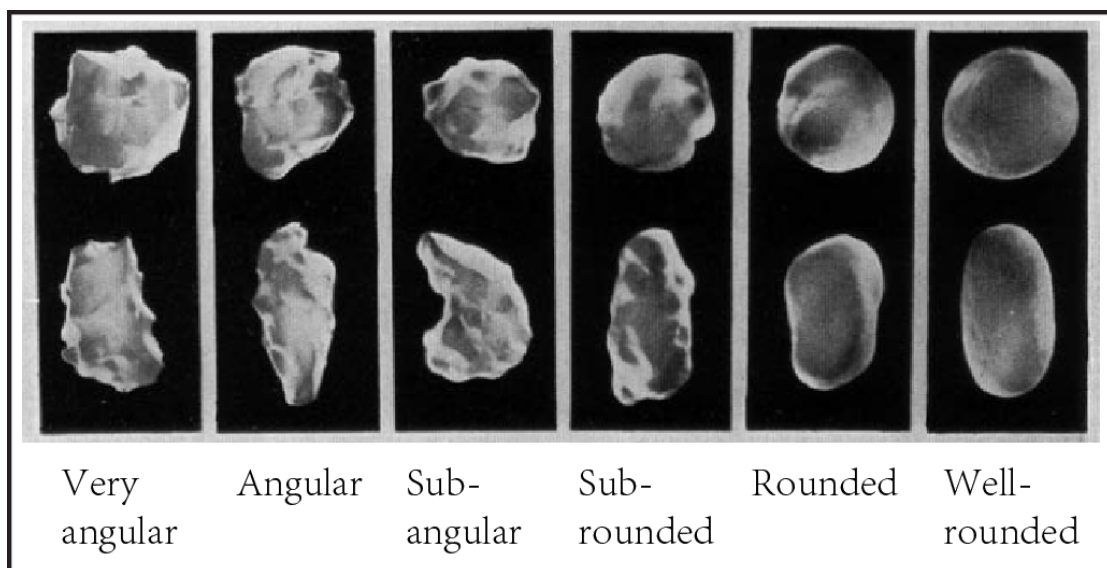
Figure 2.5 *Terminology of rounding degree of grains*(Powers, 1953).
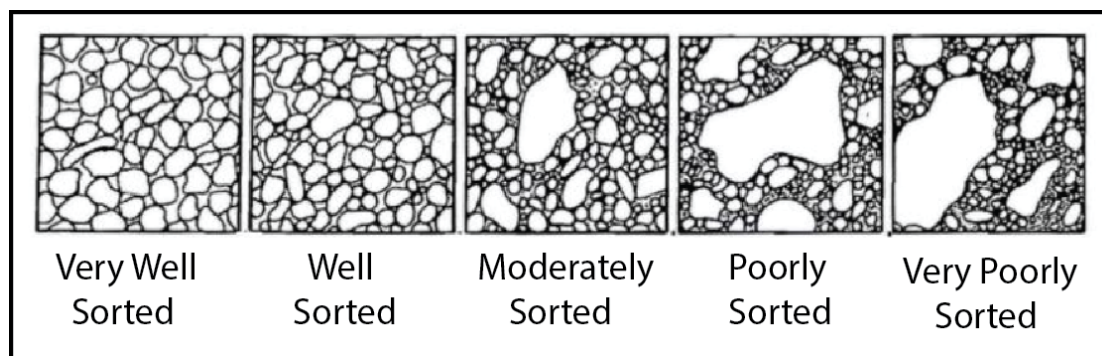
Figure 2.6 *The degree of sorting determined by Compton (1962).*

2.4.3 Scanning electron microscope (SEM)

The scanning electron microscope (SEM) was used to obtain more detailed observations of grain structures, diagenetic relations and study the clay minerals morphology. Key samples (both carbon coated thin sections and gold coated stubs) were studied by using a JEOL JSM-6460LV Scanning Electron Microscope, with LINK INCA Energy 300 (EDS) from Oxford Instruments at Department of Geosciences, UiO. The SEM produces images by scanning the sample with electrons. The electrons interact with atoms which producing signals which could be detected by secondary electrons (SE), back-scattered electron images (BEI), characteristic X-ray and light (cathodoluminescens) (CL). The SEM was handled by the author under supervision by Berit Løken Berg.

2.4.4 X-ray diffraction analysis (XRD)

Bulk XRD analysis

Thirty-one field samples were analyzed by XRD at Department of Geosciences, University of Oslo (Table 2.2). The XRD analysis is useful both for analyzing mineralogy for the bulk rock assemblages, and for studying the clay fraction. The analyzes were conducted by Maarten Aerts, and all data was collected on a Bruker D8 Advance Diffractometer equipped with a Lynxeye linar PSD detection. The equipment was operated at 40 kV and 40 mA, using Ni-filetered Cu Kα radiation.

2. Method

All field samples were first crushed to rock powder. The soft clay samples were crushed by using a "swing-mill" and the hard sandstone samples were crushed in an agate mortar. Then the rock powder of the samples was micronized to finer powder using a McCrone micronizer in 12 min. Finally the samples were packed into glass holders, in order to run in the X-ray diffraction.

Each mineral has a specific unit cell and character distance in the mineral lattice. When diffracted x-ray beams, each mineral will produce a specific d-value and 2θ angle, as a function of unit cell (Moore & Reynolds, 1997). The d-value can be described as the space of the atomic planes in the mineral lattice. The d-value, 2θ angle and intensities of a matter from the XRD-diagram could be used for mineral identification.

In this thesis, the author used the Diffrac. EVA software for peak interpretation. Each sample was analyzed the mineral content by using semi-quantitative. The semi-quantitative analysis is based on the intensity of the strongest reflection of the interest mineral. Some minerals were taken the second largest peak into account, since their main reflection in the same position as many other minerals (e.g. quartz). The results are not true percentages, only estimations (Appendix C).

Table 2.4 *Utilized d-values in semi-quantitative analysis (From Chen, 1977)*

Mineral	d-value (Å)
Quartz	4.26
K-feldspar	3.24
Plagioclase	3.19
Mica	10.08
Mixed layer clay	10-13
Chlorite	3.54
Kaolinite	3.58
Calcite	3.04
Dolomite	2.89
Pyrite	2.71
Montmorillonite	15-17

Clay fraction separation

Thirteen samples were selected for the clay fraction analysis (Table 2.2). All samples were crushed in the "swill mill" to a size of 1-2mm. Taking 3-5g sample was then suspended in ca. 350ml distilled water mixed with sodium carbonate Na_2CO_3 (0.0125g) to prevent flocculation. The suspended sample was mixed randomly by a plastic stirring rod in the laboratory tumbler. After the artificial mixture, the tumbler was put in VWR Ultrasonic Bath to undergo disaggregation for 10 min. This process was done to accelerate the dispersion of the clay particles. After the ultrasonic treatment, pour into more distilled water mixed with sodium carbonate reach to approximately the maximum volume of the tumbler, then left it for 6 hours. During the six hours, the clay particles were separated where the coarser material set down to the bottom. A hose was injected into the tumbler and removed the suspended clay mineral out of the

tumbler into a laboratory plastic box. The lower 5cm liquid containing coarser material was left in the tumbler, and then thrown away. The clay fraction (<2mm) was run through a Millipore filter by using the Millipore vacuum technique. Shaking the sample to mix clay material homogeneous before put them on the filter. After filtering the material was flushed with $MgCl_2$ to induce cation exchange. Then the sample was inverted onto round Pyrex glass platform and placed in aluminum holders for future analysis in the Bruker D8 XRD instruments. All samples experienced four different treatments: air-dried, ethylene glycol, heated-1 (350℃) and heated-2 (550℃).

In this thesis, five main clay minerals groups were identified: illite, smectite, kaolinite, interstratified illite-smectite layer, and chlorite based on their X-ray diffraction maximum, termed as "peak". According to the method described in Biscaye (1965), Moore and Reynolds (1997), the identification of the mineral groups was accomplished. The qualitative analysis of the XRD clay fraction was performed by using the Diffrac. EVA and the quantitative analysis were performed by using NEWMOD version 2.3 (Reynolds, 1985).

3. Result

3.1 Outcrop Description and Presentation of the sedimentary logs

During the field work in October-November 2014 in the northern and southern parts of the Mandawa Basin (Figure 1.1), three time equivalent formations, Makonde Fm., Kiturika Fm. and Kihuluhulu Fm. (Aptian-Mid Turonian) were sampled and logged. Two outcrops were logged in detail, whilst another two outcrops were worked out as sketch logs. In addition, some outcrops samples were only collected. Most of the outcrops are observed in the central/south Mandawa Basin, just one outcrop, WP-92, was logged in the northern part.

3.1.1 WP-92 – Kipatimu-Kihuluhulu Fm.

The WP-92 locality is located on track TR-4 not far from Nanayui village (Figure 1.1) (Hudson, 2011). Outcrops are exposed in the ditch along the main roadside and the total thickness is approximately 26.6m (Figure 3.1). The section is logged in scale 1:50 (Figure 3.2) and started from latitude S05º14, 291and longitude E90º56, 245 to latitude S05º14, 568and longitude E90º56, 095, and the value of natural gamma radiation is noted in the logs (Appendix A).

The section of WP-92 log is characterized as the Kipatimu-Kihuluhulu Fm (Figure 3.1). The lower 10m is present the Upper Kipatimu Fm, which consists of cross-bedded sandstones, grain supported conglomerates and claystones (Figure 3.1a). Clay rip-up clasts are observed in most of the sandstones and conglomerates. Some sand units show weakly degree of bioturbation as well. The Kihuluhulu Fm. starts with a unit of weakly laminated claystone interbedded with sandstone lenses/stringers, which played a dominant role in the Kihuluhulu Fm (Figure 3.1c). Several thin sandstone layers were discovered among the claystone alternately. Half meter thickness of the fossiliferous conglomerate is present the end of the section, with

moderate degree of bioturbation.
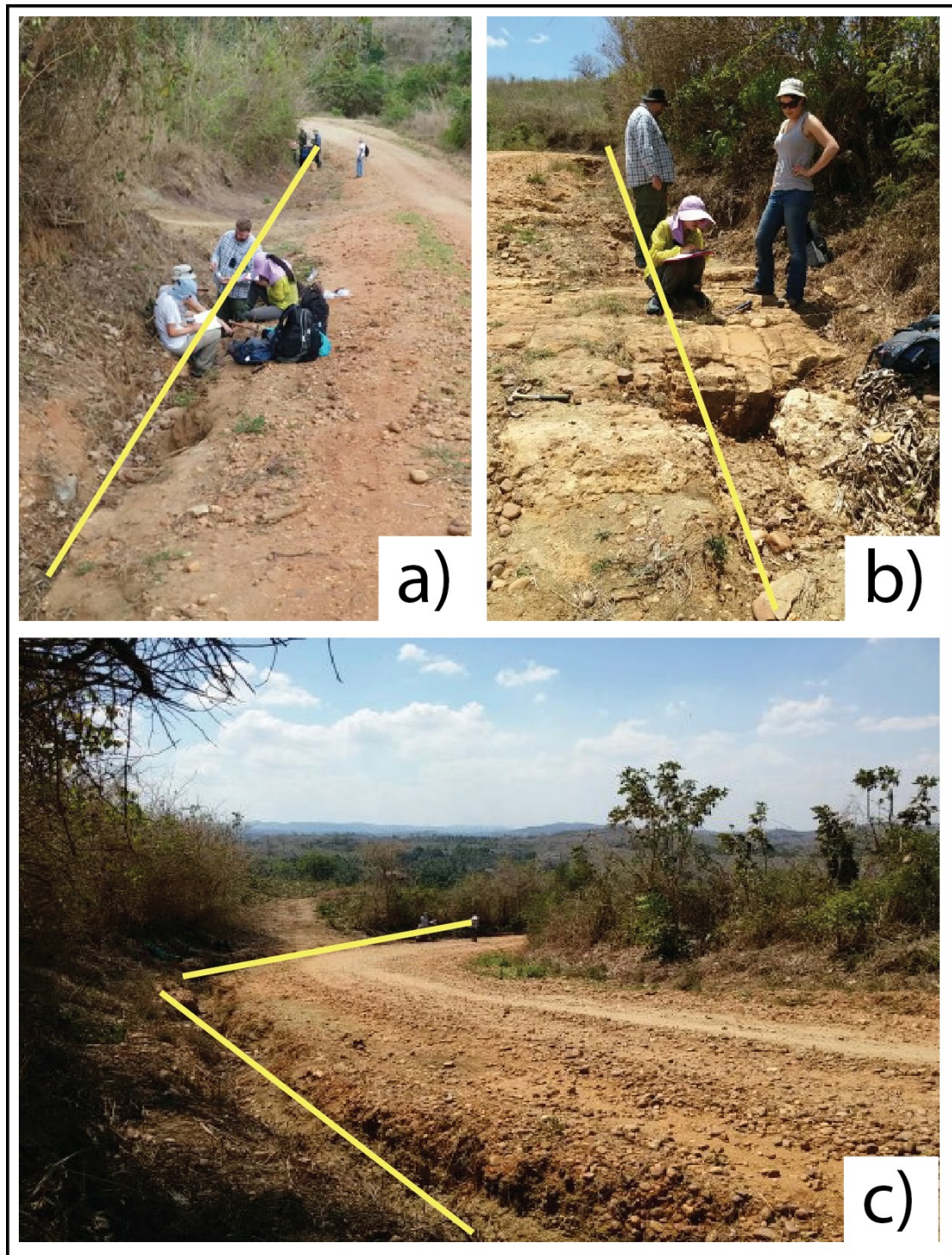
Figure 3.1 *Overview of WP-92 locality, a)-b)-c) shows stratigraphic upward. The yellow lines indicate the logged section. a) shows the first few meters of the lowest part of the locality, upper Kipatimu Fm.; b) shows few meters of the middle part of the section; c) shows the most abundant facies of Kihuluhulu Fm, which located in the upper part of this section.*
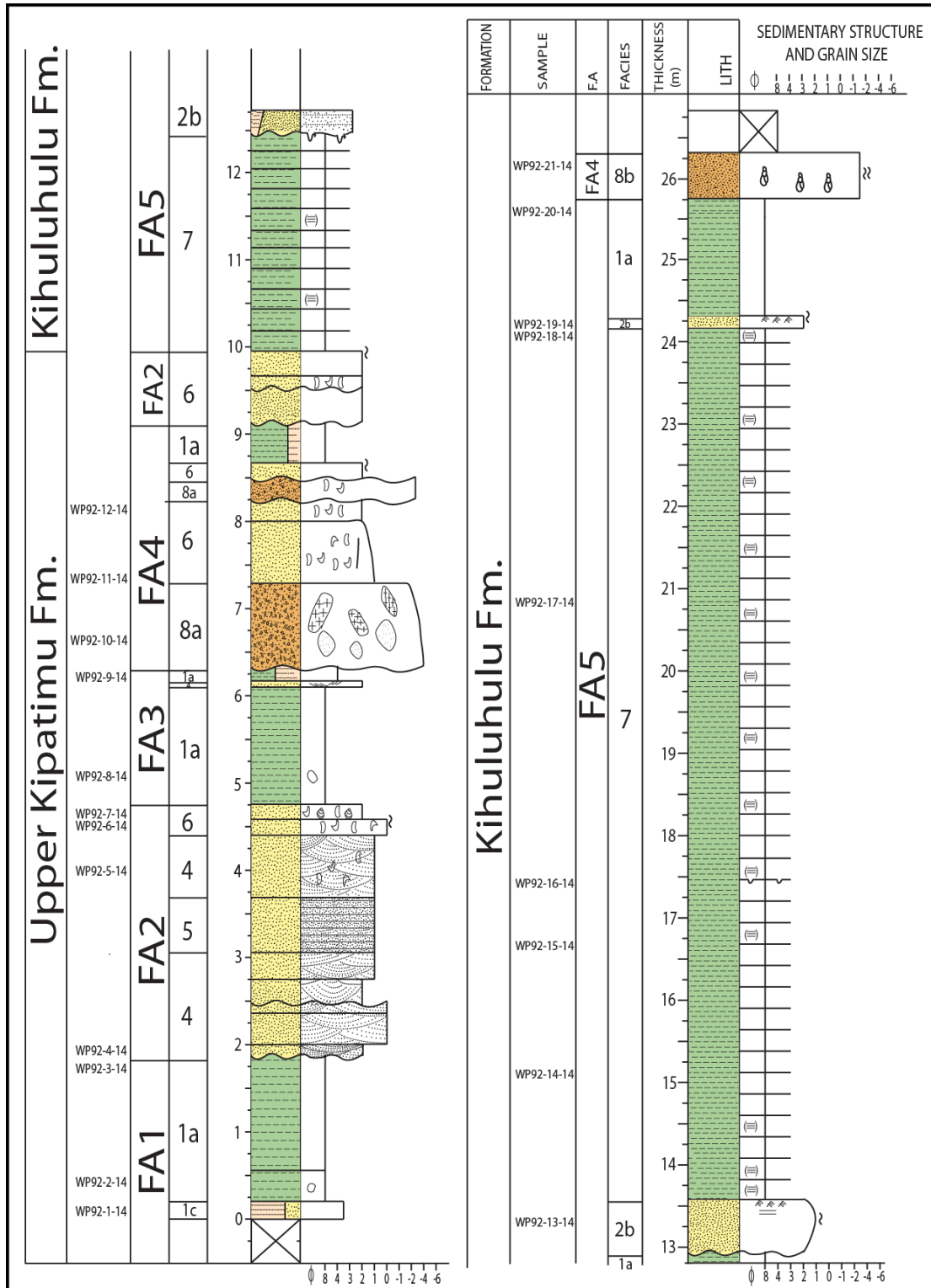
Figure 3.2 *The sedimentological log of WP-92. See figure 2.4 for legend.*

3.1.2 WP-223 –Kihuluhulu Fm.

The WP-223 locality is situated at the central/ southern part of the Mandawa Basin and located on TR-20 as Hudson (2011) referred (Figure 1.1). The coordinates of this location is S 05º37, 623 and E 89º88, 991. This outcrop is exposed closely to the Kilwa-Lindi highway (Figure 3.3). The sedimentary log was logged in the scale of 1:20 and the measurements of the natural gamma radiation are noted in the log (Figure 3.4).
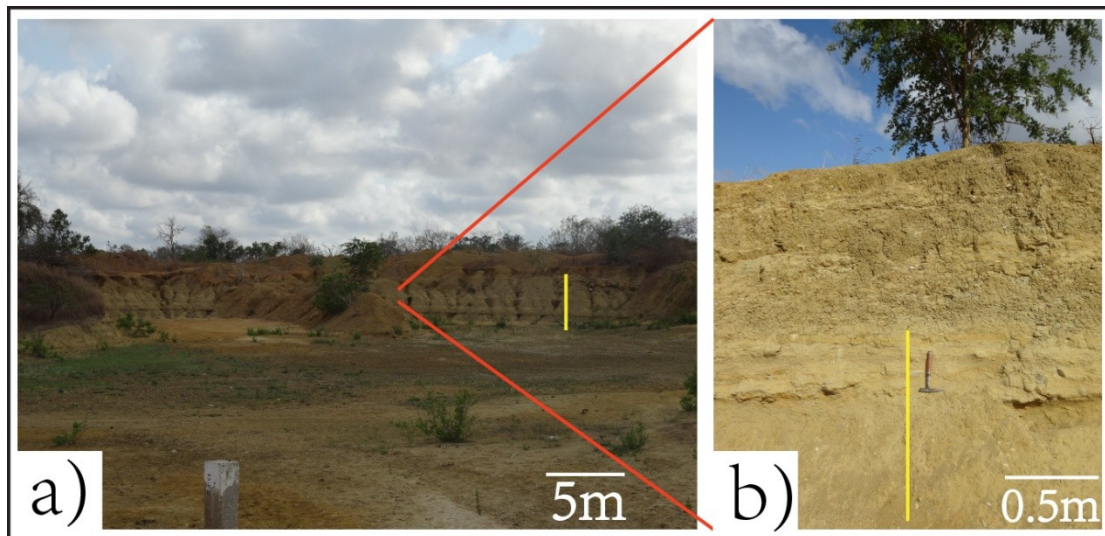
Figure 3.3 *Overview of the outcrop at WP-223 locality, and yellow lines mark the logged section; b) Shows the lowest 1m of the section, then moved southward (showed as yellow line in figure 3.3a).*

This section of the Kihuluhulu Fm. is dominated by thicker clayey siltstones interbedded with thinner sandstone beds (Figure 3.4). The siltstones are enriched in cephalopod fossils with both belemnites and ammonites. Ammonites are well preserved in the sandstone units as well. Two different morphological ammonites, straight and coiled, are appeared together. The clay/clayey siltstone beds displayed some different zonations and consolidation variations from pure clay (very soft and could squeeze with fingers) to friable sandy siltstone. The upper one meter part of sandstone is coarse grained and coal fragments occur. In the medium- to coarse-grained sandstones, clay rip-up clasts and iron nodule are found. However, a

conglomerate unit is found on the top of the sandstones, but could not be logged due to the time limitation.

Figure 3.4 *Logged sections of Kihuluhulu Fm at the locality of WP-223.*

See figure 2.4 for legend.

3.1.3 WP-222 – Kihuluhulu Fm.

The locality of WP-222 is not far from WP-223, which is situated at the roadside of the highway from Kilwa to Lindi (TR-20) (Figure 1.1) (Hudson, 2011). The section was not logged due to the small outcrop. The section was sampled as WP222-1-14 and WP222-2-14. The coordinate of this locality is S 05º34, 800 and E 89º96, 220. The trace fossils (Thalassinoides) are abundant at the sandstone bedding surface (Figure 3.5a), while the base of the sandstone unit displays load casts (Figure 3.5b). The sandstone is cemented with carbonate, and the value of natural gamma radiation is 67 cps. A very fine gray claystone deposited below the sandstone layers, showing 122 cps of natural gamma radiation (Figure 3.5c).
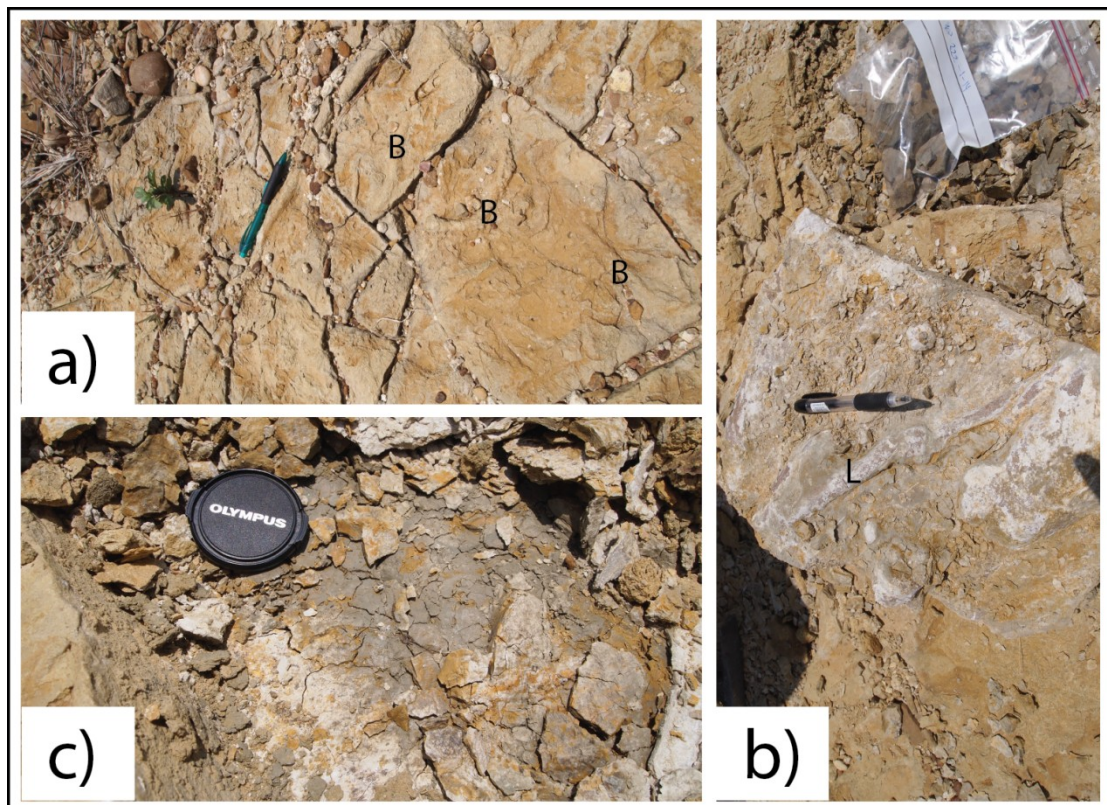
Figure 3.5 *Outcrop of WP-222 locality. a) Shows the abundant trace fossils (Thalassinoides) are present at the sandstone bedding surface (B in photo). The Thalasinoides are braching with 0.5 to 2cm tubes; load casts (L in photo) are found at the base of the sandstone unit, shown as b); c) shows the gray claystone deposited below the sandstones, with a strong reaction of HCl.*

3.1.4 N5 (N5-22, N5-26 & N5-27) – Kihuluhu Fm.

These three localities, N5-22, N5-26 and N5-27, are situated on track TR-11 in the south part of Mandawa Basin (Figure 1.1)(Hudson, 2011).

At locality N5-22 (latitude S 05º21, 488 and longitude E90º26, 105), greenish-gray claystones are poorly exposed along the road. The sample N5-22-1-14 was picked well (Figure 3.6a). The natural gamma radiation measurement was 151 cps.

At locality N5-26, with the coordinate S05º23, 733 E90º26, 005, a low relief sandstone surface was exposed along the road. The sandstone is characterized as very fine-grain very well sorted carbonate cemented sand. The color is yellowish gray and the value of natural gamma radiation was 96 cps. Two sets of fractures are observed on the sandstone bedding surface, with the major striking 146º(SE) and a minor striking 60º(ENE). Moreover, bioturbations occurred on the surface bed (Figure 3.6b). Two samples were picked of the sandstone and one sample of the claystone. The natural gamma radiation of the clay was 104 cps.

At locality N5-27 (latitude S 05º24, 211and longitude E90º26, 026), a fine- to medium-grained, greenish-gray carbonate cemented sandstone is exposed. Flute casts displayed on the sandstones. The natural gamma radiation of the sandstones was 125 cps.
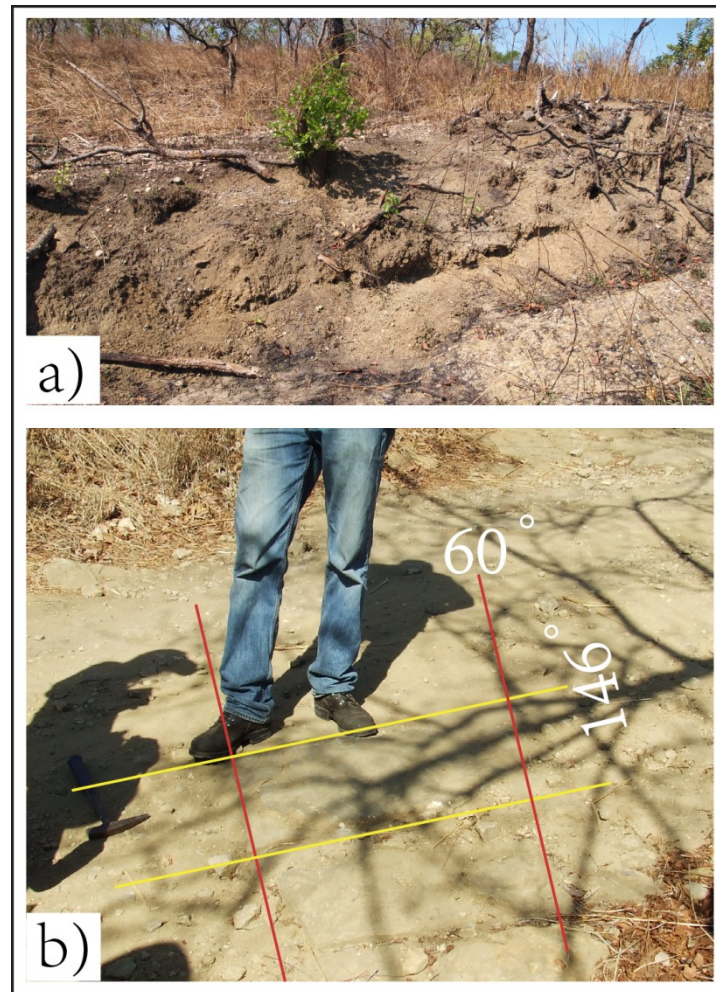
Figure 3.6 *a) Poorly exposed claystones of the Kihuluhulu Fm. at the locality N5-22;*
b) Two fracture sets (yellow and red lines) at the outcrop of N5-26.

3.1.5 WP71 – Kiturika Fm.

The Kiturika Fm. is poorly exposed at the locality WP71, which is on track TR-9 in
the southern Mandawa Basin (Figure 1.1). The coordinates of this locality is latitude
S05°19, 170and longitude E90°19, 423. This locality is dominated by reefal
limestones, which can be described as in situ coral-bearing limestones. However,
calcarenites are exposed at this locality as well. Sketch map and a section of sketch
log are operated of this locality (Figure 3.7).

Figure 3.8 is showing the sketch log that is logged from a calcarenite unit to a reefal
limestone unit. These two beds carry different dips, consequently an angular

unconformity is present along the boundary between the two layers. The nature gamma radiation of the lower calcarenite is 83 cps, while the value of upper reefal limestone 58 cps.
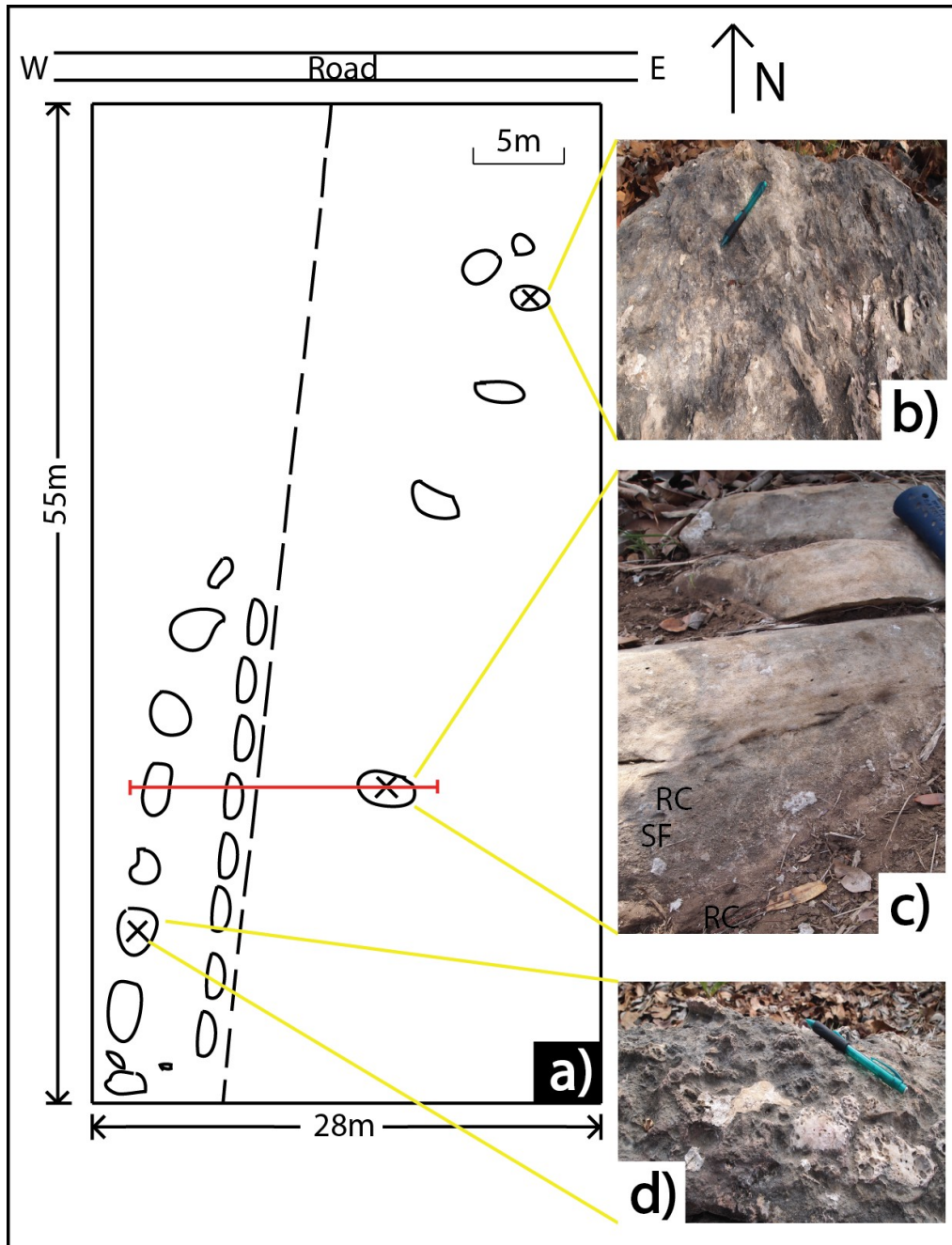
Figure 3.7 *a) Sketch map of WP-71 locality, three samples were taken. A sketch log was compiled. The red line marks the section of the sketch log; b) Carbonate cemented calcarenite, sample WP-71-3-14; c) Laminated calcarenite, sample WP71-1-14; d) Reefal limestone with highly crystallized, sample WP71-2-14.*
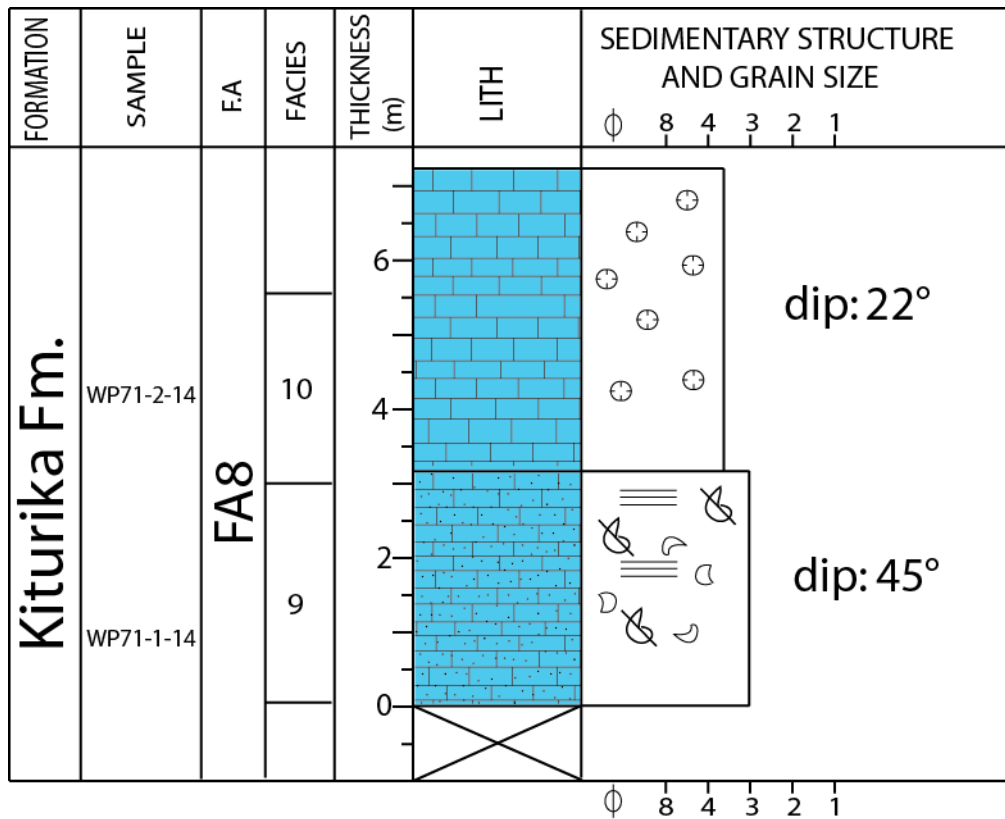
Figure 3.8 *The sketch log of Kiturika Fm., the section is logged along the red line in figure 3.7a in a scale of 1:100. The lower calcarenite is dipping in 45° while the upper reefal limestone is dipping in 22°.An angular unconformity ispresent the boundary between these two units. See for figure 2.4 for legend.*

3.1.6 WP62 – Makonde Fm.

The Makonde Fm. is exposed at WP-62 locality on track TR-9, located at a dug water hole in the south part of Mandawa Basin (Figure 1.1)(Hudson, 2011). The coordinates of this locality is latitude S05º12, 594 and longitude E90º15, 986. A short log is completed at this locality and the measured natural gamma radiation is present in Figure 3.9a. The sandstones are divided into two different parts. The lower part is recognized as grayish sandy siltstone. Small grayish clay rip-up clasts are present in this bed, as well as coal fragments (Figure 3.9b). Coarsening upward sequences are characterized the upper fine- to medium-grained sandstones. The cross bedding occurred at 30cm from the sandstone base, showing two sets of different direction (Figure 3.9c).
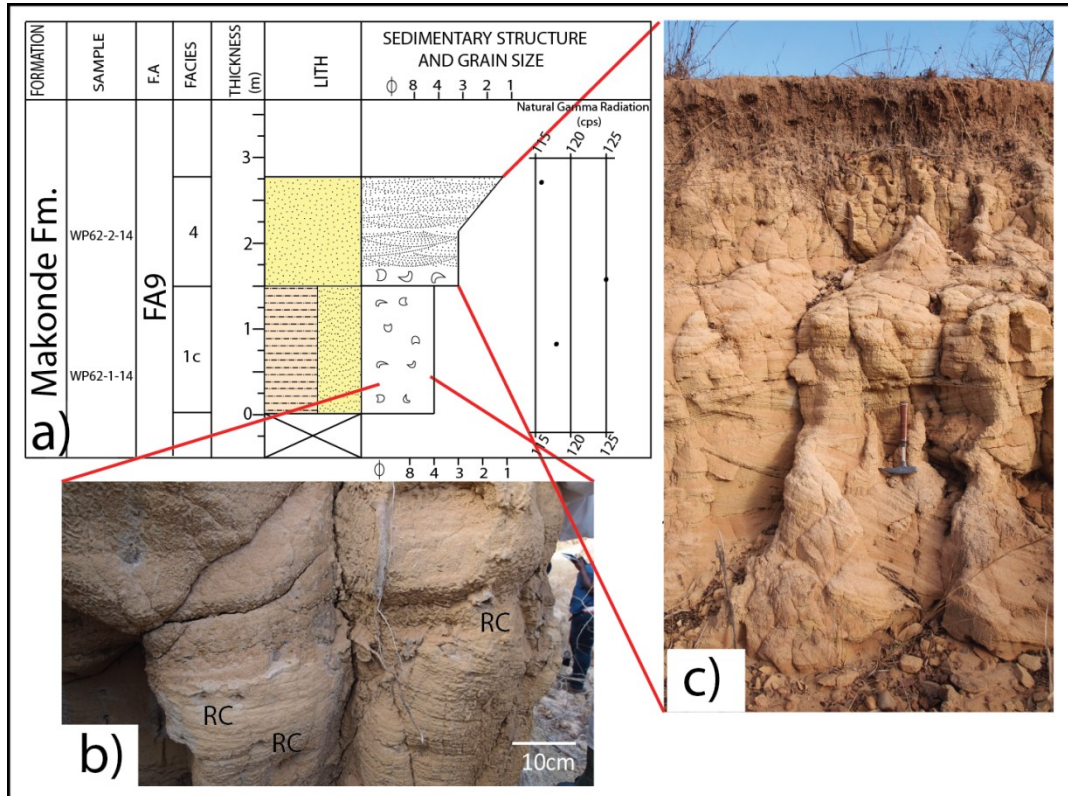
Figure 3.9 *a) Sedimentary log of Makonde Fm. at the WP-62 locality, in a scale of 1:50(see for figure 2.4 for legend);b) Small clay rip up clasts (RC in photo) occurred in the sandy siltstone; c) Well cross-stratification bedded layers of the coarsening upward sandstones.*

3.2 Facies

Table 3.1 *Description of sedimentary facies of Kihuluhulu, Kipatimu, Kiturika and Makonde formations identified the field outcrops.*

Facies nr	Facies	Grain Size	Description	Figure
1a	Clay /clayey siltstone	Clay to silt	No apparent structures, light yellowish brown to dark gray, very weak reaction of HCl. Some units contain belemnites, straight and curled ammonites (iron oxidation reaction) and erosive base.	3.10a,b,e,f; 3.11f
1b	Laminated clayey siltstone	Clay to silt	Parallel laminated, light yellowish brown.	3.10a
1c	Sandy siltstone	Silt to very fine sand	Color is pink to yellowish brown; some units contain small clay rip-up clasts.	3.9a
2a	Massive sandstone	Silt to very fine sand	No apparent bedding, light yellowish brown to pinkish. Some units contain clay rip-up clasts /mud lenses, bioturbation, shell fragments, and erosive base.	3.10c
2b	Ripple-bedded sandstone	Fine to Medium sand	Color is yellowish brown, bioturbation. Some units show gradual grain size variations.	3.11e.f.g
3	Massive sandstone	Very fine to coarse sand	Light yellowish brown to gray, coal fragments, iron oxide nodule. Some units consist of clay rip-up clasts.	3.10f
4	Cross-bedded massive sandstone	Fine to coarse sand	Trough cross-bedded layers, color is white to yellowish brown. Some units contain erosive base and clay rip-up clasts.	3.9; 3.11a,
5	Planar laminated massive sandstone	Fine to medium	Planar laminated, color is yellowish brown to white, some units consist erosive base, flute cast.	

6	Massive sandstone	Very fine to coarse sand	No apparent bedding, light yellowish brown to pinkish. Some units contain clay rip-up clasts /mud lenses, bioturbation, shell fragments, and erosive base, and display upward fining developments.	
7	Claystone inter-bedded with silty sandstone lenses/stringers	Clay to very fine sand	Thin sandstone stringers within claystone. Some sand units have loading structure at the base of the sands. Moderate to strong action of HCl. Weakly laminated/bedded. Grayish to brownish colored.	3.11f
8a	Grain supported conglomerate	Granule/Pebble	Well rounded pebbles in a medium sand matrix, pinkish, well carbonate cemented. Some units contain clay rip-up clasts, basement clasts and Kipatimu sandstone clasts. In addition, upward fining sequence occurred in some units.	3.11b,c,d
8b	Fossiliferous conglomerate	Granule/Pebble	Grain supported, clay rip up clasts. Rich in fossils (gastropods, reefs et al), bioturbation.	3.11h
9	Calcarenite grainstone	Very fine to fine sand	Carbonate cemented, well sorted, weakly bedded, shell fragments. Some of the units displayed internal grain size variations. Clay rip-up clasts is observed in some units.	3.7b,c
10	Reefal limestone	Silt to very fine	Very well cemented with carbonate, highly recrystallized. Corals are exposed well.	3.7d

Facies 1 Clay and siltstone (Table 3.1)

a) Clay and clayey siltstone: Facies 1a is the predominant facies at the WP-223 section of Kihuluhulu Fm. (Figure 3.4) and this facies occurred at WP-92 locality of Kipatimu Fm. and Kihuluhulu Fm. (Figure 3.2). The average thickness of facies 1a at WP-223 is approximately 70cm. The color is dark brown and has a light yellowish brown weathering color. It contains abundant cephalopod fossils with both belemnites and ammonites present. Both straight and coiled ammonites were found together. The fossils are oxidized by iron, hence, the color displayed yellowish brown (Figure 3.10e & f). However, in the Kipatimu Fm. and the Kihuluhulu Fm. at the location of WP-92, no fossils were found in this facies (Figure 3.2 & 3.11f). The color here is greenish-gray, containing some iron-oxide nodules.

b) Laminated clayey siltstone: This facies is present at the lowest part of the section at WP-223 locality (Figure 3.4). Parallel laminated siltstone with light yellowish brown weathered color is the characteristic of the facies 1b (Figure 3.10a).

c) Sandy siltstone: This facies is represented the lowest part of WP-92 section of Kipatimu Fm as a 20cm thick siltstone unit (Figure 3.2). This layer displayed pinkish color. In addition, this facies is present in the lower unit of WP-62 section of Makonde Fm. as a 150cm thick unit. This unit displayed a weathering color of light yellowish brown (Figure 3.9a).

Facies 2 Sandstone (Table 3.1)

The facies 2 is present in the Kihuluhulu Fm. both at the WP-92 and WP-223 localities (Figure 3.2 & 3.4). The difference of facies 2a and 2b is the bedding structures.

a) Massive sandstone: The facies 2a is only displayed at the location of WP-223 (Figure 3.4). The sandstone units contain about 40% silt. It is carbonate cemented and has a light yellowish brown weathering color. It appears light gray on a fresh surface. Scattered bioturbations does occur, as well as ammonites (Figure 3.10c).

b) Bedding structural sandstone: Both parallel lamination and climbing ripples were observed in the sandstones (Figure 3.11e & f). Some of the units consist of flute casts at the base, which indicated the current transport from east to west (Figure 3.11f). In addition, the facies displays scattered bioturbation.

Facies 3 Massive Sandstone (Table 3.1)

The facies 3 appeared at the upper part of Kihuluhulu Fm. at the location of WP-223 (Figure 3.4). This facies consists of very fine to coarse sand with coal fragments, iron nodules and clay rip-up clasts occasionally (Figure 3.10f). The fresh surface is colored as gray but the weathering color is light yellowish brown.

Facies 4 Cross-bedded Massive Sandstone (Table 3.1)

This facies is characterized as fine- to coarse-grained massive sandstones, showing clearly cross-stratification structures. The facies 4 are present both in the Kipatimu Fm. and Makonde Fm (Figures 3.2, 3.9 & 3.11a). Several small clay rip-up clasts are found in both two formations. Some of the sandstone layers of Kipatimu Fm. contain erosive base. The color of this facies in Kipatimu Fm. is white, while the sandstones of Makonde Fm. carry a light yellowish brown weathering color.
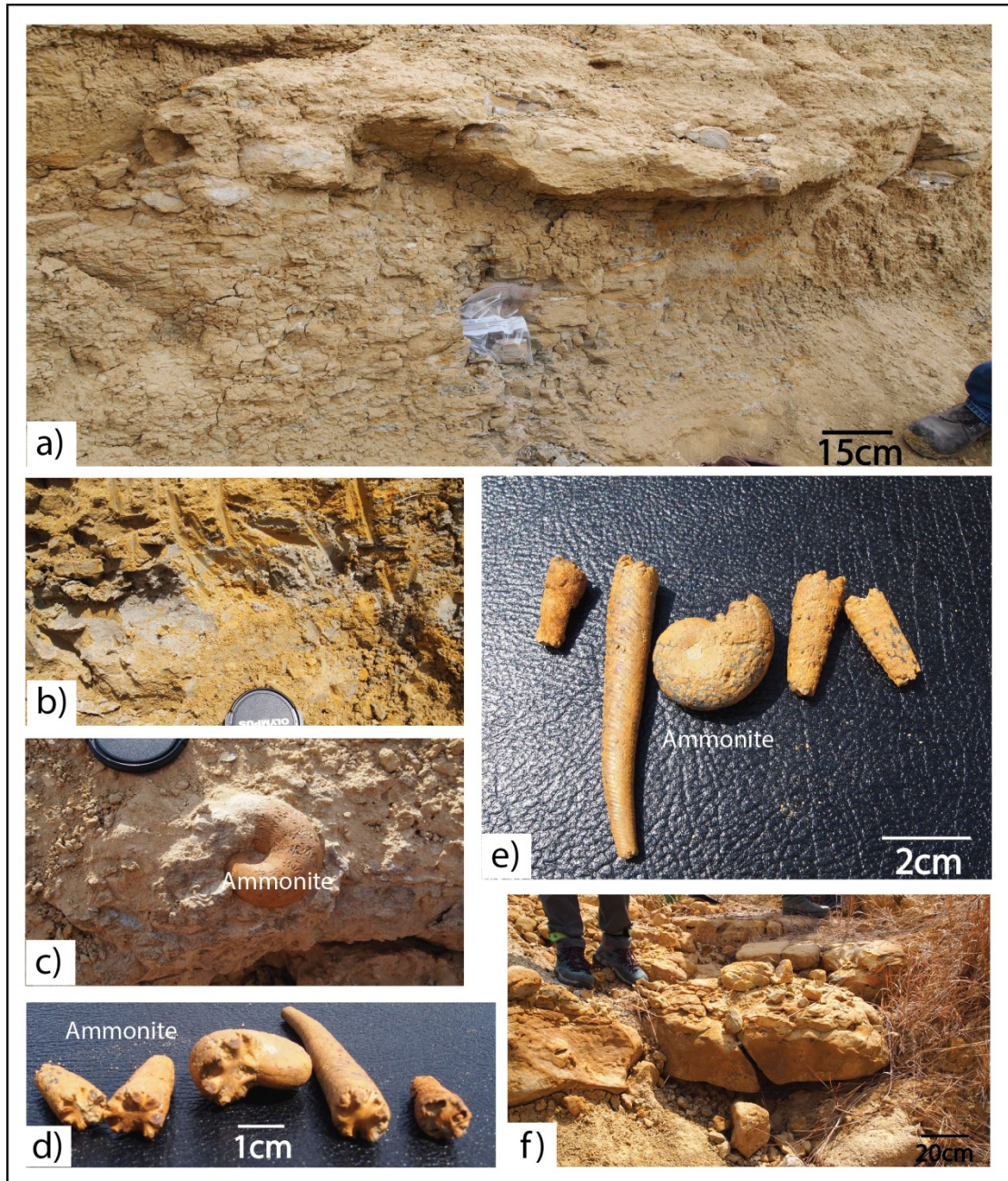
Figure 3.10 *a) Shows the lowest part of the section of WP-223 log. Sample WP223-1-14 (level 0.25min Figure 3.4)is picked for the friable siltstone; b) Very soft pure clay that could be squeezed by any fingers. The dark gray color is from the fresh surface while the weathered surface is colored by light yellowish brown; c) Shows a well preserved ammonite with suture lines occurred in situ at the top of sandstone beds (Facies 2a) (level 1.2m in Figure 3.4), the lower part of the section; d) & e) show two different morphological ammonites (straight and coiled) found at the WP-223 locality. All of them are colored by secondary iron oxides. d) Shows the view of the aperture while e) shows the holistic view; f) Presents the sandstone of Facies 3, located at the upper part of this section.*

Facies 5 Planar Laminated Massive Sandstone (Table 3.1)

The sandstones with planar lamination are present in the Kipatimu Fm. of WP-92 locality (Figure 3.2). This facies consists of fine- to medium-grain sandstones accompanied with planar laminations. This facies is whitish in color in the Kipatimu Fm. (Figure 3.11f).

Facies 6 Massive Sandstone (Table 3.1)

The facies 6 is present in the Kipatimu Fm. of WP-92 locality (Figure 3.2). The grain size of these sandstones varies from very fine to coarse, with light yellowish brown weathering color. Most of the unit contains clay rip-up clasts, and display an erosive base and scattered bioturbation.

Facies 7 Claystone Interbedded with Silty Sandstone Lenses/Stringers (Table 3.1)

This facies is the predominant facies of the Kihuluhulu Fm. at the location of WP-92 (Figure 3.2). Facies 7 is made up of claystones and thin silty sandstone lenses/stringers interbedded (Figure 3.11f). The thickness of this facies is more than 10m. The claystones show weak lamination, and have a moderate to strong reaction of the acid. Load structures could be seen along the base of various sand units (level 17.5m in Figure 3.2).

Facies 8 Conglomerate (Table 3.1)

a) Grain supported conglomerates: This facies is present in the Kipatimu Fm. at WP-92 locality (Figure 3.2). It contains two conglomerate units. The first one is characterized as an upward fining sequence, which is grain supported carrying well rounded pinkish pebbles in a medium sand matrix (Figure 3.11c & d). This

conglomerate contains Kipatimu sandstone clasts that up to 53cm, and well-rounded basement clasts that up to 9cm. Another conglomerate unit is described as pinkish grain supported conglomerate. Clay rip-up clasts occurred on the top of the layer, as well as the base is eroded (Figure 3.11b).

b) Fossiliferous conglomerate: The facies 8b is the end unit of the Kihuluhulu Fm. of the WP-92 section (Figure 3.2). A certain number of fossils and traces are present in this facies. Several large gastropods are displayed on the surface of the conglomerate (Figure 3.11h).

Facies 9 Calcarenite (Table 3.1)

This facies is present in the Kiturika Fm. at the location of WP-71 (Figure 3.8). The calcarenite is well cemented with carbonate, and the grains are well sorted. The calcarenites are weakly bedded, accompanied with internal grain size variations (Figure 3.7b&c). Some clay rip-up clasts are present along the bedding planes. Shell fragments appear as well.

Facies 10 Reefal Limestone (Table 3.1)

Reefal limestones are the dominant facies of Kiturika Fm. in WP-71 (Figure 3.8). This facies is characterized as very well sparitic cemented, highly recrystallized fossiliferous limestones (Figure 3.7d).
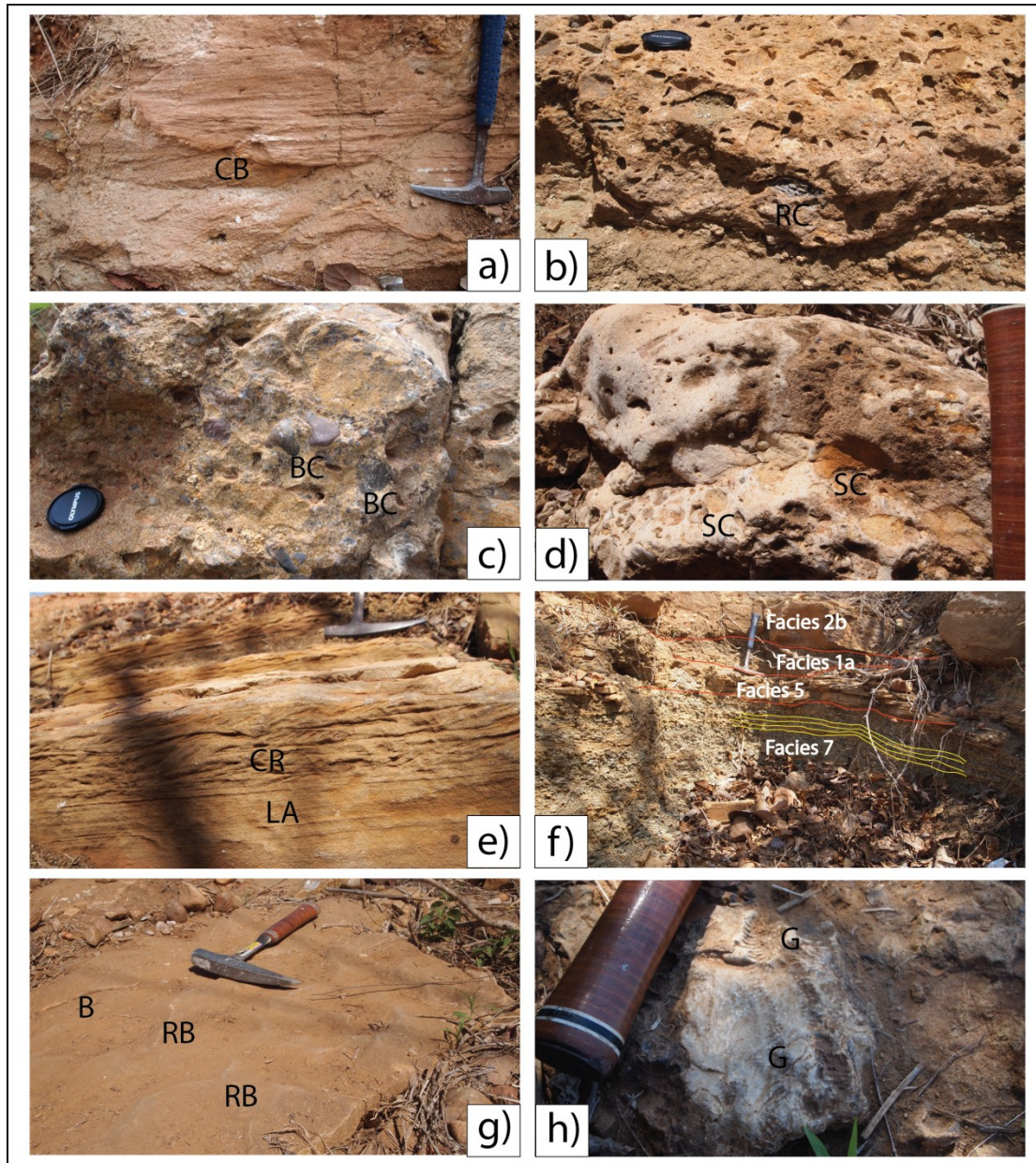
Figure 3.11 a) Shows the cross-bedded sandstones (CB in photo) of the Kipatimu Fm, representing the facies 4 (level 2-3m in Figure 3.2); b) Shows the conglomerate unit with clay rip-up clasts (RC in photo) of the Kipatimu Fm (level 8.25-8.5m in Figure 3.2); c) & d) Show the conglomerate bed of the Kipatimu Fm.(level 6.26-7.26m in Figure 3.2). c) Displays the basement clasts (BC in photo) in the conglomerate while d) displays the Kipatimu sandstone clasts (SC in photo) in the conglomerate. The remaining four pictures show the examples of Kihuluhulu Fm. at WP-92. e) Shows the sandstone contains climbing ripples (CR in photo) and laminations (LA in photo); f) Shows a minor section of the Kihuluhulu Fm. The figure displays four different facies (Facies 1a, 2b, 5, 7).g) Shows the ripple-bedded structures (RB in photo) and bioturbations (B in photo) on the surface of facies 2b; h) Shows the large gastropods (G in photo) occur on the top of the facies 8b, situated at the end of Kihuluhulu Fm. of WP-92.

43

3.3 Facies Association and Sedimentological Description

Five facies association have been determined according to the facies description, which were named FA1 to FA8 (Table 3.2). In the following paragraphs, facies association and sedimentological descriptions are illustrated in detail.

Table 3.2 *Classification of facies association of Kihuluhulu, Kipatimu, Kiturika and Makonde formations.*

Facies Association	Facies	Figure	Locality
FA1	1a,1c	3.2	WP-92
FA2	4,5,6	3.2	WP-92
FA3	1a,4	3.2	WP-92
FA4	1a,6,8a,8b	3.2	WP-92
FA5	1a,2b,7	3.2	WP-92
FA6	1a,1b,2a	3.4	WP-223
FA7	3	3.4	WP-223
FA8	9,10	3.8	WP-71
FA9	1c,4	3.9	WP-62

FA1

FA1 is recognized at the location of WP-92, located in the northern Mandawa Basin (Figure 1.1) (Table 3.2). This facies association is composed of three facies, facies 1a, and 1c, which are dominated by clay and siltstones (Figures 3.2 and 3.4). The grain sizes vary from clay to very fine sand, and the color of the clay and siltstone is various from light yellowish brown to dark gray (Figures 3.10a and b). FA1 is observed at the lowest part ofWP-92 locality, at level of 0-1.8m.

FA2

The FA2 is identified in the northern Mandawa Basin, WP-92, which is dominated by massive sandstones (Figure 3.2). It contains three sandstone facies, facies 4, 5 and 6 (Table 3.2) (Table 3.2). Facies 4 and 5 display distinctive stratification structural characters while it is hardly to observe any structures of facies 6. Further, the facies 4 is present trough cross bedding structures (Figure 3.11a) while facies 5 displays planar lamination. Clay rip-up clasts and erosive base are identified in facies 4. The grain size of facies association FA2 varies from silt to coarse sand. The color of these sandstones is white to light yellowish brown. This facies association is recognized in Kipatimu Fm., at the level of 1.8-4.8m (Figure 3.2).

FA3

Facies association 3 (FA3) is recognized at the location WP-92 of the northern part of the Mandawa Basin and the location WP-223 of the south Mandawa Basin (Figure 1.1). FA3 is composed of facies 1a and facies 4, which is a combination of clay/siltstones and massive sandstones (Figures 3.2 and 3.4) (Table 3.2). The facies 1a is described as clayey siltstone with no distinctive bedding. Some of the units contain certain amounts of belemnites and ammonites in situ. The sandstone facies 4 displays a thin unit of 7cm thick. FA3 is present in the Kipatimu Fm., at levels of 4.8-6.3m (Figure 3.2).

FA4

FA4 is composed of light yellowish brown sandstone facies 6, grain supported conglomerates facies 8a and 8b and claystones facies 1a (Figure 3.2) (Table 3.2). FA4 is present in the Kipatimu and Kihuluhulu formations, located at the location WP-92 of the north Mandawa Basin (Figure 1.1). The facies 6 is characterized as

homogenous sandstone unit with clay rip-up clasts and scattered bioturbation. The conglomerates facies are carbonate cemented; grain supported well rounded pebbles/granules in the medium sand matrix. Some units of facies 8a contain basement clasts and Kipatimu sand clasts. The facies 8b is rich in fossils (e.g. gastropod, reef et al.). FA4 display a thick unit in the Kipatimu Fm, at level of 6.3-9.1m, and it is present at the top of the Kihuluhulu Fm with the thickness of 1m (level 25.8-26.8m) (Figure 3.2).

FA5

This clay and siltstones association is dominated by dark gray clay facies 1a and 7, interbedded with homogenous sandstone units (15-28 cm in thickness) of facies 2b (Figure 3.2) (Table 3.2). FA5 is present in the Kihuluhulu Fm. of the WP-92 locality (Figure 1.1), which it constitutes 15.8m (level of 10-25.8m) of the log, making FA5 the dominant facies association. Facies 7 is dominating this facies association, which is described as clay interbedded with sandstone lenses/stringers. Facies 2b displays planar lamination and ripple-bedded structures.

FA6

FA6 is the dominant facies association in the location WP-223, located at the southern/central part of the Mandawa Basin (Figure 1.1). This facies association displays a similar composition with FA5, consisting of the dominant siltstone facies 1a and 1b interbedded with sandstone facies 2a (Table 3.2). Facies 1a can be described as fossiliferous siltstone, which contains amounts of belemnites and ammonites (Figure 3.10d & e). Parallel lamination can be observed in facies 1b. The sandstone facies 2a displays no distinctive structures, some units contain ammonites and scattered bioturbation (Figure 3.10c). FA6 is present at level of 0-3.45m in the WP-223 locality.

FA7

The facies association FA7 only consists of facies 3, presenting at the top of the WP-223 locality (Figure 1.1) (Table 3.2). Facies 3 comprises medium- to coarse-grained sandstone and siltstone. Coal fragments are present in both two beds. In the sandstone unit, clay rip-up clasts and iron-oxide nodules are discovered as well.

FA8

Kiturika Fm. is poorly exposed at southern Mandawa Basin, the location WP-71 has been studied in this thesis (Figure 1.1). FA8 is dominated by reefal limestones (Facies 10), which is very well carbonate cemented with highly crystallized corals (Figure 3.7d) (Table 3.2). The corals are easily apparent on weathered surfaces. Three samples were collected from this location (Figure 3.7). Calcarenites (Facies 9) are exposed at this locality as well, which is characterized as well carbonate cemented, well sorted, alternating grain size between finer and coarser laminated calcium limestone (Figure 3.7c). At the base of the calcarenite, clay rip-up clasts (RC in Figure 3.7c) and shell fragments are present (SF in Figure 3.7c).

FA9

FA9 represents the Makonde Fm, located at the location WP-62 of the southern Mandawa Basin (Figure 1.1). This facies association consists of facies 1c and 4 (Table 3.2), displaying an upward coarsening succession. Clay rip-up clasts are present in facies 1c and the base of the facies 4. The thickness of FA9 is about 2.8m (Figure 3.9).

3.4 Petrographic Description

3.4.1 Kihuluhulu Fm. (Aptian-Mid Turonian)

Two sections are represented this formations, which are located at localities WP-223 and WP-92 respectively.

3.4.1.1 WP-92

XRD results
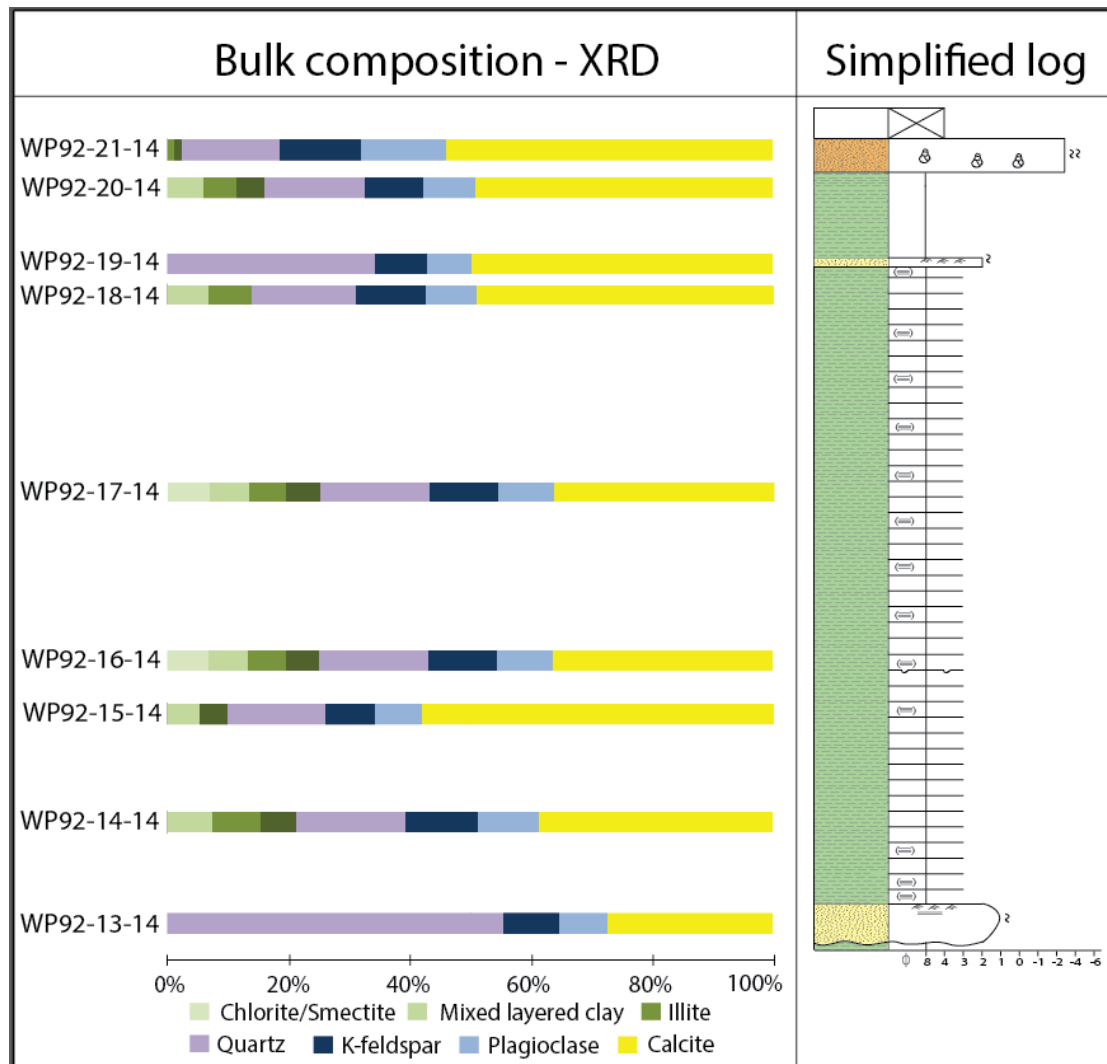
Figure 3.12 *Quantitative XRD results are present with the simplified log of WP-92 section*

The bulk mineralogical compositions of the nine samples from Kihuluhulu Fm. at the WP-92 locality were analyzed by XRD (Figure 3.12). All the bulk samples are carbonate cemented, with an average carbonates cementation of 46.4%. The predominant mineral is quartz, varying in concentration between 16.1% and 55.6%, with an average value of 24.1%. Feldspar (19.3%) is subdivided into K-feldspar (10.2%) and plagioclase (9.1%) (Appendix C). The quartz/feldspar ratio varies between 0.6 and 3.2. The samples contain on the average 5.5% clay minerals, except in the two sandstone samples (WP92-13-14 and WP92-19-14).

The clay fraction has been analyzed of four samples (WP92-14-14, WP92-17-14, WP92-18-14 and WP92-20-14) (Appendix D). All the clay samples are dominated by interstratified illite-smectite mixed layer clay mineral, with an average value of 53.0%. Illite and chlorite are also present with average values of 18.0% and 8.8% respectively.

Petrographic and mineralogical description

The petrography of four samples from Kihuluhulu Fm. of WP-92 location was studied in thin section (WP92-13-14, WP92-16-14, WP92-19-14 and WP92-21-14). All samples can be classified as arkosic sandstone (Appendix E). The samples constitute mainly subrounded to subangular grains. The samples are basically weakly compacted, and display mostly tangential grain contacts, with several long and concave contacts observed (Figure 3.13a). The grain size is dominated by fine- to medium- sand. All samples are carbonate cemented, with the concentration varying between 18% and 48.8%. The porosity was observed both in WP92-13-14 and WP92-19-14 samples and dominated by secondary porosity, represents minor amounts (1.5%) which makes up of dissolved feldspar and dissolved carbonate cement. According to the results of point counting, all of the samples display a high abundance of quartz and weathered feldspar. Monocrystalline quartz with straight extinction is the dominant quartz type

with values up to 66.1%, where both undulatory (26.3%-39.1%) and polycrystalline (14.2%-28.3%) quartz and chert (0.25%-1%) were observed. Feldspar grains are poorly preserved with the majority of grains being classified as category 4-5 (Table 2.3). Pyrite present in the samples makes up of the value up to 3.5%. Some pore filling kaolinite and biotite are present in the samples as well. Authigenic chlorite coated of both quartz and feldspar grains have been revealed during light microscope and by SEM analysis (Figure 3.13e). SEM studied displayed that chlorite precipitated in the secondary porosity which caused by the dissolution of K-feldspar. Albitization of K-feldspar and small amounts of pyrite were observed by the SEM analysis as well (Figure 3.13d).
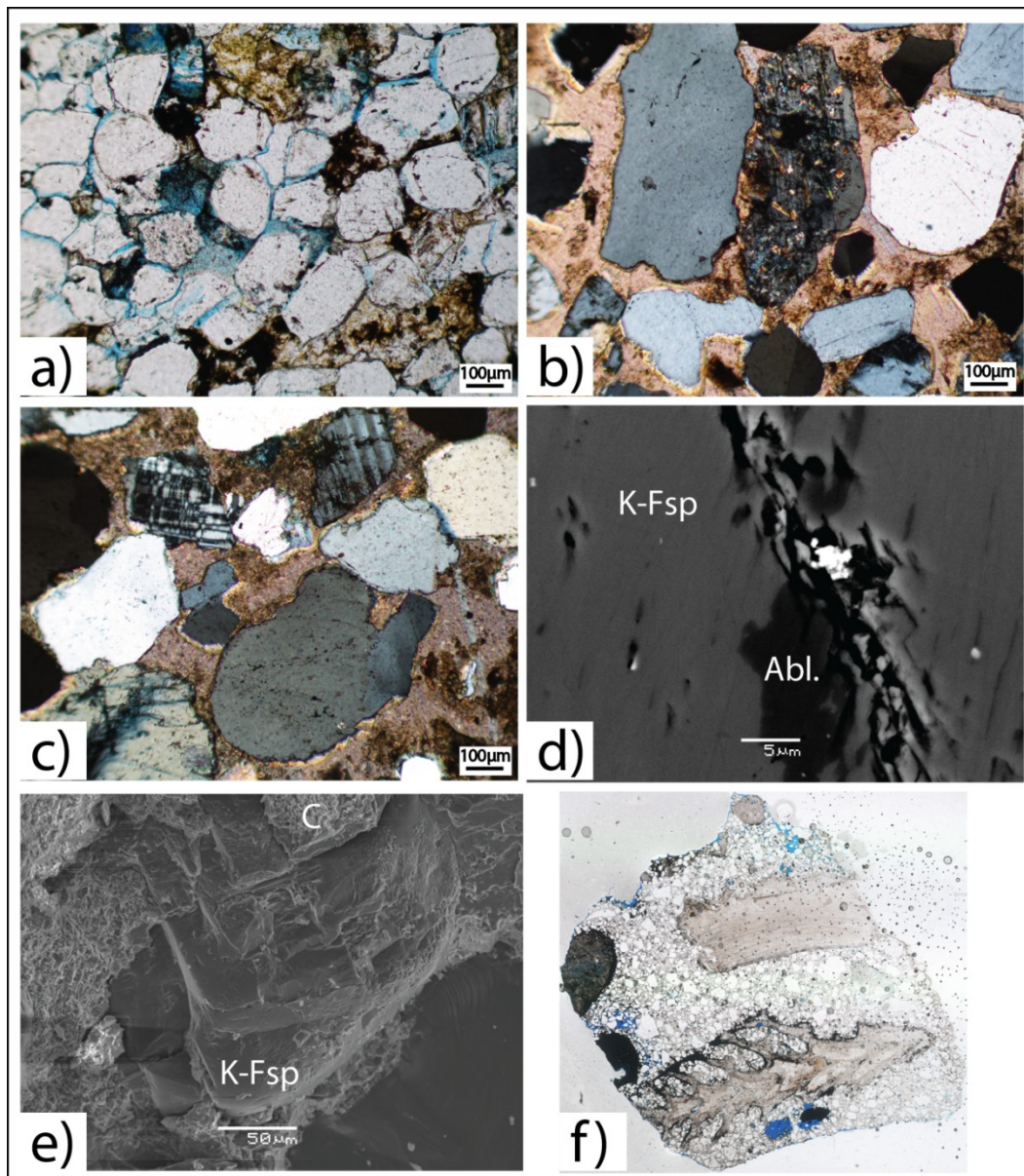
Figure 3.13 *a) Plane polarized micrography of subrounded to rounded grains of sample WP92-13-14. The grains are well sorted with long and tangential contacts and are surrounded by sparitic calcite cement. The secondary porosity is the result of feldspar dissolution. The feldspar preservation is category 5 (Table 2.3); b) Cross polarized micrography of sample WP92-19-14. The feldspar is dissolved and altered to smectite. Some grains are surrounded by clay coating; c) Cross polarized micrography of subangular-subrounded grains of sample WP92-19-14. The sample is well cemented by sparry calcite, with quartz/feldspar ratios about 3; d) A backscatter image taken in SEM of sample WP92-19-14, displaying feldspar albitization and microporosity; e) SEM image of K-feldspar (K-Fsp in photo) surrounded by chlorite coating (C in photo) of sample WP92-16-14; f) Scanned thin section of sample WP92-21-14 from Kihuluhulu Fm. showing the foraminifera.*

3.4.1.2 WP-223

XRD results

Six samples of the Kihuluhulu Fm. at WP-223 locality are analyzed by bulk XRD (Figure 3.14) (Appendix D) and two samples are analyzed by clay fraction analysis (Appendix D).

The bulk samples can be divided into two groups, the lower four samples are cemented with carbonate, with an average value of 35.5%, while the upper two samples have no carbonate cementation. Quartz is the dominant mineral in the upper sandstone samples with an average value of 86.9% and the quartz/feldspar ratio are 8 and 10 respectively. In the lower siltstone/sandstone samples, quartz makes up an average of 27%. The feldspar content has an average value of 32.1%, subdivided into K-feldspar (14%) and plagioclase (18.2%) (Appendix C). The quartz/feldspar ratio displays an average value of 0.85.

WP223-2-14 and WP223-4-14 samples were selected for clay mineral analysis. The illite-smectite interlayer is the dominant phase of the clay minerals, making up 52.7%. Illite is present in both samples, with a similar value approximately 21.5%. Smectite appears in these two samples, and display closed values between 26.4% and 28.4%. The amounts of kaolinite within the two samples vary from 0.9% to 8.6%. Chlorite was only observed in sample WP223-2-14, with proportion of 19.0%
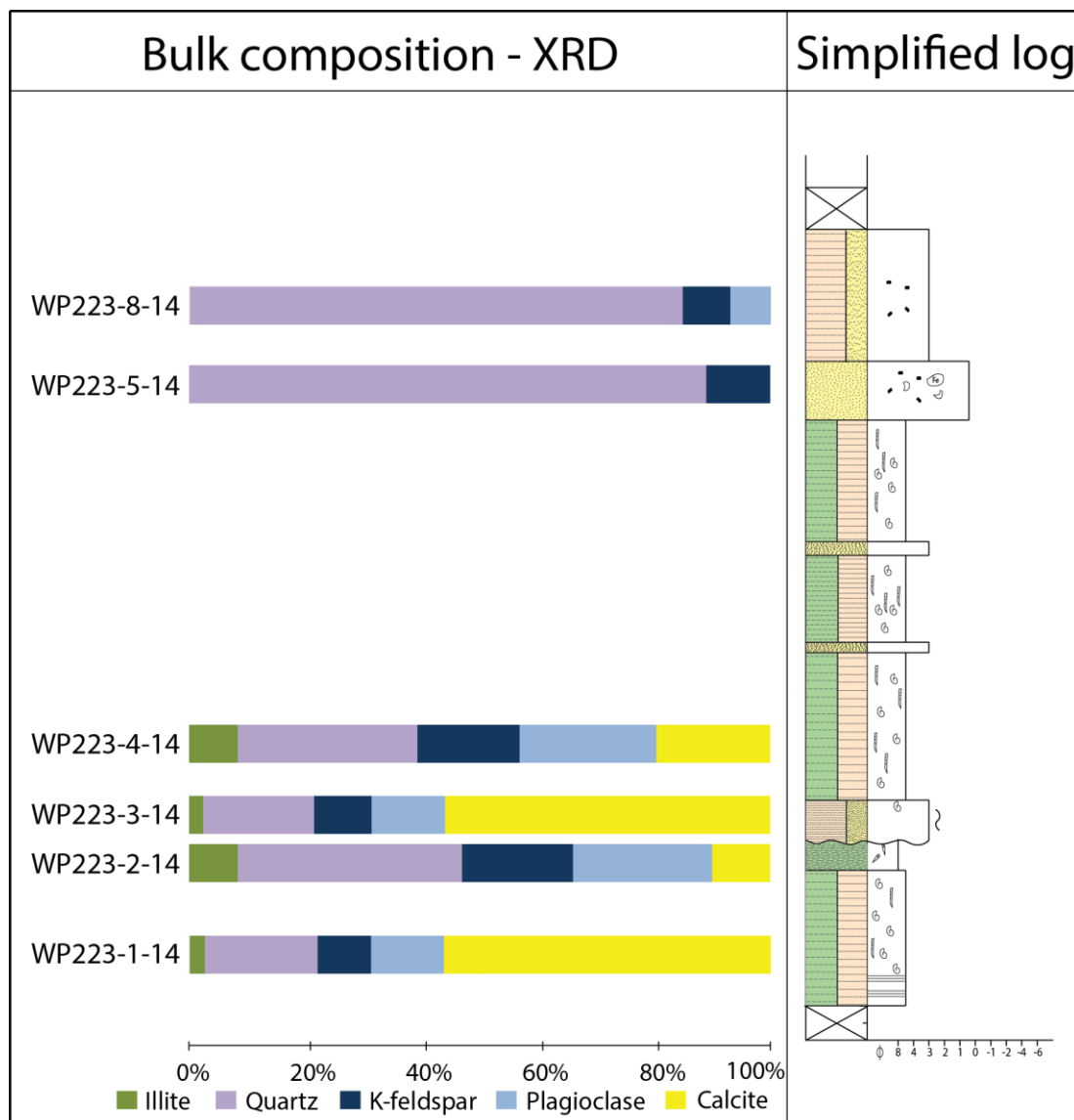
Figure 3.14 *Quantitative XRD results are present with the simplified log of WP-92 section, indicating where the analyzed samples were taken in the logged section.*

Petrographic and mineralogical description

Four siltstone and sandstone samples were point counted and studied by using optical microscopy. Samples WP223-1-14 and WP223-3-14 can be classified as arkosic sandstone, while the other two samples (WP223-5-14 and WP223-8-14) are classified as subarkosic sandstone (Appendix E). The arkosic sandstone is carbonate cemented, making up between 5.5% and 30.0%. Clay matrix varies from 8.8% to 51.3% (Figure 3.15b). Quartz is the dominant mineral of grains, with the value various from 17.8% and 30.6%. Monocrystalline quartz grains are the most abundant grains various between 15.3% and 26.9%. Undulatory quartz makes up the percentage of 6.8% and 9.3%. Feldspar grains consist of K-feldspar (1%-4%) and plagioclase (2.3%-7.0%). The preservation category of feldspar is around category 4-5. Porosity is present in the samples, with the total value of 2.5% and 9.5%. The other compositions are heavy minerals (1.3%), kaolinite (1.3%), biotite (0.5%-2.0%), Fe-oxide (3.0%) and pyrite (0.3%-10.0%). The subarokic sandstones vary in grain size from very fine to medium. The finer sample comprises clay matrix with the value of 51.3%, and poor sorting (Figure 3.15a). The larger grains display subrounded-rounded grain shapes while the smaller grains are subangular-subrounded. These samples are dominated by quartz, with the value up to 47.8%. Monocrystalline quartz makes up the predominant quartz grains with the value up to 37.3%. The quartz grains with undulating extinction display the value up to 16.5%. Porosity occurs in both samples, with the value various between 5.0% and 25.8%. The coarser sandstone display quartz cementation (6.8%) and clay coating (11.0%) (Figure 3.15d). A less abundant kaolinite (0.3%-0/5%) presents in the subarkosic sandstones. The sandstone is moderate sorted with subrounded grains.
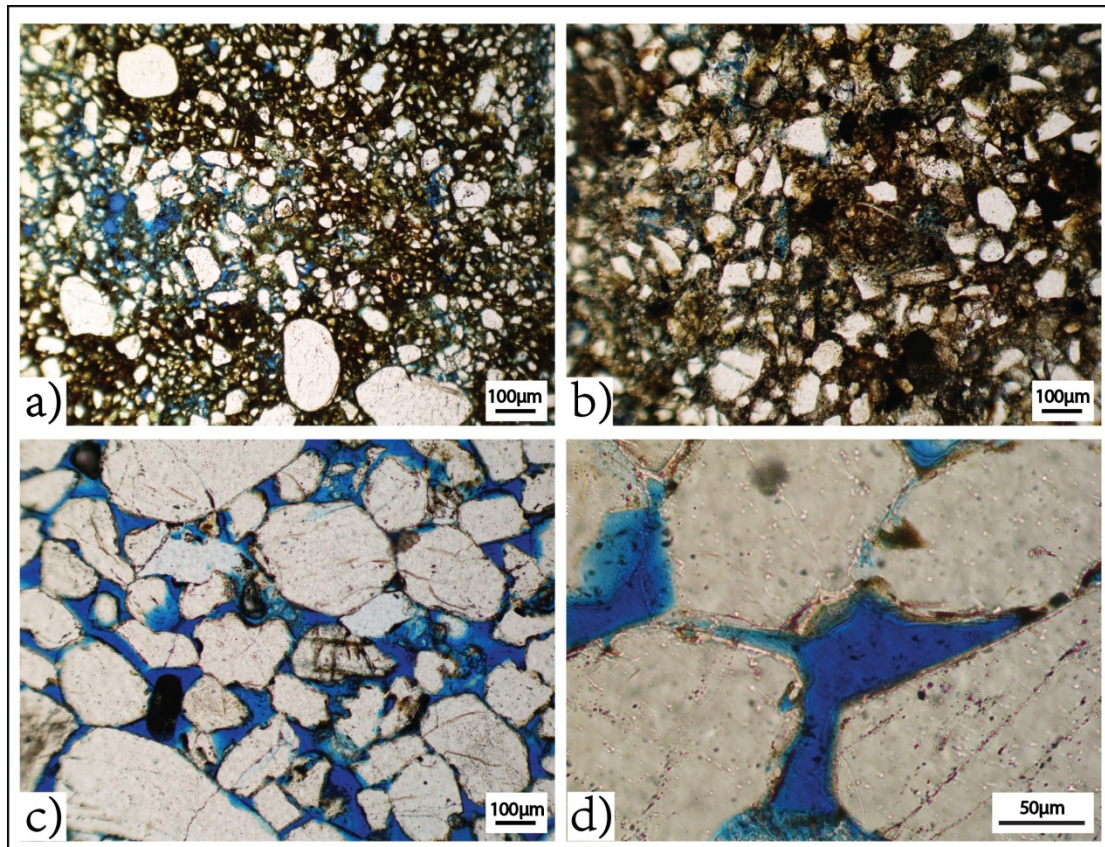
Figure 3.15 a)Plane polarized micrography of poorly sorted siltstone of sample WP223-8-14. The siltstone consists of coarser subrounded grains and finer subangular grains; b) Plane polarized micrography of subangular-subrounded, moderate sorted siltstone of sample WP223-3-14. The siltstone is cemented by carbonate; c) Plane polarized micrography of moderate sorted medium sandstone of sample WP223-5-14; d) The image display quartz cementation and clay coating around the grains of sample WP223-5-14.

3.4.1.3 WP-222

XRD results
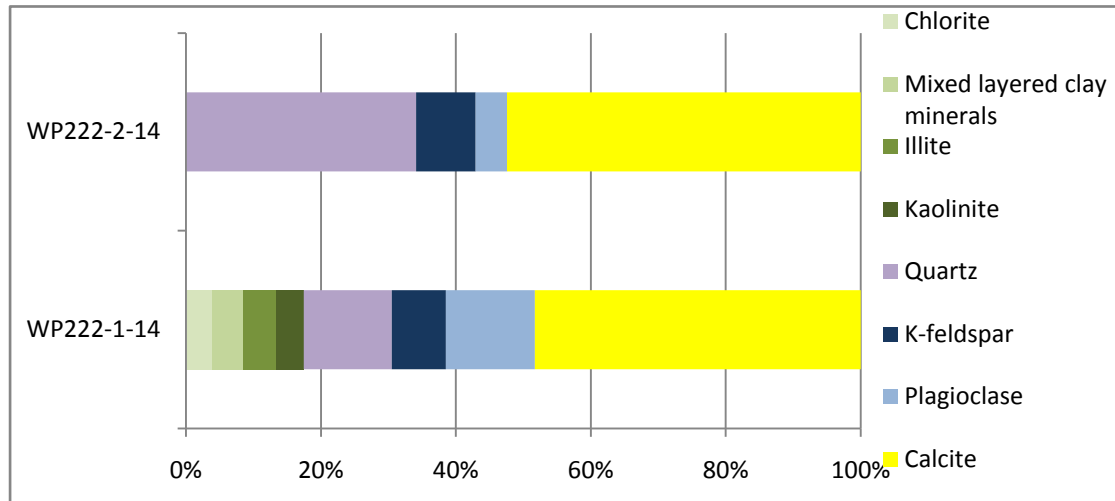
Figure 3.16 *Quantitative XRD results from the Kihuluhulu Fm. of WP-222 locality.*

The bulk mineral compositions of two samples (WP222-1-14 and WP222-2-14) from Kihuluhulu Fm. of the locality WP-222 were analyzed by XRD (Figure 3.16) (Appendix C). Both samples consist of high amount of calcite which makes up to 52.4% of the bulk composition. Sample WP222-1-14 was in addition to bulk also run for clay mineralogical analysis. Quartz comprises 13% of the total composition while feldspar comprises 21.2%, subdivided into K-feldspar (8%) and plagioclase (13.2%). In the clay fraction, the sandstone sample, WP222-2-14, is dominated by quartz which makes up to 34.1%. Feldspar comprises 13.4% with 8.8% K-feldspar and 4.6% plagioclase.

The clay minerals of sample WP222-1-14 (Appendix D) consist of illite, smectite, kaolinite and interlayered illite-smectite. The mixed illite-smectite layer is the predominant phase with value of 66.0%, while the illite and kaolinite make up the minor amount in the clay minerals, presenting the value between 4.0% and 5.0%. Smectite display the amount of 25% within the whole clay mineral.

Petrographic and mineralogical description

One samples from Kihuluhulu Fm. of WP-222 locality, WP222-2-14, was studied in

thin section under a petrographic microscope. The sandstone can be classified as arkosic sandstone (Appendix F). This sample consists of fine sand with carbonate cemented. The sorting is moderate to well, and the grain shapes vary from subangular to subrounded. Most of grains have long grain contacts, the others are more tangential. Monocrystalline quartz grains with straight extinction are the most abundant mineral with values up to 73.7%. Polycrystalline quartz grains makes up 8.4% of the quartz grains whilst the quartz grains with undulatory character are 21.6%. The preservation category of feldspar varies between 4 and 5. The plagioclase/K-feldspar ratio is 3, constituting the total feldspar with values up to 6%. The value of the calcite cementation makes up 50.3%. Biotite, chert and fossils were observed in the sandstone.
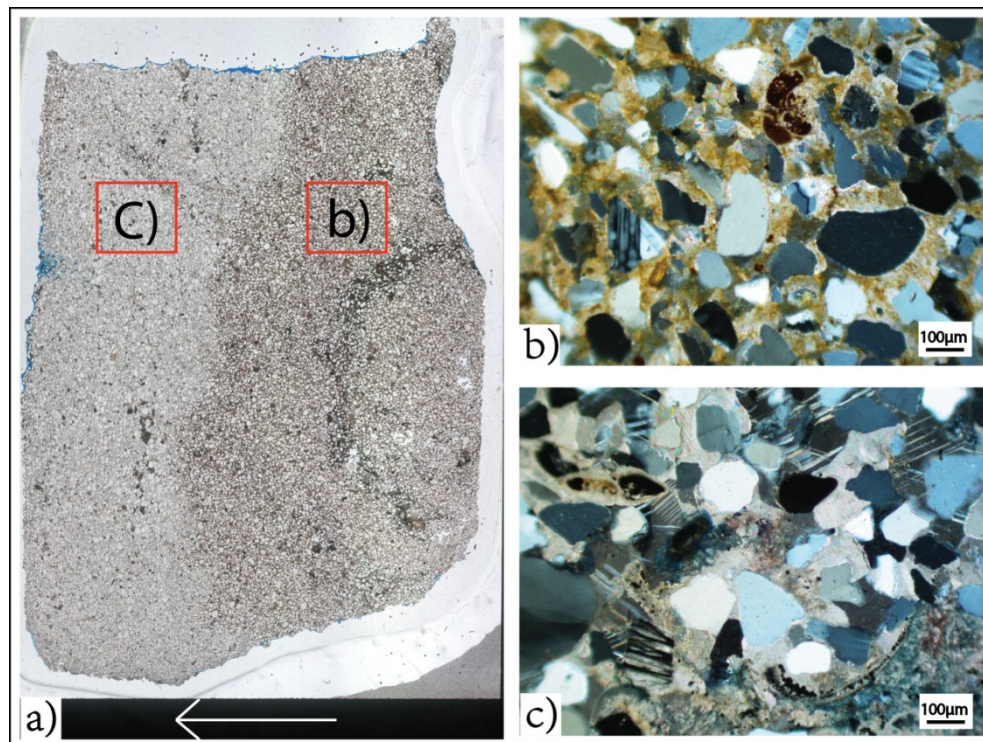
Figure 3.17 *a) Scanned thin section of WP222-2-14, displaying the clay matrix decreased up toward the stratigraphy. The arrow shows the direction of stratigraphy up; b) Cross polarized micrography of the lower stratigraphic part of this sample, displaying clay matrix covered on the calcite cement; c) Cross polarized micrography of the upper stratigraphy, showing the subangular-subrounded grains are surrounded by calcite cement, with less abundant clay matrix. The feldspar grains show relative poor preservation, with the category 3-4.*

3.4.1.4 N5 (N5-22, N5-26 & N5-27)

Six samples from Kihuluhulu Fm. location N5 (Figure 1.1) were analyzed by bulk XRD (Figure 3.18) (Appendix C) and the clay fraction of two clay samples were analyzed (Appendix D).

XRD results
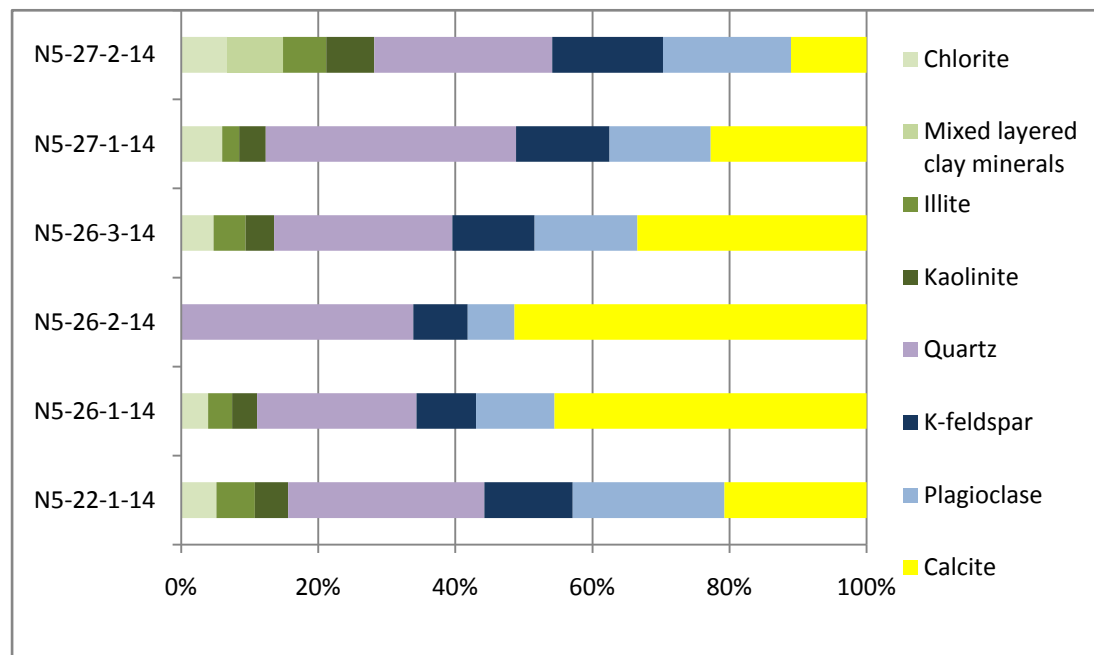
Figure 3.18 *Quantitative XRD results from the Kihuluhulu Fm. of N5-22, N5-26 and N5-27 localities.*

The samples comprise of up to 28.1% clay minerals, except for sample N5-26-2-14 which did not contain any according to the XRD analysis (Appendix C). All samples are cemented with calcite from 11% to 51.4%. Sample N5-26-2-14 excepted, all samples show nature similar mineral composition (Figure 3.18). They comprise of quartz (23.3%-36.5%), feldspar (14.7%-35.1%) subdivided into K-feldspar (7.9%-16.2%) and plagioclase (6.8%-22.2%).

The N5-26-3-14 and N5-27-2-14 samples were selected for the clay mineral analysis.

Four clay phases are observed in these two samples. The clay minerals are dominated by interstratified illite-smectite, making up maximum 57.9%. Smectite consists of the secondary highest percentage of the clay minerals, where the value is up to 34.8%. Illite (5.3%-21.2%) and kaolinite (7.6%-15.0%) are present in the samples as well.

Petrographic and mineralogical description

The petrography of two sandstone samples from Kihuluhulu Fm. (N5-26-2-14 and N5-27-1-14) was studied in thin section and optically point count. The two samples present similar mineral content and grain characteristics. The amount of monocrystalline quartz dominates the polycrystalline quartz, making up an average value of 85.5% (Figure 3.19b). Quartz with undulating extinction is less abundant than straight with an average value of 21.6%. The fine-grained sands are subangular and calcite cemented, displaying moderately to well sorting character. The contacts between grains are tangential characters (Figure 3.19). Feldspar grains are poorly preserved in these two samples with mostly category 5 preservation and seldom category 4 (Table 2.3). Pyrite and biotite were observed in both two samples. In addition, few fossils (0.25%) existed in the samples. These two samples are classified as arkoses based on results from point counting (Appendix F).
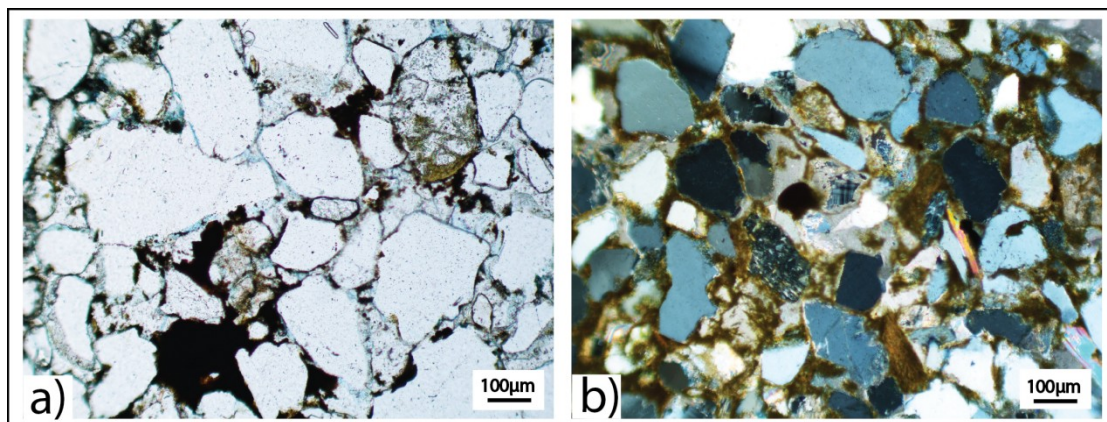
Figure 3.19 *a) Plane polarized micrography of subangular grains, displaying long and tangential contacts, from sample N5-26-2-14. Fe-oxide presents as pore fill; b) Cross polarized micrography of the moderate sorted sandstone, cemented with carbonate, from sample N5-27-1-14. Feldspar is dissolved and altered by clay.*

3.4.2 Kiturika Fm. (Aptian-Albian)

XRD result
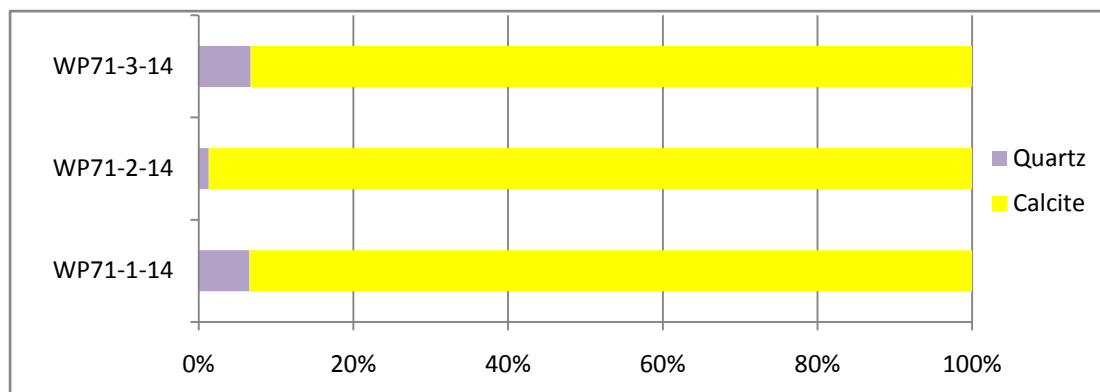
Figure 3.20 *Quantitative XRD results from the Kiturika Fm. of WP-71 locality.*

Three samples from Kiturika Fm. were analyzed by bulk XRD (Figure 3.20). Limestone samples are dominated by calcite with values up to 99.0%, quartz is only found in small accounts, from 1.0% to 7.0% (Appendix C).

Petrographic and mineralogical description

Three thin section samples of Kiturika Fm. were studied in the optical microscope and point counted. WP71-1-14 and WP71-3-14 can be classified as calcarenite and packstone, composed of majority calcite cementation and minor siliciclastic sediments. The calcite component makes up to 72.8%, dominated by sparite calcite. Quartz is the predominant mineral within the siliciclastic sediments, with value up to 12.8%. Further, monocrystalline quartz is the most abundant mineral, with values up to 10.3%.

Quartz with undulose extinction is fomed between 2.3% and 2.5% (Figure 3.21a). Feldspar appears occasionally in these two samples, makes up value range from 0.5% to 1.3%. The preservation of feldspar varies from category 3 to 5 (Table 2.3), for both K-feldspar (0.3%-1.0%) and plagioclase (0.3%). Fossils are observed in both two samples; vary values between 1.5% and 4%. Iron oxide pore fill (0.3%) and pyrite pore fill (1.3%-2.0%) present as well (Appendix C). WP71-2-14 can be classified as mudstone. This mudstone contains 94.5% carbonate, and 2.5% fossils (Appendix C). Most fossils are iron oxide (Figure 3.21b).
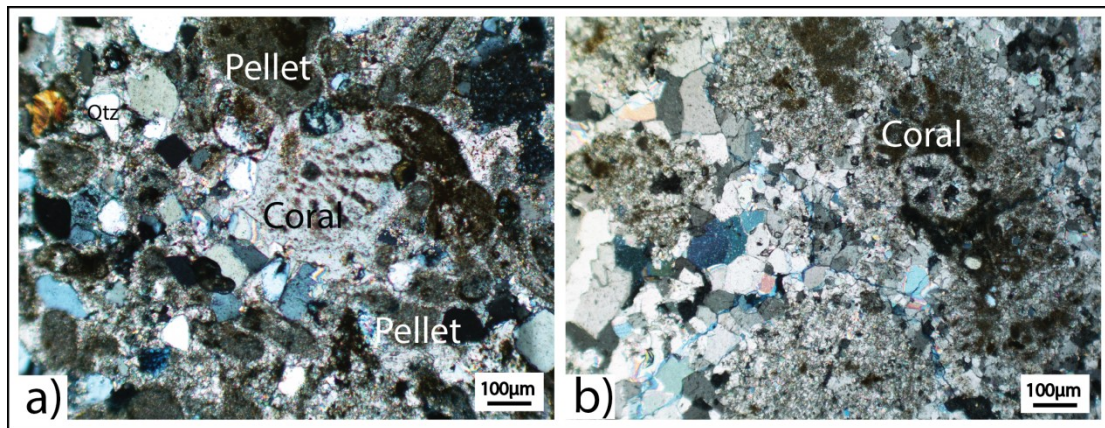
Figure 3.21 *a) Cross polarized micrography of calcarenite. The calcarenite consists of sparitic cement, pellets and corals, from sample WP71-1-14; b) Cross polarized micrography of reefal limestone of sample WP71-2-14. Foraminifera are iron oxide.*

3.4.3 Makonde Fm. (Aptian-Albian)

XRD results

Two samples (WP62-1-14 and WP62-2-14) (Figure 1.1) from Makonde Fm. were analyzed by bulk XRD (Figure 3.22) and the clay fraction of sample WP62-1-14 (Appendix D).
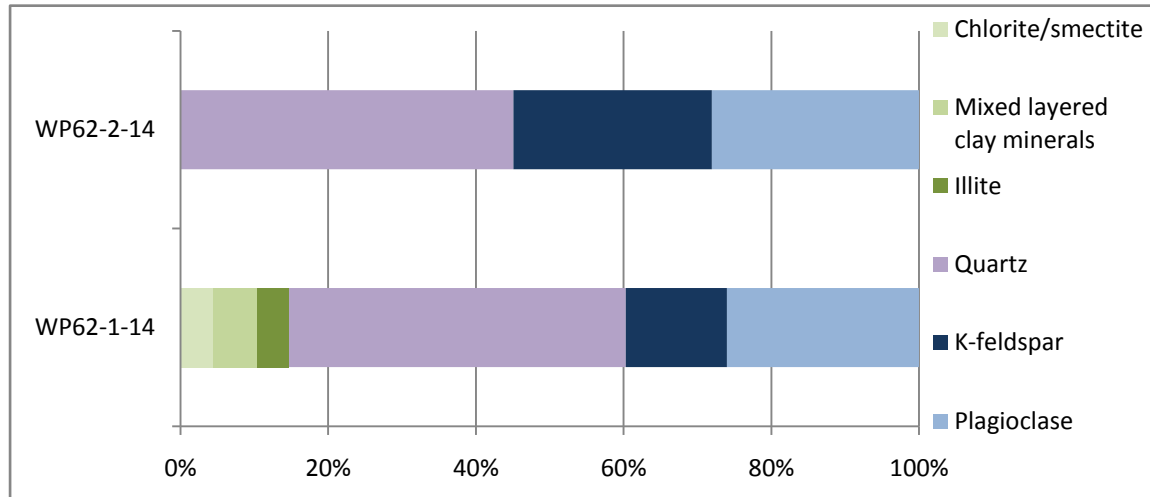
Figure 3.22 *Quantitative XRD results from the Makonde Fm. of WP-62 locality.*

These two samples show the comparable contents of quartz making up about 45.0%. Feldspar content varies value from 39.7% to 54.9%, with the plagioclase being the most abundant feldspar mineral with values up to 28.0%. K-feldspar is present with amounts between 13.7% and 26.9% (Appendix C). The quartz/feldspar ratios are 1.1 and 0.8 of WP62-1-14 and WP62-2-14 samples respectively. WP62-1-14 also consists of clay minerals, with chlorite/smectite (4.5%), mixed layered clay (6.0%) and illite (4.3%) (Appendix C).

WP62-1-14 sample was studied of the clay mineralogy (Appendix D). In the clay fraction, the mixed layered clay presents the most abundant minerals, which consists of illite-smectite interlayer (30.3%) and smectite-chlorite interlayer (32.7%). Smectite display a relative high value compares to the illite. The percentage of smectite is 29.1% while the percentages of illite is7.9%.

Petrographic and mineralogical description

The sandstone sample of Makonde Fm. was studied in the optical microscope (WP62-2-14). The sandstone sample is classified as arkosic sandstone (Appendix). Feldspar preservation ranges from category 3 to 5 for both K-feldspar and plagioclase

(Figure 3.23c). Monocrystalline quartz makes up the dominant mineral phase with values up to 47.5%, while quartz grains with undulatory character varies between 6.7% and 11.8% of the total samples. The quartz feldspar ratio varies between 3 and 5. In addition chert, biotite, pyrite and heavy minerals have been formed in the samples. Total porosity makes up values between 10.8% and 16.4%. In addition, primary porosity is the dominate porosity type in the samples, with values up to 13.4%. Secondary porosity is present as dissolved feldspar grains, microcracks, shrinkage voids, with values 2.5-3% of the total porosity. Kaolinite is present as pore fill with values of 7.3% (Figure 3.23a & b). 3.1% of the grains are clay coated. Clay matrix (4.4%) and pyrite (2.8%) appear in the sample (Figure 3.23d).
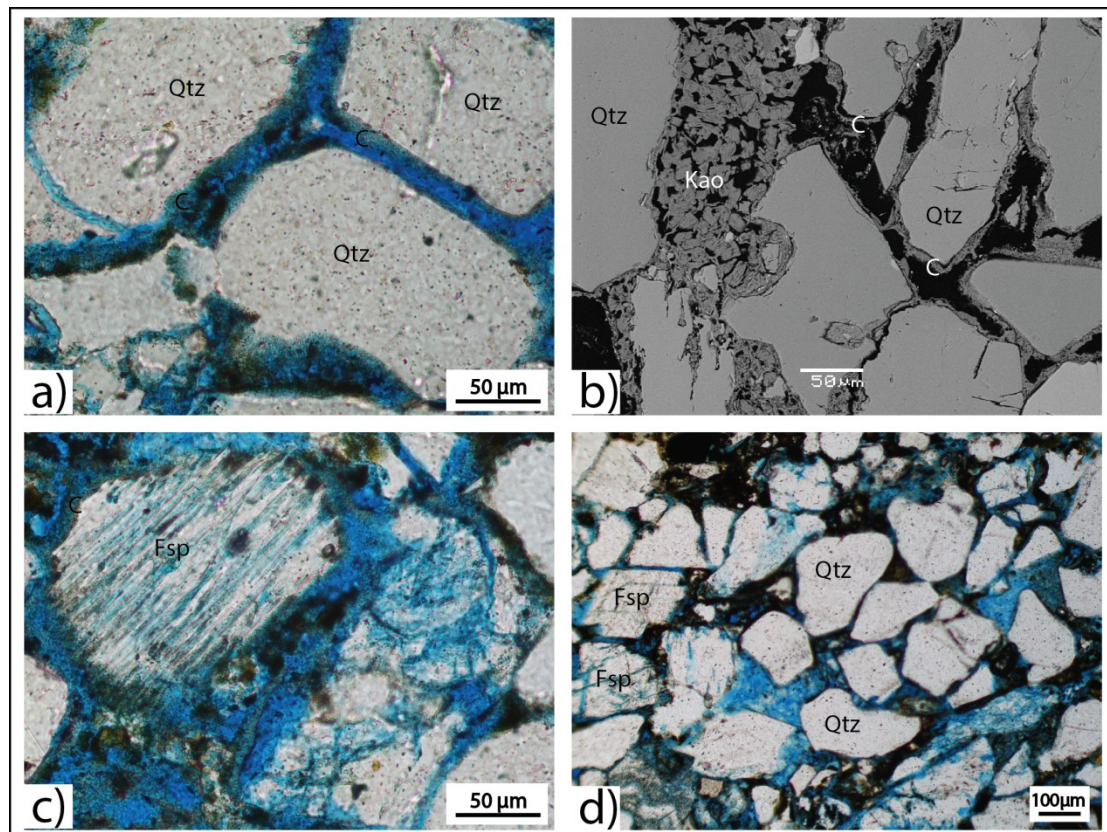
Figure 3.23 *Some photos of sample WP62-2-14. a) Plane polarized micrography of grains with clay coating of sample; b) The backscatter image was taken in SEM, display pore fill kaolinite and clay coating; c) The image shows the feldspar preservation of category 5 (Table 2.3); d) Plane polarized micrography with well sorted subangular grains, with long and tangential grain contacts.*

3.4.4 Samples from the Dublin collection of Hudson (2010)

Nine samples from the Dublin collection of Hudson (2010) were sampled by Hudson and Nicholas studied under optical microscope. Three of them were analyzed by point counting from Kihuluhulu Fm. and Makonde Fm.

Petrographic and mineralogical description

In thin section, two samples (MDW 10 and MDW 62) from Kihuluhulu Fm. can be classified as arkosic sandstone (Appendix F). Both samples are carbonate cemented, with the average calcite percentage of 42.5%. Quartz is the dominant mineral in the samples, makes up the value between 44.3% and 48.8%. In addition, monocrystalline quartz presents the highest proportion up to 41.8%. The quartz grains with undulating extinction make up to 9.5%. Feldspar grains can be subdivided into K-feldspar and Plagioclase, consisting of the total value between 7.0% and 7.8% (Appendix B). The preservation of feldspar varies from category 3 to 5 (Table 2.3). Fossils (4.8%) are observed obviously in MDW 62 (Figure 3.24a). Few biotite and secondary porosity appear in the samples as well.

Sample MDW 09-08 from Makonde Fm. can be classified as arkose (Appendix F). The sample is dominated by quartz grains, 54.4% of which 46.3% is monocrystalline. The grains with undulating extinction comprise of 7.4% percent of total quartz. Feldspar consists of K-feldspar and plagioclase, with the total value of 16.4% (Appendix B). The feldspar grains are preserved as category 3-5 (Table 2.3). Porosity types can be divided into primary and secondary porosity, and the primary porosity is the dominant type with the percentage of 13.4% while secondary porosity is 3.0%. Kaolinite appears as pore filling mineral with the value of 4.5%. Heavy minerals (1.5%) and clay coatings (6.7%) occurs in the sample (Appendix B).
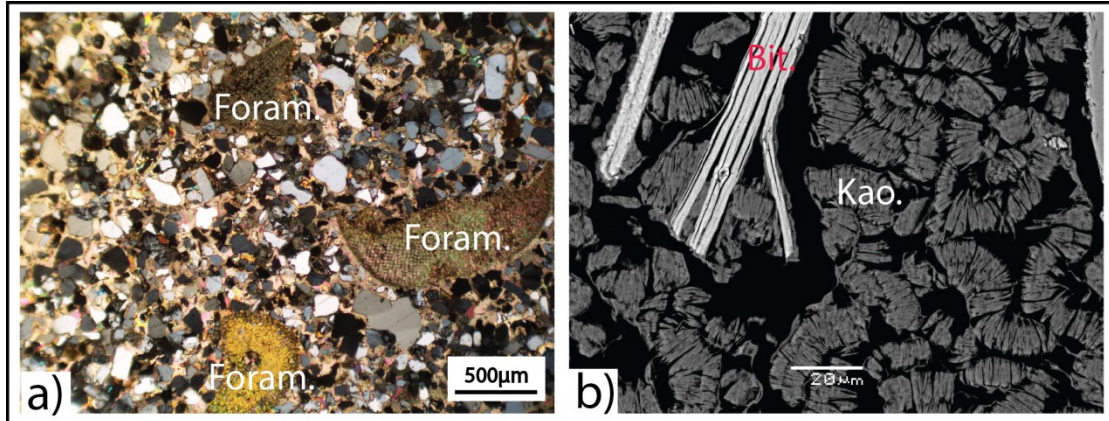
Figure 3.24 a) *Cross polarized micrography of Kihuluhulu Fm. from the Dublin collection of Hudson (2010) (Sample MDW 62). Foraminifera (Foram. in photo) are observed in this sample; b) A backscatter image taken by SEM of sample MDW 10. A booklet kaolinite (Kao. in photo) precipitated in the porous, and mechanical formed mica (Bit. in photo) is present in the sample. This sample represent Makonde Fm.*

4 Discussion

4.1 Facies associations and depositional environment

The facies associations described from logged field outcrops comprises Kihuluhulu Fm., Kiturika Fm. and Makonde Fm. of Early Cretaceous and Kipatimu Fm. of Upper Jurassic. In the following chapter, the author will focus on the facies associations from the formations of Early Cretaceous. The Kihuluhulu Fm. contains four facies associations, FA4, FA5, FA6 and FA7. The facies association FA8 is identified in the Kiturika Fm. and FA9 is identified in the Makonde Fm. In addition, the author will compare the outcrops characters to the core samples from well sites 24 and 21, which has discussed by Gundersveen (2014) of the Kihuluhulu Fm.

4.1.1 Kihuluhulu Fm.

Four facies associations can be recognized in the Kihuluhulu Fm.

FA4

A part of the facies association FA4 is present in the Kihuluhulu Fm. A conglomerate unit (Facies 8b) is located on the top of the FA2 facies association. Facies 8b composes of grain-supported well rounded pebbles in a medium sand matrix. Large gastropods, reefs and moderate bioturbation are characteristic in this conglomerate. The association of clay-conglomerate could indicate more shallower and/or continental inputs are carried into the marine setting, during a significant regressive process (Berrocoso et al., 2015, Hudson, 2011). This facies association might interpret to be a shallow beach depositional environment, where Stearns (1945) described a similar beach conglomerate characteristic.

4. Discussion

FA5

The FA5 facies association is dominated by facies 7 (Figure 3.2), and studied at Namayuni (WP-92) locality (Figure 1.1). This facies association can be interpreted as an outer shelf depositional environment (Hudson, 2011). Facies 7 is characterized by claystone interbedded with very fine sandstone lenses/stringers. The claystones display color characters vary from greenish-gray to brown. The facies are formed in quite leads up to 10m thickness. The claystones show weak lamination and alternation with thin sandstone stringers and could be interpreted to be the product of hemipelagic deposition with minor intermittent low density turbidity flows. The rhythmic character of facies 7 indicates the action of recurrent flow with comparable hydrodynamic characteristics (Dixon et al., 2012). The overall characterization of facies 7 gives an interpretation of low energy calm environment and high energy turbidites appear alternately. This facies association also contains a pure clay facies (Facies 1a) indicating a quiet depositional environment as well.

The sandstone facies present in the FA5 facies association is identified as facies 2b, totally three sandstone leads of facies 2b are formed. Facies 2b is characterized by the very fine- to medium-grained sand displaying apparent bedding structures. The bedding structures comprise of both parallel lamination and climbing ripple bedded layers. The normal, inverse and absent grading are representing the individual sandstone beds within the facies 2b. The parallel bedding might be interpreted as representing the T_b or T_d divisions of the Bouma sequence. Further, if the parallel laminated bed passes up into a rippled interval, the parallel laminae could be divided into T_b division. The occurrence of ripple bedding is usually interpreted as T_c unit within the Bouma Sequence (Shanmugam, 1997). In some cases, it is hard to recognize the original transport mechanism where the sands in a parallel or rippled laminae. The original transport mechanism might be either suspended load turbidity current or bedload bottom current. However, climbing ripples are formed, as a result,

when suspended sands fall rapidly onto a bed with the turbidity current moving within the ripple bedform field, the climbing ripples might be taken for the evidence for turbidity-current deposition (Jobe et al., 2012, Shanmugam, 1997, Sanders, 1960). The inverse graded bed passed up to the fining upward sequence might indicate a combination of T_a and T_c units. The upward coarsening might be interpreted to be the lowest part of Bouma Sequence, which is described as debris flow deposits within the turbidity current (Shanmugam, 1997).

FA6

The FA6 facies association is dominated by silt and sand and is weakly bioturbated (Table 3.2) (Figure 3.4), and studied at the central/ south part of Mandawa basin, WP-223 locality (Figure 1.1). An outer shelf environment is suggested for the sediments in FA6 (Hudson, 2011). The clayey siltstone facies 1a and 1b are the predominant silt facies, while facies 2a is made up of sand facies. Facies 1b consists of parallel laminated claystone, which grades into homogeneous clay and siltstone (Facies 1a). The siltstones contain amount of fossils, such as belemnites and different types of ammonites, which could indicate the depositional period of Kihuluhulu Fm. Two different morphological ammonites are found together, straight and curled. Referred to Walaszczyk, et al. (2014), the straight ammonites display the similar characteristics with *Parasolenoceras Splendens Collignon*, and the curled ones perform the similarity of macroconch. Powell (1963) also described the similar ammonite occurred in lower and middle latitudes of the early Turonian, which was named *Pseudaspidoceras flexuosum*. Because the shells of ammonite sank quickly to the sea floor with short transport distance (Ifrim, 2013), a great many well preserved cephalopod fossils (ammonites and belemnites) can be formed in the siltstones indicating a relatively quiet environment. Moreover, as the chemocline determines the maximum dwelling depth of ammonite, the ammonite might only have existed in the upper water layers (Ifrim et al., 2011a, 2011b).

Facies 2a is characterized by sparsely bioturbated sandstones, with a variation between sharp and erosional bases towards to the underlying clay- and siltstones. The thickness of the different sandstone units display upward decreasing trend, vary from dm- to cm- scale. The sandstone beds of facies 2a are interpreted as high energy deposits which might be turbidity flow, since the facies 2a display the similar characteristics as facies 2b. The turbiditic currents might be generated from suspension flow, which formed by storm activity on a shelf, for example Mulder & Alexander (2011).

FA7

The section of WP-223 locality terminates with the FA7 facies association. The facies is coarse sand compared to the facies 2a sands containing coal fragments. Iron nodules and clay rip-up clasts are observed in some units within this facies. The terrestrial material occurred in a marine setting could be interpreted as higher energy depositional environment in comparison with the clay and siltstones (Facies 1a and 1b) with FA6. The occurrence of terrestrial material (e.g. coal fragment) might indicate the depositional environment moves proximity to the land. This is because the increasing energy of water flux has ability to transport the terrestrial material into the marine setting. The depositional environment of FA7 might be terminal distributary channel of the river-dominated delta (Olariu & Bhattacharya, 2006).

4.1.2 FA8– Kiturika Fm.

The FA8 facies association is found within the sketch logged section of Kiturika Fm., was studied at WP-71 locality (Figure 1.1). The FA8 facies association consists of calcarenite and reef limestone facies, identified as facies 9 and facies 10 respectively. FA8 indicates a shallow water marine depositional environment based on the combination of coral-bearing limestones and calcarenites. These calcareous

limestones comprise of calcareous metazoans (e.g., corals and bivalves) which survived in the shallow water (James & Wood, 2010).

Facies 9 is described as calcarenite, which is dominated by sparitic calcite cement with minor silisiclastic grains. The calcarenite consists of well sorted, subrounded grains within the biosparitic calcite cement. Shell fragments of bivalves and clay rip-up clasts are observed as well. In some units of facies 9, weakly laminated units are present in the calcarenite, with grain sizes alternating between finer and coarser grains (Figures 3.7c and 3.8). These sedimentary features might indicate the siliclastic-carbonate depositional systems, where sedimentation is characteristically reciprocal. The siliciclastic sediments input is increasing during sea-level falls (Tropeano & Sabato, 2000).

Facies 10 is characterized as highly recrystallized reef limestone and the dominant facies of the FA4 facies association. Corals are exposed well within the limestone. Corals are most commonly presented in shallow, well-oxygenated, tropical to subtropical waters of normal marine salinity (Hanken et al., 2010). This limestone bed is dipping 22º, deposited over the facies 9 with dip 45º, indicating an angular unconformity between the two beds. The Kiturika Fm. extends for approximately 20km from the east to the west of the Mandawa Basin (Figure 1.1). This could indicate that reefs have developed as an extensive carbonate platform on a gentle slope (Hudson, 2011). According to the Wilson (1975) comprehensive model of the carbonated facies belts (Figure 4.1), the reef limestone from Kiturika Fm. matches with platform foreslope carbonate facies (zone 4) and platform margin carbonate facies (zone 5).
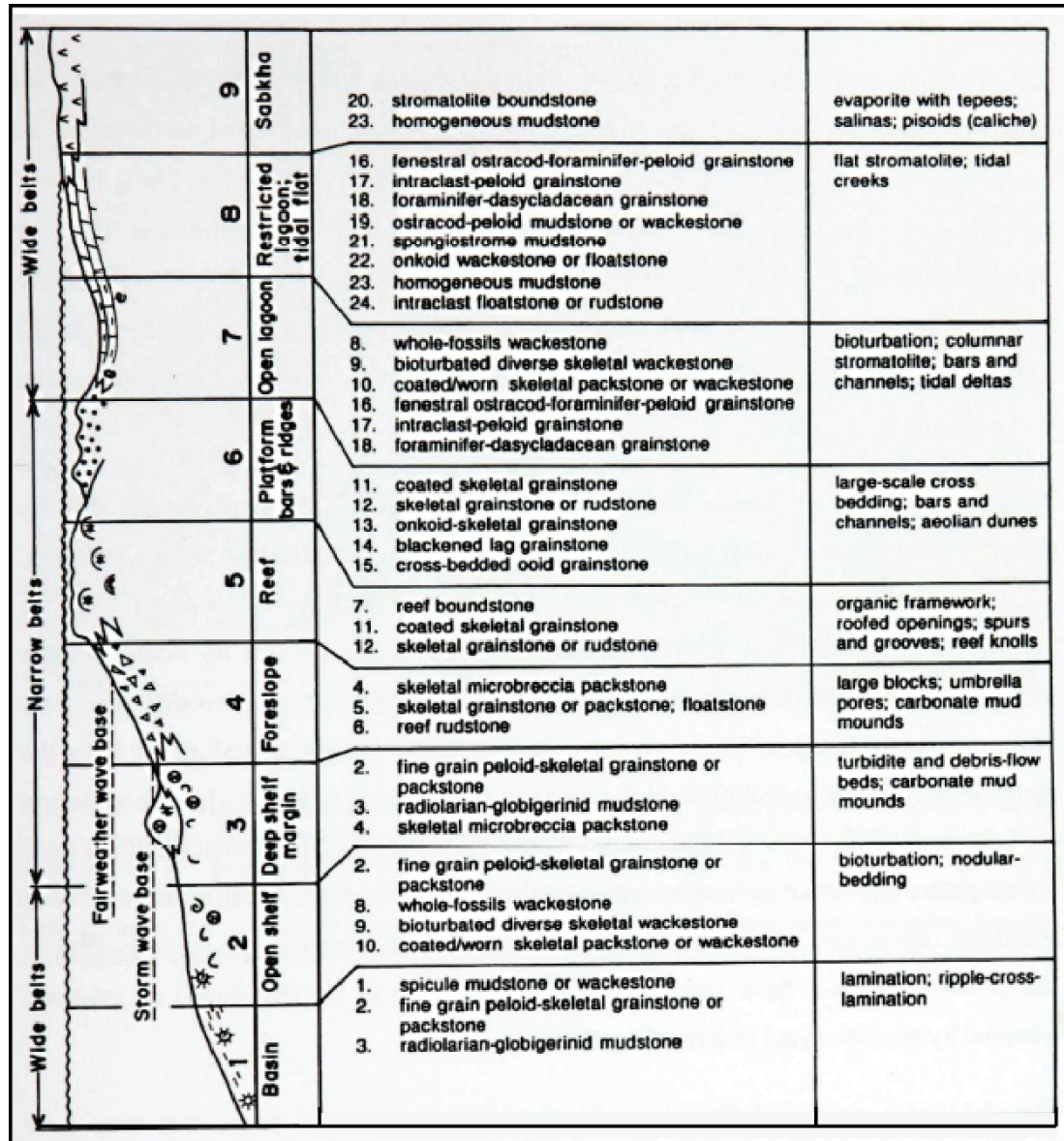
Figure 4.1 Wilson's comprehensive model of the carbonated facies belts (Modified from Wilson, 1975).

4.1.3 FA9 – Makonde Fm.

The FA9 facies association is found within the sketch logged section of Makonde Fm., was studied at Mbate (WP-62) locality (Figure 1.1). This facies association consists of sandy siltstone and sandstone facies, identified as facies 1c and facies 4 respectively (Figure 3.9). FA9 facies association shows coarsening upward sequence, grading from siltstone at the base to cross-bedded sandstone at the top. This character could reflect mouth bar depositional environment, during a regressive (forced regression) period

70

(Reading & Collinson, 1996, Bhattacharya, 2006, Overeem et al., 2003).

Facies 1c comprises of sandy siltstone with silt content up to 60%. Small clay rip-up clasts are the predominant structures of this facies. The rip-up clasts are the product of fragments eroded from decelerated current activity and redeposited in succedent high energy environments (Garzanti, 1991, Morad et al., 2010). The upper part of the FA9 facies association is dominated by graded sandstones (Facies 4). The distinctive structures of the very fine to medium sandstones are cross stratification and some units display trough cross-beds. Mud rip-up clasts are present in the lower part of facies 4. These cross-layers and clay rip-up clasts could represent terminal distributary channel deposits of the river-dominated delta (Olariu & Bhattacharya, 2006).

In general, the depositional environment of FA9 is proposed to be terminal distributary channel facies overlap the mouth bar deposits (Schomacker et al., 2010, Olariu & Bhattacharya, 2006). Due to the progradation of the delta, mouth bars are incised by terminal distributary channels (Schomacker et al., 2010).

4.2 Petrography and diagenetic process

The following chapters will discuss the petrography and diagenetic history of the studied sandstones from field outcrops.

4.2.1 Kihuluhulu Fm.

Kihuluhulu Fm. is interpreted to represent outer shelf depositional environment. Studied sandstone samples from Kihuluhulu Fm. display very fine to medium grain sizes, and are only weakly to moderately compacted. Most of the sandstones show moderately-well sorted, while minor samples are poorly sorted. The grain shapes are mainly subrounded with a minority of subangular grains. Except for two poorly cemented samples are classified as subarkose, the calcite cemented sandstones are classified as arkosic sandstone. The samples cemented with carbonate display the

quartz/feldspar ratios vary from 3 to 7, with an average value of 5, samples consisting of terrestrial materials (e.g. coal fragment) show a higher quartz/feldspar ratio up to 11. This means the sandstones without cementation are more mature than that carbonate cemented samples. Moreover, the plagioclase/K-feldspar ratios with variation values between 0.5 and 1.7 for all studied samples, representing the variant weathering degree of different localities. The preservation category of feldspar is dominated by category 5, while some feldspar shows preservation categories of 3 and 4 (Table 2.3). This degree of preservation might indicate that weathering is at a maximum, as a consequence of strongly weathering under a tropical climate (Carroll, 1970). Generally, the monocrystalline quartz is dominating the quartz fraction of the samples. In addition, the strain-free grains display three times in quantity as strained (undulatory) ones on an average. The high percentages of non-undulatory quartz most widely reflect that the grain assemblages experienced several sedimentary episodes rather than derive from igneous or metamorphic source rocks (Conolly, 1965).

Gundersveen (2014) has described the petrographic characters of core samples from well sites 24 and 21. The core samples are time equivalent as Kihuluhulu Fm. Compare the surface samples (taken from field outcrops) with the core samples (well sites 24 and 21), the quartz/feldspar ratio display somewhat lower values in the surface samples. This could indicate that the core samples are more mature than the surface samples (Gundersveen, 2014). However, the surface samples may have undergone more recent weathering than the core samples, based on the feldspar preservation degrees. According to Gundersveen (2014), feldspars in the core samples are mostly showed category 3 while the surface samples are mostly classified as category 5 (Table 2.3).

The analyzed Kihuluhulu Fm. samples show either none or only small amounts of kaolinite. This might be a result of lack of meteoric flushing in a distal depositional environment. The sandstone beds are commonly overlain by clay units. Consequently

the meteoric water may have been reduced into these sandstones. The core samples (Gundersveen, 2014) also carry just minor amounts of kaolinite. Consequently weathering might plays hardly any role in the precipitation of kaolinite.

Carbonate Cementation is the most abundant cement in most samples from the Kihuluhulu Fm. outcrops (except WP223-5-14 & WP223-8-14). Calcite is the dominant mineral determined by XRD results. The clastic grains display elongate to tangential contact in the carbonate cements, where the loosely packed framework indicates the calcite cementation is interpreted to be the earliest diagenetic process. According to Pettijohn et al. (1972), the sandstones within marine depositional environment may very well carry carbonate cement as an early diagenetic phase. Calcite cementation occurred in the loose sediments where the pore fluid saturated with respect to calcite precipitated in primary or secondary pores (Flügel, 2010).

In the SEM studies, the calcite cement displays to be comprised of low-Mg calcite, which is the most stable form. Nevertheless, this might not be used as evidence that no high-Mg calcite or aragonite precipitated, since the both may recrystallize to the more stable low-Mg cement through time (Flügel, 2010; Bjørlykke et al., 1989).The sparry calcite is dominating the cement, which may reflect the recrystallized products of earlier deposited and dissolved skeletal fragments in shelf sediments (Dypvik & Vollset, 1979). The calcite cementation within the sandstones displays continuously cemented layers, but in the clay/siltstones, calcite cements occurs as concretions

The carbonate cements of the outcrop samples show the similar features as the core samples from well sites 24 and 21 (Gundersveen, 2014). The outcrop samples consist of more calcite cements and no samples carry dolomite or ankerite. In Gundersveen's results, some samples are dominated by dolomite or ankerite, while the calcite is present in minor amounts. This might indicate that the formation of the core samples experience dolomitiation during late burial deposits. Mg^{2+} is more easily hydrated

than Ca^{2+} in sea water, and the magnesium hydrate ($Mg(H_2O)_6^{2+}$) is hard to enter a crystal position at relative low temperature. Further, with increasing water temperature, the hydration decreases and dolomitisation might happen (Bjørlykke, 2010).

Authigenic clay mineral could have been formed through reactions between the precursor minerals on framework grains and contained waters during regeneration, and precipitated during burial diagenesis (Aagaard et al., 2000, Wilson & Pittman, 1977). Authigenic clay minerals in the outcrop samples consist of kaolinite, chlorite, smectite, and interstratified illite/smectite by the clay fraction of XRD analysis.

The chlorite was observed as the grain coatings under the optical microscope and in SEM studies. The chlorite coatings were formed during the hydrothermal runs. In the SEM analysis, the extensive chloritic grain coatings seem to be neoformed or recrystallized, and are similar in appearance to naturally-occurring chlorite coatings (Aagaard et al., 2000). In order to produce chlorite coatings, a suitable Fe-rich precursor and appropriate temperature are the necessary factors. The simplified equation could follow by Eq (1) of Bjørlykke et al., (1989):

Smectite + Fe^{3+} + Kaolinite = Illite + Chlorite (1)

In addition, some of the calcite cement is present within the chlorite in the SEM, and pores display around the grains with chlorite coating. This might indicate that the chlorite coating occurred prior to the calcite cement.

Smectite forms only when the porewater is oversaturated by silica, where the concentration of silica is significantly higher than the quartz saturation. Consequently the smectite is most common in sandstones which derived from volcanic sources, however, rare in arkosic and feldspathic sandstones (Aagaard & Helgeson, 1982;

Bjørlykke et al., 1989). Sponge spicules and chert could support the necessary silica for smectite precipitation (Stonecipher et al., 1984). In the clay fraction of XRD analysis, the smectite constitutes an average value of 15% within the whole clay mineral.

The interstratified illite/smectite is the predominant clay minerals phase, making out to 45% of the clay fraction. The conversion of smectite layers to illite layers is likely a dissolution and reprecipitation process. This transformation might comprise the addition of Al and K and the release of Si and H_2O (Boles and Franks, 1979; Lynch et al., 1997; Peltonen et al., 2009). The S-I reaction is simplified in Eq (2)

$$Smectite + K^+ \rightarrow Illite + SiO_2 + H_2O \qquad (2)$$

In this reaction, the type of smectite present (trioctahedral or dioctahedral) and the source of K^+ will control on the amount of SiO_2 released (Peltonen et al., 2009). During burial diagenesis, the random-ordered mixed-layer I/S (R0) with more than 50% smectite transforms into the ordered mixed-layer I/S (R1) with illite dominated at the temperature approximately between 60 and 90 ℃ (Peltonen et al., 2009). In the clay fraction analysis of the studied samples, most of the mixed-layer I/S comprises high amount of iron, and the Fe^{2+} may gain from the chemical changes during the transition (Lynch et al, 1997).

Authigenic kaolinite appears as pore filling cement in the optical microscope studies. From clay fraction analyses, kaolinite makes up an average value of 8% of the total clay minerals. The authigenic kaolinite observed in the SEM analysis commonly shows the characteristic booklet stacks (Lanson et al., 2002). The authigenic kaolinite might precipitate at the expense of feldspar and micas in pore waters and commonly formed in meteoric pore waters, which requires porosity and permeability (Bjørlykke et al., 1989). The formation of the authigenic kaolinite follows the fellow reactions

(Eqs 3 and 4) (Bjørlykke & Jahren, 2010).

$$2K(Na)AlSi_3O_8 + 2H^+ + 9H_2O = Al_2Si_2O_8(OH)_4 + 4H_4SiO_4 + 2K^+(2Na^+) \qquad (3)$$

Feldspar   Kaolinite

$$2KAl_3Si_3O_{10}(OH)_2 + 2H^+ + 3H_2O = 3Al_2Si_2O_5(OH)_4 + 2K^+ \qquad (4)$$
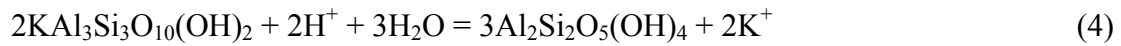
  Muscovite   Kaolinite

Siltstones and sandstones experiencing early carbonate cementation will have reduced porosity and permeability. Therefore, the authigenic kaolinite only comprises small amounts of the clay minerals in these beds. Further, in the tight framework of the siltstones and sandstones, kaolinite forms in the secondary pores caused by feldspar dissolution. In conclusion, the formation of authigenic kaolinite in the studied samples most widely was formed after the feldspar dissolution.

The pyrite cement is considered to be of the early diagenetic minerals, forming before the calcite cement. The pyrite is presumed to have formed in reducing conduction. The Fe-oxide cement is considered to be of the latest diagenetic minerals, which is presumed to form in the oxidation environment.

The sequence of diagenetic events is summarized in Figure 4.2. Early diagenesis includes (1) Initial mechanical compaction; (2) smectite; (3) calcite cement; (4)mixed layer – I/S; (5)chlorite coating; (6)feldspar dissolution; (7) kaolinite pore fill; (8) pyrite;(9) Fe-oxide.

Diagenetic Sequence	Time: Start —————————————→ Today
Mechanical compaction	——————————————
Smectite	————
Chlorite coating	—————————
Calcite cement	—————————
Mixed layer-I/S	————————
Feldspar dissolution	———————— ————————
Kaolinite pore fill	————————
Pyrite	————
Fe-oxide	————————
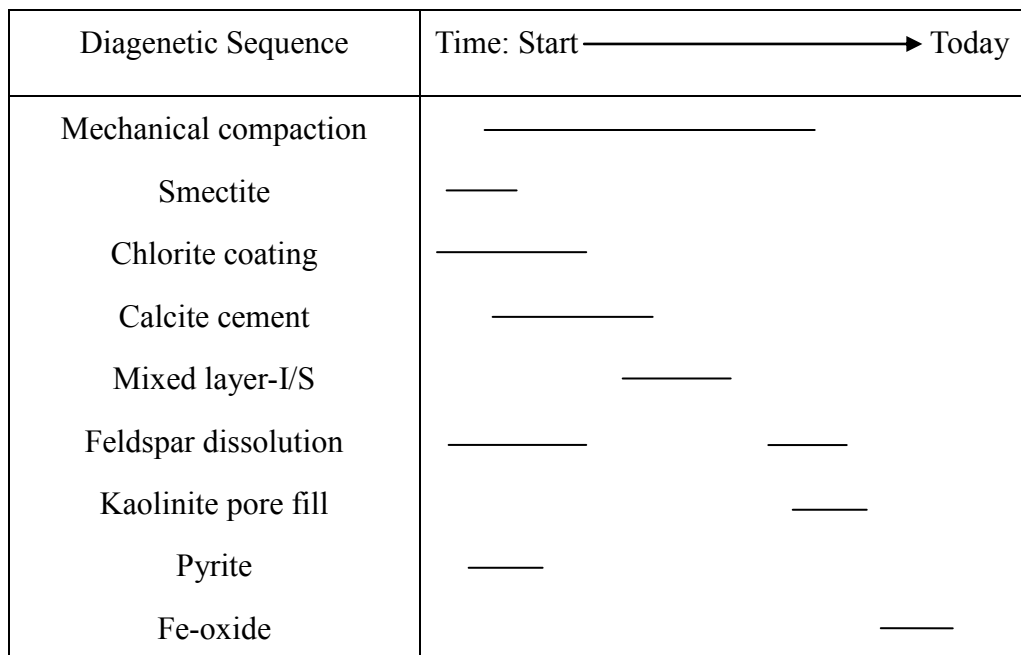
Figure 4.2 Generalized diagenetic sequence of Kihuluhulu Fm.

4.2.2 Kiturika Fm.

Kiturika Fm. is interpreted to represent shallow marine depositional environments. The studied samples from the Kiturika Fm. consist of two major rock types; calcarenite and reefal limestone. The calcarenite (WP71-1-14 & WP71-3-14) displays very fine siliceous sediments with calcite cement. The sparitic calcite cement makes up of the dominant cement (43.2-51.7%) according to the results of point counting under the microscope. Faecal pellets are present in the calcarenite. The reefal limestone is dominated by micrite (48.5%) without any siliceous sediment. According to the Dunham (1962) classification, the reefal limestone sample can be classified as mudstone (Figure 2.3). The carbonate cement is dominated by calcite, with value up to 89.8%.

Reefs are building up along the shelf margins, after affected by high waves and tidal activity, making sure that the constant movement of vast quantities of supersaturated

marine waters through the stable, porous reef framework. Several authors have described a process of the carbonate cementation within the reef frame (e.g. Land & Moore, 1980, Ginsburg & Schroeder, 1973). Marine water loses CO_2 rapidly by agitation, warming, and organic activity, which give rise to the water saturation with respect to $CaCO_3$. The early calcite cements, and most widely, abiotic cements precipitated directly from marine waters (Schroeder, 1986). Reef cementation normally takes place just centimeters beneath the sea floor, before the burial diagenesis takes place. The shallow burial near-surface diagenesis is affected by changing pore water chemistry, temperature and pressure processes (Flügel, 2010). In the sample WP71-2-14, micrite is the dominate cement, making up the relative ratio of 54% with respect to sparite. This might indicate that the micrite was formed as early cementation. In the samples WP71-1-14 and WP71-3-14, the sparry calcite cement displays much higher amounts compare to sample WP71-2-14. The grains (e.g. minor siliciclastic grains, pellets) display point to short line grain contact, which could indicate the mechanical compaction process occurred before the formation of calcite cement. During the burial process, part of the micrite was recrystallized by sparry calcite cement, due to the increased temperature. In addition, the sparitic cement could precipitate since micritic calcite experienced pressure solution. Carbonate reactions are, unlike silicate reactions, relatively fast even at low temperatures and chemical compaction (Hanken et al., 2010). Aragonite and high Mg calcite are metastable minerals in the marine environment. Aragonite fossils (e.g. corals) that consist of acicular aragonite might be recrystallized by the coarse sparry calcite (Flügel, 2010, Bathurst, 1982). In general, the diagenetic history of the Kiturika Fm. might be suggested by mechanical compaction, near-surface and marine diagenesis, and burial diagenesis (coarse sparry calcite cements). The similar diagenesis process is illustrated by Flügel (2010).

4.2.3 Makonde Fm.

The Makonde Fm. is interpreted to be mouth bar deposits. The Makonde Fm. displays

fine- to medium-grain sizes with moderately to well sorting, and subangular to subrounded grain shapes. Feldspar grains show a preservation grade of category 3-5 (Table 2.3). The feldspars are presented the similar preservation degree compare to the Kihuluhulu Fm., which is thought to be both these two formations underwent the similar exposure time in the weathering system. An average quartz/feldspar ratio of 4 indicates that these sandstones display the comparable maturities.

According to the results of clay mineral analysis, three different clay minerals are comprised in the Makonde Fm., which are smectite, illite, smectite-chlorite and kaolinite.

The mixed-layered smectite-chlorite clay minerals are formed as grain coating in the Makonde Fm. Under the SEM analysis, the coatings display a similar SEM energy dispersive spectrum as Ku and Walter (2003) described, which could thought to be smectite-chlorite coating. The observation of SEM tallies with the XRD result with respect to the coatings. The crystal morphology and the radial orientation could indicate the clay coating is suggested to be authigenic. According to Wilson and Pittman (1977), the crystalline habits characteristic of the authigenic clays is the most useful criterion to distinguish the authigenic clays from the allogenic ones.

The smectite clay minerals can be formed in distal, fluviolacustrine and interdune facies under warm, arid to semiarid conditions, where the meteoric water flow is limited (Morad et al., 2000). In the Makonde Fm., the smectite might be considered as the precursor mineral that was introduced by mechanical infiltration. The smectite precursor might regenerate and transform into a mixed smectite-chlorite. Further, the smectite-chlorite transition is as fundamental an aspect of the low-grade metamorphism of the clastic rocks (Salemn et al., 2000, Pettjohn et al., 1972, Schiffman & Fridleifsson, 1991). The percentage of chlorite in the mixed smectite-chlorite increases continuously with increasing temperature, which means

along with the burial depth increased, more smectite transfers into chlorite (Schiffman & Fridleifsson, 1991). In other word, chlorite displays more stable than the smectite. Smectite precipitation requires a sufficient silica concentration (Figure 4.3). Since quartz shows very low precipitation rates at low temperatures, the silica concentration may have been higher than the quartz saturation. It allows formation of silica-rich phases, such as smectite (Bjørlykke et al., 1989, Bjørlykke, 2010). As the previous discussion in the Kihuluhulu Fm, the high silica content are often found in sediments derived from volcanic rock. The Makonde Fm. displays a relative high amount smectite, which might indicate that the sediments could derive gneiss with the Mozambique belt east of the Tanzania craton, which contain soluble silicates (Nerbråten, 2014).

Illite is a product by mica (muscovite and biotite) with potassium where replaced by water (H_2O, H_3O^+) (Bjørlykke, 2010). Kaolinite might be the source of illite, which could be replaced by illite. The similar process has discussed in Kihuluhulu Fm.

The authigenic kaolinite displays the least abundant of the clay minerals in Makonde Fm., contain about 4%. Studies in SEM and the optical microscope show pore fiiling authigenic kaolinite in the sandstone samples. Kaolinite is most widely the result of early diagenetic process by meteoric water flow. The pore flow could dissolve the feldspar and mica. Kaolinite precipitation is usually effected by the weathering reaction (Eq (3)).According to the equation, kaolinite precipitation requires silica and potassium must be removed from the system. A low K^+/H^+ ratio in the pore water will drive this reaction to the right if the K^+ (Na^+) concentrations are low (Bjørlykke & Jahren, 2012, Bjørlykke, 2014) (Figure 4.3).
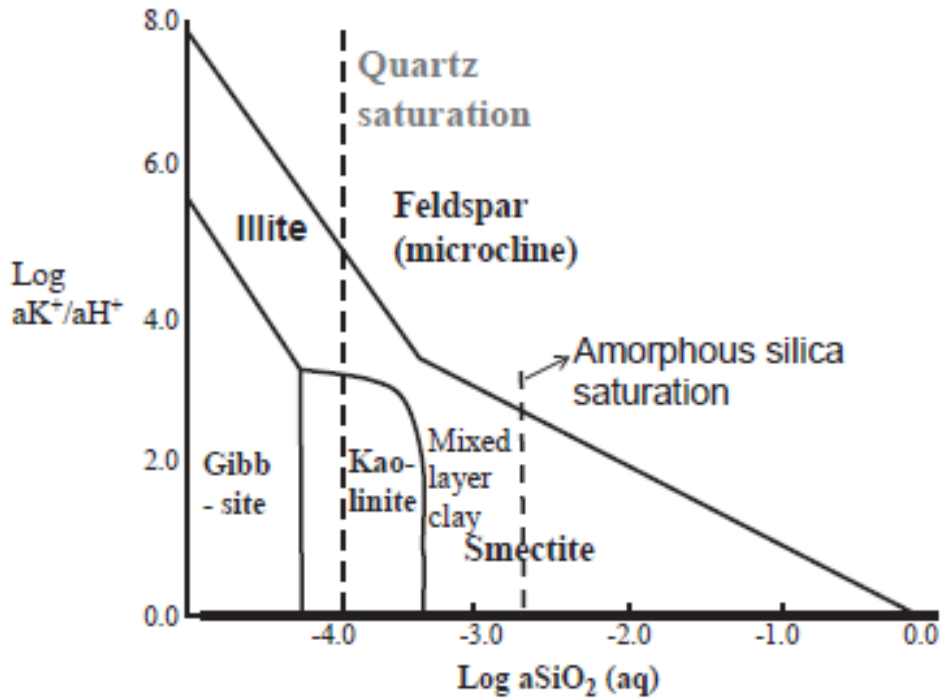
Figure 4.3 Logarithmic activity diagram shows kaolinite is only stable at a low
K+/H+ ratio and low silica concentrations (Bjørlykke, 2014).

The sequence of diagenetic events in the Makonde Fm, as determined from thin
section, SEM examinations and the clay fraction results are summarized in Figure 4.4.
Early diagenesis includes (1) Initial mechanical compaction; (2) pore filling detrital
smectite; (3) smectite-chlorite coating; (4) dissolution of feldspar; (5) authigenic
kaolinite; (6) product of minor pore filling Fe-oxide.

Diagenetic Sequence	Time: Start ⟶ Today
Mechanical compaction	————————
Smectite pore fill	———
Smectite-chlorite coating	————
Feldspar dissolution	————
Kaolinite pore fill	————
Fe-oxide (pore fill)	———

Figure 4.4 Generalized diagenetic sequence of Makonde Fm.

81

In general, for both Kihuluhulu and Makonde formations, alternation of the sampled outcrops may undergo during the recent weathering process, and it is difficult to distinguish the chemical weathering from the diagenetic alteration.

Further work

Further studies of the clay minerals in Kihuluhulu Fm. of the core samples are necessary to obtain information about the origin of the clay minerals. Further studies should include analysis of clays with respect to the clay clasts and clay matrix in the Kihuluhulu Fm. clay/siltstones and sandstones. In addition, little information about the onshore-offshore was obtained by this study. Further analysis must be concentrate on the offshore samples, in order to provide the comparison with the outcrop samples.

5 Conclusion

Kihuluhulu Fm., Kiturika Fm. and Makonde Fm. were deposited in Early Cretaceous. From west to east within the Mandawa Basin, these three formations deposited laterally as time-equivalent. The depositional environments vary from deltaic channel, pass into the shallow marine and finally deposit outer shelf marine sediments (Figure 5.1).

Kihuluhulu Fm. (Figure 5.1): The clay/siltstones are interbedded with fine to medium sandstones in the Kihuluhulu Fm were probably deposited in the outer shelf marine environment. Both clay/siltstones and sandstones are highly cemented by carbonate cements, and dominated by calcite. The sandstones are thought represent turbiditic deposits, deposited from turbiditic currents on the upper slope. After deposition, the Kihuluhulu Fm. only underwent weak compaction due to the early carbonate cementation. Clay minerals transitions occurred during the diagenetic history. Smectite precipitated and transform into the mixed layer – I/S. Some sandstones consist of chlorite coating. The dissolution of feldspar might be caused by the meteoric water influx, and kaolinite formation is a result of the feldspar dissolved. The major dissolution of feldspar happened before the calcite cementation. Compare to the core samples from well site 24 and 21, the surface samples contain more clays and poorer feldspars preservation, which might be suggested to experience much more weathering process. The porosities are in general low, secondary porosity is the dominate type in the carbonate cemented layer.

Kiturika Fm. (Figure 5.1): Kiturika Fm. represents shallow marine depositional environments. This formation is dominated by reefal limestone with calcarenites. Corals and foraminifera are the dominant fossils in the Kiturika Fm. The carbonate rocks are mainly cemented by calcite cements, which may have been recrystallized the aragonite fossils and micrite. The Kiturika Fm. experienced initial mechanical

83

compaction before the carbonate cementation.

Makonde Fm. (Figure 5.1): Makonde Fm. is interpreted to be deposited in mouth bar depositional environment, where the trough cross-stratification is the dominant sedimentary structure. The diagenetic process display weak to moderate mechanical compaction. The sandstones experience shallow diagenesis where silisiclastic minerals like feldspar and mica were highly dissolved. Clay minerals comprise mechanical infiltrated and authigenic clay minerals. The mechanical infiltrated clay is dominated by the pore filling smectite, and the authigenetic clay includes smectite-chlorite coating and pore filling kaolinite. The amount of kaolinite is a somewhat higher than that in the Kihuluhulu Fm., which might reflect higher porosities compare to the calcite cement sanstones.

A summarizing illustration of the depositional environments and the diagenesis of the studied formations in the Mandawa Basin are present in Figure 5.1.

Makonde Fm. Kiturika Fm. Kihuluhulu Fm.
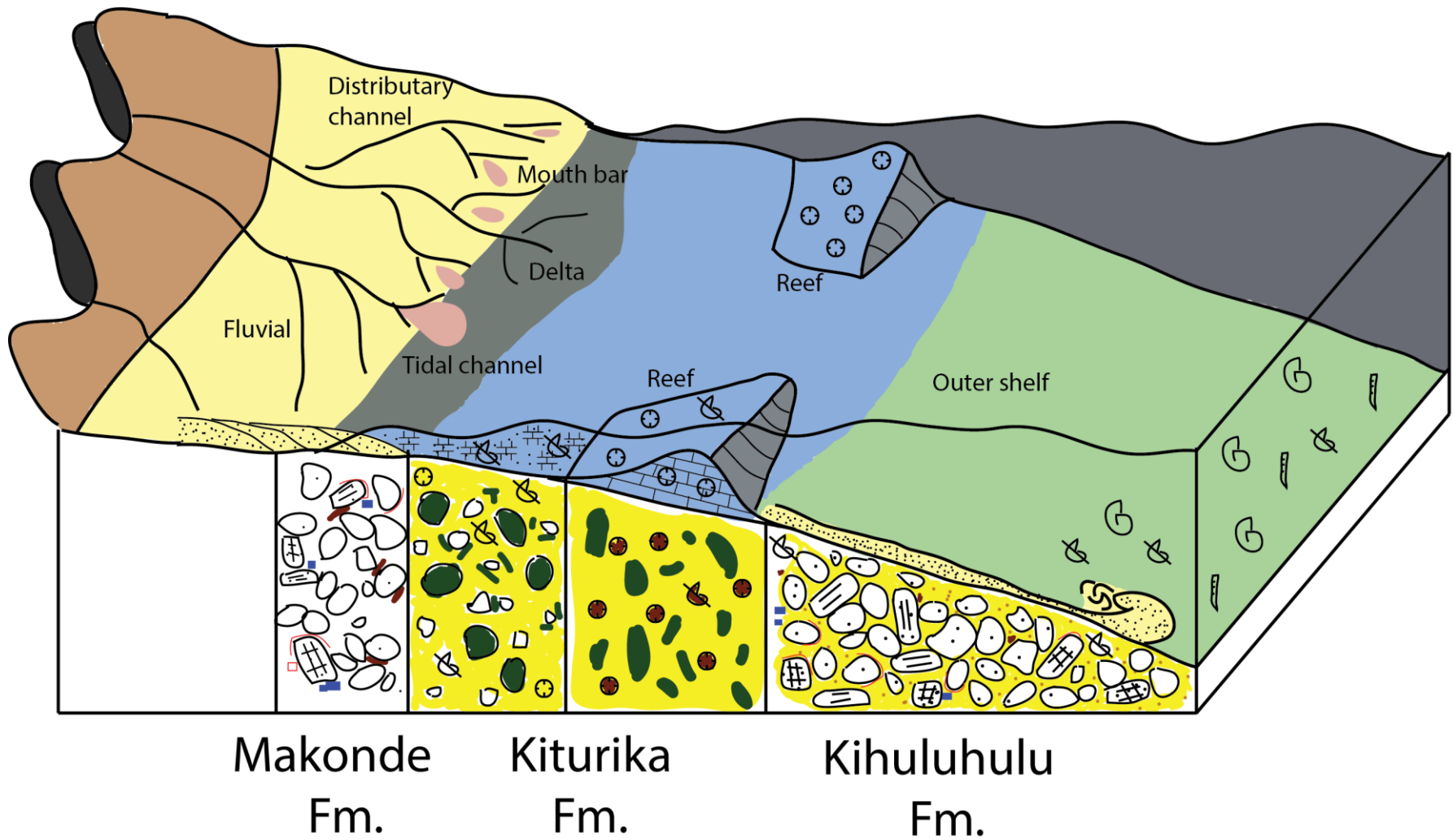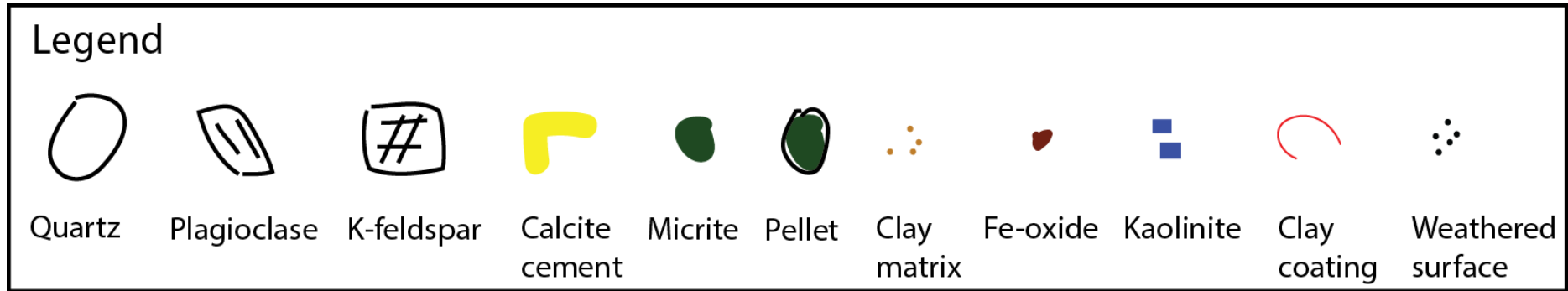
Figure 5.1 *Summarizing figure showing the depositional environments and diagenesis of the three studied formations within the Mandawa Basin. Makonde Fm. deposited in mouth bar. Kiturika Fm. deposited in shallow marine environment, dominated by reefal limestone and calcarenite. Kihuluhulu Fm. deposited in outer shelf marine environments, with carbonate cemented.*

References

AAGAARD, P., & HELGESON, H. C. (1982). Thermodynamic and kinetic constraints on reaction rates among minerals and aqueous solutions; I, Theoretical considerations. *American Journal of Science, 282*, 237-285.

AAGAARD, P., JAHREN, J., HARSTAD, A., NILSEN, O., & RAMM, M. (2000). Formation of grain-coating chlorite in sandstones. Laboratory synthesized vs. natural occurrences. *Clay Minerals, 35*, 261-269.

BALDUZZT, A., MSAKY, E., TRINCLANTI, E., & MANUM, S. B. (1992). Mesozoic Karoo and post-Karoo Formations in the Kilwa area, southeastern Tanzania- a stratigraphic study based on palynology, micropalaeontology and well log data from the Kizimbani Well. *Journal of African Earth Sciences, 15*, 405-427.

BATHURST, R. C. (1982). Genesis of stromatactis cavities between submarine. *Geol. Soc. London, 139*, 165-181.

BERROCOSO, A. J., & MACLEOD, K. G. (2010). Lithostratrigraphy, biostratigraphy and chemostratigraphy of Upper Cretaceous sediments from southern Tanzania: Tanzania drilling project sites 21-26. *Journal of Aafrican Earth Sciences, 57*, 47-69.

BERROCOSO, J. A., HUBER, B. T., MACLEOD, K. G., PETRIZZO, M. R., LEES, J. A., WENDLER, I., et al. (2015). The Lindi Formation (upper Albian-Coniacian) and Tanzania Drilling Project Sites 36-40 (Lower Cretaceous to Paleogene): Lithostratigraohy, biostratigraphy and chemostratigraphy. *Journal of African Earth Sciences, 101*, 282-308.

BHATTACHARYA, J. P. (2006). Deltas. I R. S. WALKER, & N. P. JAMES, *Facies Model:Response to Sea-leval Change* (ss. 157-177). Geol. Assoc. Can.

BISCAYE, P. E. (1965). Mineralogy and sedimentation of recent deep-sea clay in the Atlantic Ocean and adjacent seas and oceans. *Geological Society of America Bulletin, 76*, 803-832.

References

BJØRLYKKE, K. (2014). Relationships between depositional environments, burial history and rock properties. Some principal aspects of diagenetic process in sedimentary basins. *Sedimentary Geology, 301*, 1-14.

BJØRLYKKE, K. (2010). Sedimentary Geochemistry. I K. BJØRLYKKE, *Petroleum Geoscience: From Sedimentary Environments to Rock Physics* (ss. 87-111). Berlin: Springer-Verlag.

BJØRLYKKE, K., & JAHREN, J. (2012). Open or closed geochemical systems during diagenesis in sedimentary basins: Constraints on mass transfer during diagenesis and the prediction of porosity in sandstone and carbonate reseviors. *AAPG BULLETIN, 96*, 2193-2214.

BJØRLYKKE, K., & JAHREN, J. (2010). Sandstones and Sandstone Reservoirs. I K. BJØRLYKKE, *Petroleum Geoscience: From Sedimentary Environments to Rock Physics* (ss. 113-140). Berlin: Springer-Verlag.

BJØRLYKKE, K., RAMM, M., & SAIGAL, G. C. (1989). Sandstone diagenesis and porosity modification during basin evolution. *Geologische Rundschau, 78/1*, 243-268.

BOLES, J. R., & FRANKS, S. G. (1979). Clay diagenesis in Wilcox sandstones of Southwest. *Journal of Sedimentary Petrology, 49*, 55-70.

CARROLL, D. (1970). *Rock Weathering*. New York: Plenum Press.

CHEN, P. Y. (1977). Table of key lines in x-ray powder diffraction patterns of mineral in clays and associated rocks. *Geological Survey* .

COMPTON, R. R. (1962). Manual of field geology. *Soil Science* , 295.

CONOLLY, J. R. (1965). The occurrence of polycrystallinity and undulatory extinction in quartz in sandstones. *Journal of Sedimentary Research, 35*, 116-135.

DALRYMPLE, R. W., & JAMES, N. P. (2010). *Facies Models 4.* Geological Association of Canada.

DIXON, J. F., STEEL, R. J., & OLARIU, C. (2012). River-dominated, shelf-edge deltas: delivery of sand across the shelf break in the absence of slope incision.

References

Sedimentology, 59, 1133-1157.

Dott JR, H. R. (1964). Wacke, Graywacke and Matrix -- What Approach to Immature Sandstone Classification? *Journal of Sedimentary Research* , 34.

DUNHAM, R. J. (1962). Classification of carbonate rocks according to depositional texture. I W. E. HAM, *Classification of Carbonate Rocks* (ss. 108-121). Tulsa, OK: American Association of Petroleum Geologists Memoir 1.

DYPVIK, H., & VOLLSET, J. (1979). Petrology and Diagenesis of Jurassic Sandstones from Norwegian Danish Basin, North Sea. *AAPG Bulletin, 63*, 182-193.

FLÜGEL, E. (2010). Diagenesis, Porosity, and Dolomitization. I E. FLÜGEL, *Microfacies of Carbonate Rocks* (ss. 267-338). Berlin: Springer - Verlag.

FOSSUM, K. (2012). Sedimentology, petrology and geochemistry of the Kilimatinde Cement, central Tanzania. *Master Thesis, Department of Geosciences, UiO* .

GAINA, C., TORSVIK, T. H., HINSBERGEN, D. J., MEDVEDEV, S., WERNER, S. C., & LABAILS, C. (2013). The African Plate: A history of oceanic crust accretion and subduction since the Jurassic. *Tectonophysics* .

GARZANTI, E. (1991). Non-carbonate intrabasinal grains in arenites: their recognition, significance, and relationship to eustatic cycles and tectonic setting. *JOURNAL OF SEDIMENTARY PETROLOGY, 61*, 959-975.

GINSBURG, R. N., & SCHROEDER, J. H. (1973). Growth and submarine fossilization of algal cup reefs, Bermuda. *Sedimentology, 20*, 575-614.

GUNDERSVEEN, E. (2014). Sedimentology, Petrology and Diagenesis of Mesozoic Sandstones in the Mandawa Basin, Coastal Tanzania. *Master Thesis,Department of Geoscienses, UiO* .

HANKEL, O. (1994). Early Permian to Middle Jurassic rifting and sedimentation in East African and Madagascar. *Geol Rundsch, 83*, 703-710.

HANKEN, N.-M., BJØRLYKKE, K., & NIELSEN, J. K. (2010). Carbonate Sediments. I K. BJØRLYKKE, *Petroleum Geoscience: From Sedimentary Environments to Rock Physics* (ss. 141-200). Berlin: Springer-Verlag.

References

HUDSON, W. E., & NICHOLAS, C. J. (2014). The Pindiro Group (Triassic to Early Jurassic Mandawa Basin, southern coastal Tanzania): Definition,palaeoenvironment, and stratigraphy. *Journal of African Earth Sciences, 92*, 55-67.

HUDSON, W. (2011). The Geological Evolution of the Petroleum Prospective Mandawa Basin Southern Coastal Tanzania.

IFRIM, C. (2013). PALEOBIOLOGY AND PALEOECOLOGY OF THE EARLY TURONIAN (LATE CRETACEOUS) AMMONITE PSEUDASPIDOCERAS FLEXUOSUM. *PALAIOS* , 9-22.

IFRIM, C., GÖTZ, S., & STINNESBECK, W. (2011a). Fluctuations of the oxygen minimum zone at the end of Oceanic Anoxic Event 2 reflected by benthic and planktic fossils. *Geology, 39*, 1043-1046.

IFRIM, C., VEGA, F. J., & STINNESBECK, W. (2011b). Epizoic stramentid cirripedes on ammonites from Mexican late Cretaceous platy limestones. *Journal of Paleontology, 85*, 526-538.

JAMES, N. P., & WOOD, R. (2010). Reefs. I N. P. JAMES, & R. W. DALRYMPLE, *Facies Models 4* (ss. 421-447). Canada: Geological Association of Canada.

JOBE, Z. R., LOWE, D. R., & MORRIS, W. R. (2012). Climbing-ripple successions in turbidite systems: depositional environments, sedimentation rates and accumulation times. *Sedimentology, 59*, 867-898.

KAPILIMA, S. (2003). Tectonic and Sedimentary Evolution of the Coastal Basin of Tanzania during the Mesozoic Times. *Tanz.J.Sci, 29(1)*, 1-16.

KU, T., & WALTER, L. M. (2003). Syndepositional formation of Fe-rich clays in tropical shelf sediments, San Blas Archipelago, Panama. *Chemical Geology, 197*, 197-213.

LAND, L. S., & MOORE, C. H. (1980). Lithification, micritization and syndepositional diagenesis of biolithites on the Jamaican island slope. *Sediment. Petrol, 50*, 357-370.

LARSON, B., BEARFORT, D., BERGER, G., BAUER, A., CASSAGNABERE, A.,

References

& MEUNIER, A. (2002). Authigenic kaolin and illitic minerals during burial diagenesis of sandstones: a review. *Clay Minerals, 37*, 1-22.

LYNCH, F. L., MACK, L. E., & LAND, L. S. (1997). Burial diagenesis of illite/smectite in shales and the origins of authigenic quartz and secondary porosity in sandstones. *Geochimica et Cosmochimica Acta, 61*, 1995-2006.

MBEDE, E. I. (1991). The sedimentary basins of Tanzania - reviewed. *Journal of African Earth Sciences, 13*, 291-297.

Miall, D. A. (2003). Sands, gravels. and their lithified equivalents. *Sedimentology* , 960-966.

MOORE, D. M., & REYNOLDS, R. C. (1997). *X-Ray Diffraction and the Identification and Analysis of Clay Minerals.* Oxford: Oxford University Press.

MORAD, S., AL-RAMADAN, K., KETZER, J. M., & DE ROS, L. F. (2010). The impact of diagenesis on the heterogeneity of sandstone reservoirs: A review of the role of depositional facies and sequence stratigraphy. *AAPG BULLETIN, 94*, 1267-1309.

MORAD, S., KETZER, I. M., & DE ROS, L. F. (2000). Spatial and temporal distribution of diagenetic alterations in siliciclastic rocks: implications for mass transfer in sedimentary basins. *Sedimentology, 47*, 95-120.

MPANDA, S. (1997). Geological development of the East African coastal basin of Tanzania. *STOCKHOLM CONTRIBUTIONS IN GEOLOGY, 45(1)*, 1-116.

MULDER, T., & ALEXANDER, J. (2011). The phisical character of subaqueous sedimentary density flows and their deposits. *Sedimentology, 48*, 269-299.

NERBRÅTEN, K. (2014). Petrology and Sedimentary Provenance of Mesozoic and Cenozoic Sequences in the Mandawa Basin. *Master thesis, Department of Geosciences, UiO* .

NICHOLAS, C. J., & PEARSON, P. N. (2007). Structural evolution of southern coastal Tanzania since the Jurassic. *Journal of African Earth Sciences, 48*, 273-297.

References

NICHOLAS, C. J., PEARSON, P. N., BOWN, P. R., JONES, T. D., HUBER, B. T., KAREGA, A., et al. (2006). Stratigraphy and sedimentology of the Upper Cretaceous to Paleogene Kilwa Group, southern coastal Tanzania. *Journal of African Earth Sciences, 45*, 431-466.

OLARIU, C., & BHATTACHARYA, J. P. (2006). Terminal distributary channels and delta front architecture of river-dominated delta systems. *Journal of Sedimentary Research, 76*, 212-233.

OVEREEM, I., KROONENEBERG, S. B., VELDKAMP, A., GROENESTEUN, K., RUSAKOV, G. V., & SVRROCH, A. A. (2003). Small-scale stratigraphy in a large ramp delta: recent and Holocene sedimentation in the Volga delta, Caspian Sea. *Sedimentary Geology, 159*, 133-157.

PELTONEN, C., MARCUSSEN, Ø., BJØRLYKKE, K., & JAHREN, J. (2009). Clay mineral diagenesis and quartz cementation in mudstones: The effects of smectite to illite reaction on rock properties. *Marine and Petroleum Geology, 26*, 887-898.

PETTIJOHN, J. F., POTTER, E. P., & SIEVER, R. (1972). Diagenesis. I *Sand and Sandstoens* (ss. 383-434). Berlin: Springer - Verlag.

POWELL, J. D. (1963). Cenomanian-Turonian (Cretaceous) ammonites from Trans-Pecos Texas and northeastern Chihuahua, Mexico. *Journal of Paleontology, 37*, 309-322.

POWERS, M. C. (1953). A new roundness scale for sedimentary particles. *Journal of Sedimentary Research, 23*.

READING, H. G., & COLLINSON, J. D. (1996). Clastic coasts. I H. G. READING, *Sedimentary Environments: Processes, Facies and Stratigraphy* (ss. 154-231). Oxford: Blackwell Science.

REYNOLDS JR, R. C. (1985). NEWMOD, a computer program for the calculation of one-dimensional diffraction patterns of mixed-layered clays. *RC Reynolds* , 8.

SALEM, A. M., MORAD, S., MATO, L. F., & AL-AASM, I. (2000). Diagenesis and reservoir quality evolution of fluvial sandstones during progressive burial and

uplift: Evidence from the Upper Jurassic Boipeba Member, Reconcavo Basin, Northeastern Brazil. *AAPG bulletin, 84*, 1015-1040.

SALMAN, G., & ABDULA, I. (1995). Development of the Mozambique and Ruvuma sedimentary basins, offshore Mozamique. *Sedimentary Geology, 96*, 7-41.

SANDERS, J. E. (1960). Primary sedimentary structures formed by turbidity currents and related resedimentation mechanisms.

SCHIFFMAN, P., & FRIDLEIFSSON, G. O. (1991). The smectite-chlorite transition in drillhole NJ-15, Nesjavellir geothermal field, Iceland: XRD, BSE and electron microprobe investigations. *J. metamorphic Geol., 9*, 679-696.

SCHOMACKER, E. R., KJEMPERUD, A. V., NYSTUEN, J. P., & JAHREN, H. S. (2010). Recognition and significance of sharp-based mouth-bar deposits in the Eocene Green River Formation, Uinta Basin, Utah. *Sedimentology, 57*, 1069-1087.

SCHROEDER, J. H. (1986). Diagenetic diversity in Paleocene coral knobs from the Bir Abu El-Husein area, s. Egypt. I J. H. SCHROEDER, & B. H. PURSER, *Reef DIAGENESIS* (ss. 132-159). New York: Springer-Verlag.

SHANMUGAM, G. (1997). The Bouma Sequence and the turbidite mind set. *Earth-Science Reviews, 42*, 201-220.

STEARNS, H. T. (1945). Decadent coral reef on eniwetok island, Marshall Group. *BULLETIN OF THE GEOLOGICAL SOCIETY OF AMERICA, 56*, 783-788.

STONECIPHER, S. A., WINN JR, R. D., & BISHOP, M. G. (1984). Diagenesis of the Frontier Formation, Moxa Arch: A Function f Sandstone Geometry, Texture and Composition, and fluid flux. *American Association of Petroleum Geologists, 3*, 289-316.

TROPEANO, M., & SABATO, L. (2000). Response of Plio-Pleistocene mixed bioclastic-lithoclastic temperate-water carbonate systems to forced regressions:the Calcarenite di Gravina Formation,Puglia, SE Italy. *Geological Society,London,Special Publications, 172*, 217-243.

References

WALASZCZYK, I., KENNEDY, W. J., DEMBICZ, K., GALE, A. S., PRASZKIER, T., RASOAMIARAMANANA, A. H., et al. (2014). Ammonite and inoceramid biostratigraphy and biogeography of the Cenomanian through basal Middle Campanian (Upper Cretaceous) of the Morondava Basin, western Madagascar. *Journal of African Earth Sciences* , 79-132.

WENTWORTH, C. K. (1992). A SCALE OF GRADE AND CLASS TERMS FOR CLASTIC SEDIMENTS. *The Journal of Geology* , 377-392.

WILSON, L. J. (1975). *Carbonate facies in geologic history.* New York,N.Y.: Springer-Berlag.

WILSON, M. D., & PITTMAN, E. D. (1977). Authigenic clays in sandstones: Recognition and influence on reservoir properties and paleoenvironmental analysis. *Journal of Sedimentary Petrology, 47*, 3-31.

Appendix

Appendix A – Simplified log of WP-92 with gamma radiation measurements.
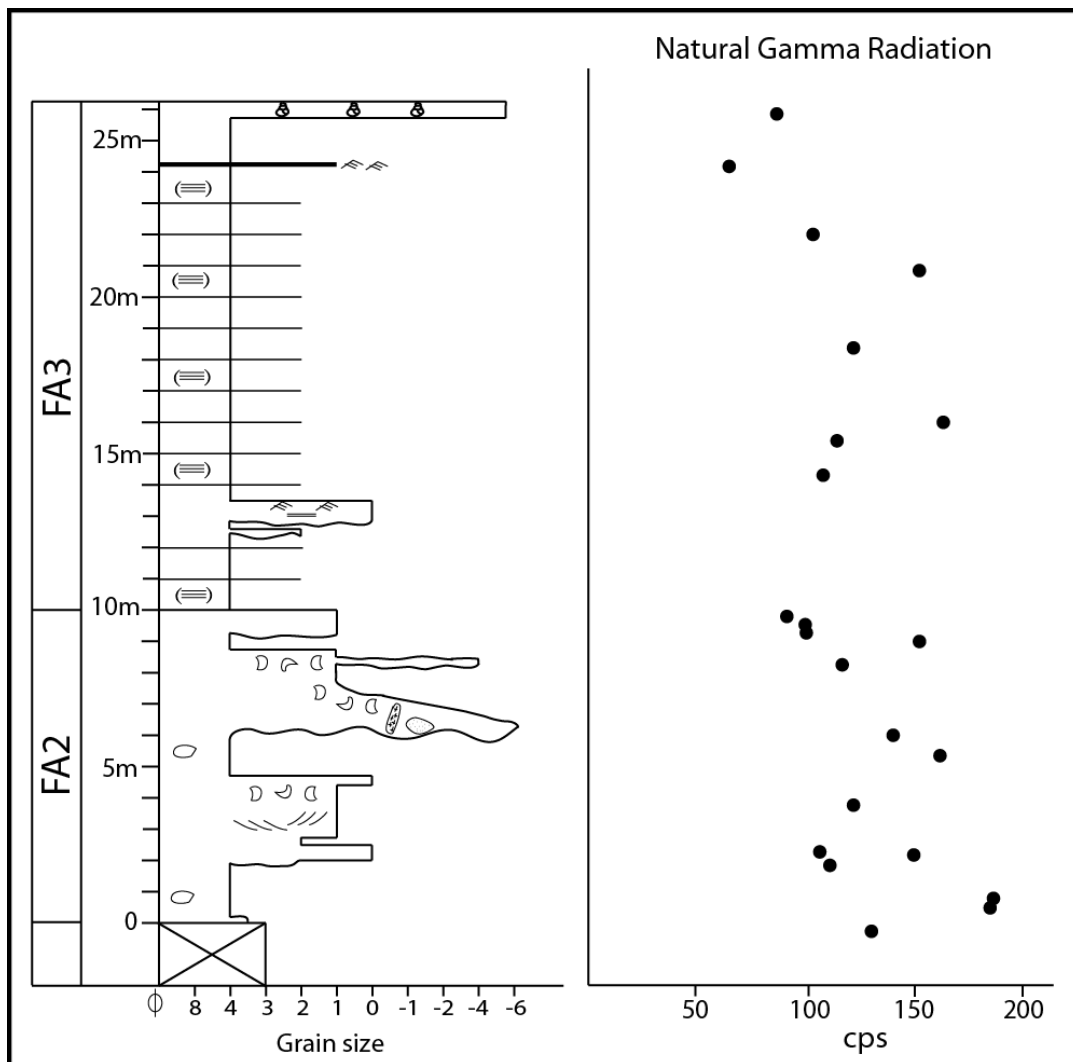
Appendix

Appendix B – Point counting.

Sample		Total	Qtz				Qtz	Total	K-Feldspar					Plagioclase					RF	Carb.	Total	Porosity		HM	Kaolin	Mica	Iron	Fossil	Chert	Pyrite	Coating	Clay	Matrix	Pellet
	%	Qtz	MonoS	MonoU	PolyS	PolyU	ogt.	Fds	1	2	3	4	5	1	2	3	4	5		cement	Poro.	Prim.	Secon.				oxide							
WP223-1-14	%	17.8	10.3	5.0	0.8	1.8	0.0	3.3	0.0	0.0	0.0	0.0	1.0	0.0	0.0	0.3	0.0	2.0	0.8	5.5	9.5	0.0	9.5	0.0	0.0	2.0	0.0	0.0	0.0	10.0	0.0	51.3	0.0	0.0
WP223-3-14	%	30.6	19.9	7.0	1.5	2.3	0.0	11.0	0.0	0.0	0.0	0.0	4.0	0.0	0.0	0.0	1.3	5.8	9.3	30.0	2.5	0.3	2.3	1.3	1.3	0.5	3.0	1.8	0.0	0.3	0.0	8.8	0.0	0.0
WP223-5-14	%	47.8	28.3	9.0	3.0	7.5	6.8	3.8	0.0	0.0	0.0	0.0	0.5	0.0	0.0	0.3	0.0	3.0	3.8	0.0	25.8	23.0	2.8	0.0	0.3	0.0	0.0	0.0	0.0	1.0	11.0	0.0	0.0	0.0
WP223-8-14	%	36.0	25.0	8.0	1.0	2.0	0.0	1.0	0.0	0.0	0.0	0.0	0.0	0.0	0.0	0.0	0.0	1.0	1.0	0.0	5.0	1.0	4.0	0.0	0.5	0.0	4.5	0.0	0.0	0.0	0.0	51.3	0.0	0.0
WP92-11-14	%	53.3	31.8	8.8	4.8	8.0	5.3	7.5	0.0	0.0	0.0	0.3	0.8	0.0	0.0	0.3	1.3	5.0	5.3	0.0	13.8	11.8	2.0	0.0	10.8	0.3	0.0	0.0	0.8	2.5	0.8	0.0	0.0	0.0
WP92-13-14	%	61.8	41.0	8.5	4.3	8.0	0.0	8.0	0.0	0.0	0.8	0.8	1.8	0.0	0.0	0.5	0.5	3.8	1.8	18.0	1.5	0.0	1.5	1.0	6.0	0.0	0.0	0.0	0.0	2.0	0.0	0.0	0.0	0.0
WP92-16-14	%	47.3	30.6	10.3	3.3	3.3	0.0	15.0	0.0	0.0	1.3	1.5	1.5	0.0	0.0	0.8	2.3	7.8	4.3	31.8	0.0	0.0	0.0	0.0	1.3	0.3	0.0	0.0	0.0	0.3	0.0	0.0	0.0	0.0
WP92-19-14	%	46.0	24.3	8.8	3.8	9.3	0.0	9.0	0.0	0.0	0.5	0.3	0.8	0.0	0.0	0.5	1.8	5.3	3.3	39.5	1.5	0.0	1.5	0.0	0.0	0.0	0.3	0.0	0.3	0.3	0.0	0.0	0.0	0.0
WP92-21-14	%	34.3	22.5	4.3	2.8	4.8	0.0	7.0	0.0	0.0	0.3	0.0	0.5	0.0	0.0	0.5	1.0	4.8	2.5	45.3	0.0	0.0	0.0	0.0	0.0	0.0	2.3	4.3	1.0	3.5	0.0	0.0	0.0	0.0
WP222-2-14	%	41.8	30.8	7.5	2.0	1.5	0.0	6.0	0.0	0.0	0.0	0.5	1.0	0.0	0.0	0.0	0.3	4.3	1.5	50.3	0.0	0.0	0.0	0.0	0.0	0.3	0.0	0.0	0.3	0.0	0.0	0.0	0.0	0.0
N5-26-2-14	%	57.5	44.5	6.0	3.8	3.3	0.0	8.8	0.0	0.0	0.3	0.0	0.8	0.0	0.0	0.3	1.0	6.5	2.3	28.3	28.3	0.0	0.0	0.0	0.0	0.5	0.5	0.3	0.5	1.0	0.0	0.5	0.0	0.0
N5-27-1-14	%	52.0	33.8	9.5	4.3	4.5	0.0	10.3	0.0	0.0	0.0	0.5	0.5	0.0	0.0	0.0	0.3	9.0	2.3	32.5	0.0	0.0	0.0	0.3	0.0	1.0	0.0	0.3	0.0	1.5	0.0	0.0	0.0	0.0
WP62-2-14	%	56.0	40.0	7.5	4.3	4.3	0.0	12.0	0.0	0.0	0.8	0.5	1.3	0.0	0.0	0.8	0.0	8.3	2.5	0.0	10.8	8.3	2.5	0.0	7.3	0.8	0.0	0.0	0.5	2.8	3.1	0.0	4.4	0.0
WP71-1-14	%	12.8	9.8	2.5	0.5	0.0	0.0	0.5	0.0	0.0	0.0	0.3	0.0	0.0	0.0	0.3	0.0	0.0	0.0	68.0	1.0	0.0	1.0	0.0	0.0	0.0	0.0	4.0	0.0	2.0	0.0	0.0	0.0	11.8
WP71-2-14	%	0.0	0.0	0.0	0.0	0.0	0.0	0.0	0.0	0.0	0.0	0.0	0.0	0.0	0.0	0.0	0.0	0.0	0.0	94.5	0.5	0.0	0.5	0.0	0.0	0.0	2.5	2.5	0.0	0.0	0.0	0.0	0.0	0.0
WP71-3-14	%	9.0	6.5	1.5	0.3	0.8	0.0	1.3	0.0	0.0	0.0	0.8	0.3	0.0	0.0	0.0	0.0	0.3	0.0	72.8	3.3	0.0	3.3	0.0	0.0	0.0	0.3	1.5	0.0	1.3	0.0	0.0	0.0	10.8
MDW 10	%	48.8	36.8	5.0	2.5	4.5	0.0	7.0	0.0	0.0	0.0	0.3	0.3	0.0	0.0	0.5	0.0	6.0	0.8	43.0	0.0	0.0	0.0	0.0	0.0	0.5	0.0	0.0	0.0	0.0	0.0	0.0	0.0	0.0
MDW 62	%	44.3	35.8	4.5	1.3	2.8	0.0	7.8	0.0	0.0	0.0	0.3	1.0	0.0	0.0	0.8	0.5	5.3	0.5	42.0	0.3	0.0	0.3	0.0	0.0	0.5	0.0	4.8	0.0	0.0	0.0	0.0	0.0	0.0
MDW09-08	%	54.4	46.3	3.7	0.7	3.7	0.0	16.4	0.0	0.0	0.7	1.5	2.2	0.0	0.0	0.7	3.0	8.2	0.0	0.0	16.4	13.4	3.0	1.5	4.5	0.0	0.0	0.0	0.0	0.0	6.7	0.0	0.0	0.0

II

Appendix C – Bulk XRD results.

Sample	Chlorite	Smectite	Mixed	Illite	Kaolinite	Quartz	K-feldspar	Plagioclase	Calcite
WP223-1-14	0.0	0.0	0.0	549.0	0.0	4069.0	1931.0	2621.0	11793.0
WP223-2-14	0.0	0.0	0.0	1265.0	0.0	5851.0	2888.0	3638.0	1517.0
WP223-3-14	0.0	0.0	0.0	636.0	0.0	5087.0	2634.0	3361.0	14896.0
WP223-4-14	0.0	0.0	0.0	1366.0	0.0	5061.0	2892.0	3856.0	3214.0
WP223-5-14	0.0	0.0	0.0	0.0	0.0	20407.0	2522.0	0.0	0.0
WP223-8-14	0.0	0.0	0.0	0.0	0.0	14942.0	1441.0	1225.0	0.0
WP92-13-14	0.0	0.0	0.0	0.0	0.0	15203.0	2488.0	2211.0	7464.0
WP92-14-14	0.0	0.0	1057.0	1094.0	835.0	2535.0	1653.0	1433.0	5427.0
WP92-15-14	0.0	0.0	947.0	0.0	808.0	2852.0	1490.0	1362.0	10300.0
WP92-16-14	0.0	0.0	0.0	419.0	546.0	8061.0	2638.0	2785.0	18027.0
WP92-17-14	0.0	1077.0	994.0	938.0	858.0	2786.0	1722.0	1396.0	5594.0
WP92-18-14	0.0	0.0	902.0	939.0	0.0	2274.0	1505.0	1121.0	6462.0
WP92-19-14	0.0	0.0	0.0	0.0	0.0	10481.0	2620.0	2316.0	15173.0
WP92-20-14	0.0	0.0	910.0	773.0	709.0	2426.0	1452.0	1260.0	7279.0
WP92-21-14	0.0	0.0	0.0	470.0	462.0	6452.0	5356.0	5609.0	21461.0
WP222-1-14	544.0	617.0	691.0	561.0	1801.0	1108.0	1823.0	6673.0	0.0
WP222-2-14	0.0	0.0	0.0	0.0	8017.0	2079.0	1090.0	12325.0	0.0
N5-22-1-14	598.0	0.0	0.0	651.0	566.0	3334.0	1505.0	2580.0	2413.0
N5-26-1-14	523.0	0.0	0.0	464.0	485.0	3098.0	1157.0	1521.0	6059.0
N5-26-2-14	0.0	0.0	0.0	0.0	0.0	8988.0	2103.0	1811.0	13634.0
N5-26-3-14	611.0	0.0	0.0	607.0	536.0	3366.0	1553.0	1942.0	4327.0
N5-27-1-14	1037.0	0.0	0.0	432.0	678.0	6346.0	2371.0	2574.0	3952.0
N5-27-2-14	701.0	0.0	850.0	663.0	732.0	2713.0	1691.0	1953.0	1155.0
WP62-1-14	567.0	0.0	758.0	547.0	5811.0	1743.0	3312.0	0.0	0.0
WP62-2-14	0.0	0.0	0.0	0.0	8804.0	5253.0	5473.0	0.0	0.0
WP71-1-14	0.0	0.0	0.0	0.0	0.0	2001.0	0.0	0.0	28639.0
WP71-2-14	0.0	0.0	0.0	0.0	0.0	433.0	0.0	0.0	33115.0
WP71-3-14	0.0	0.0	0.0	0.0	0.0	2180.0	0.0	0.0	30310.0

Appendix D – Clay fraction results.

Sample	Illite	Smectite	Kaolinite	I-S	I-S(Fe)	S-I	Chlorite	Smec-Chlo
WP92-2-14	89.1%	0.0%	0.0%	0.0%	0.0%	10.9%	0.0%	0.0%
WP92-8-14	67.6%	0.0%	0.0%	0.0%	0.0%	32.4%	0.0%	0.0%
WP92-9-14	17.3%	0.0%	17.3%	0.0%	0.0%	65.4%	0.0%	0.0%
WP92-14-14	7.8%	0.0%	11.8%	0.0%	60.8%	0.0%	8.0%	0.0%
WP92-17-14	17.6%	0.0%	7.4%	5.9%	61.8%	0.0%	10.0%	0.0%
WP92-18-14	17.0%	0.0%	7.5%	24.5%	34.0%	0.0%	17.0%	0.0%
WP92-20-14	5.5%	0.0%	8.2%	0.0%	67.0%	0.0%	19.0%	0.0%
WP222-1-14	4.3%	24.7%	5.4%	9.7%	55.9%	0.0%	0.0%	0.0%
WP223-2-14	9.9%	28.4%	8.6%	34.6%	0.0%	0.0%	19.0%	0.0%
WP223-4-14	20.0%	26.4%	0.9%	18.2%	34.5%	0.0%	0.0%	0.0%
N5-26-3-14	21.2%	34.8%	7.6%	11.0%	25.0%	0.0%	0.0%	0.0%
N5-27-2-14	5.3%	21.8%	15.0%	25.6%	32.3%	0.0%	0.0%	0.0%
WP62-1-14	7.9%	26.3%	3.9%	30.3%	0.0%	0.0%	0.0%	31.6%

Appendix

Appendix E – Classification: Kihuluhulu Fm.
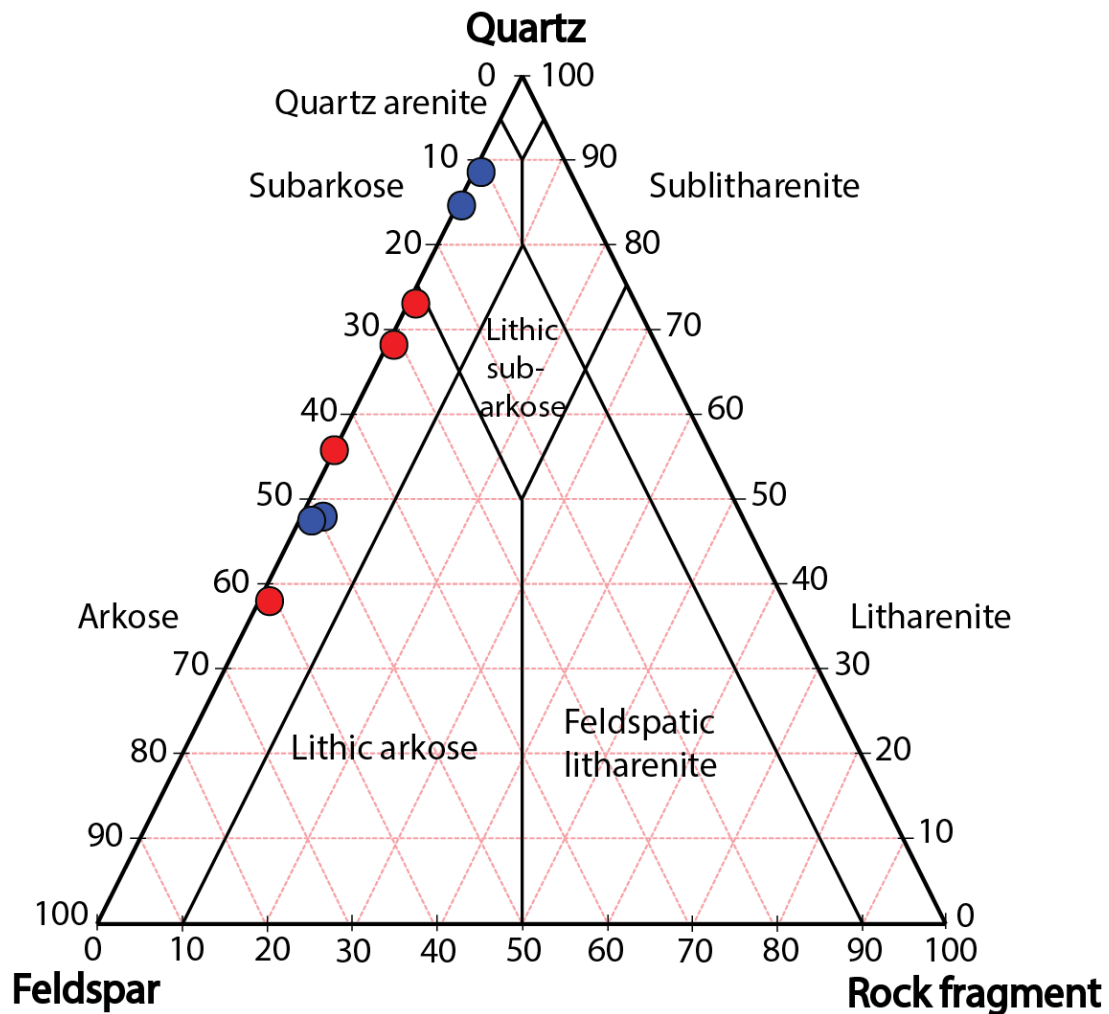
Stratigraphical unit	Sample	Clay matrix (%)	Classification
Kihuluhulu Fm.	WP92-13-14	0.0	Arkose
	WP92-16-14	0.0	Arkose
	WP92-19-14	0.0	Arkose
	WP92-21-14	0.0	Arkose
	WP223-1-14	51.3	Arkose
	WP223-3-14	8.8	Arkose
	WP223-5-14	0.0	Subarkose
	WP223-8-14	51.3	Subarkose

Appendix F – Classification: Makonde Fm. & Kihuluhulu Fm.
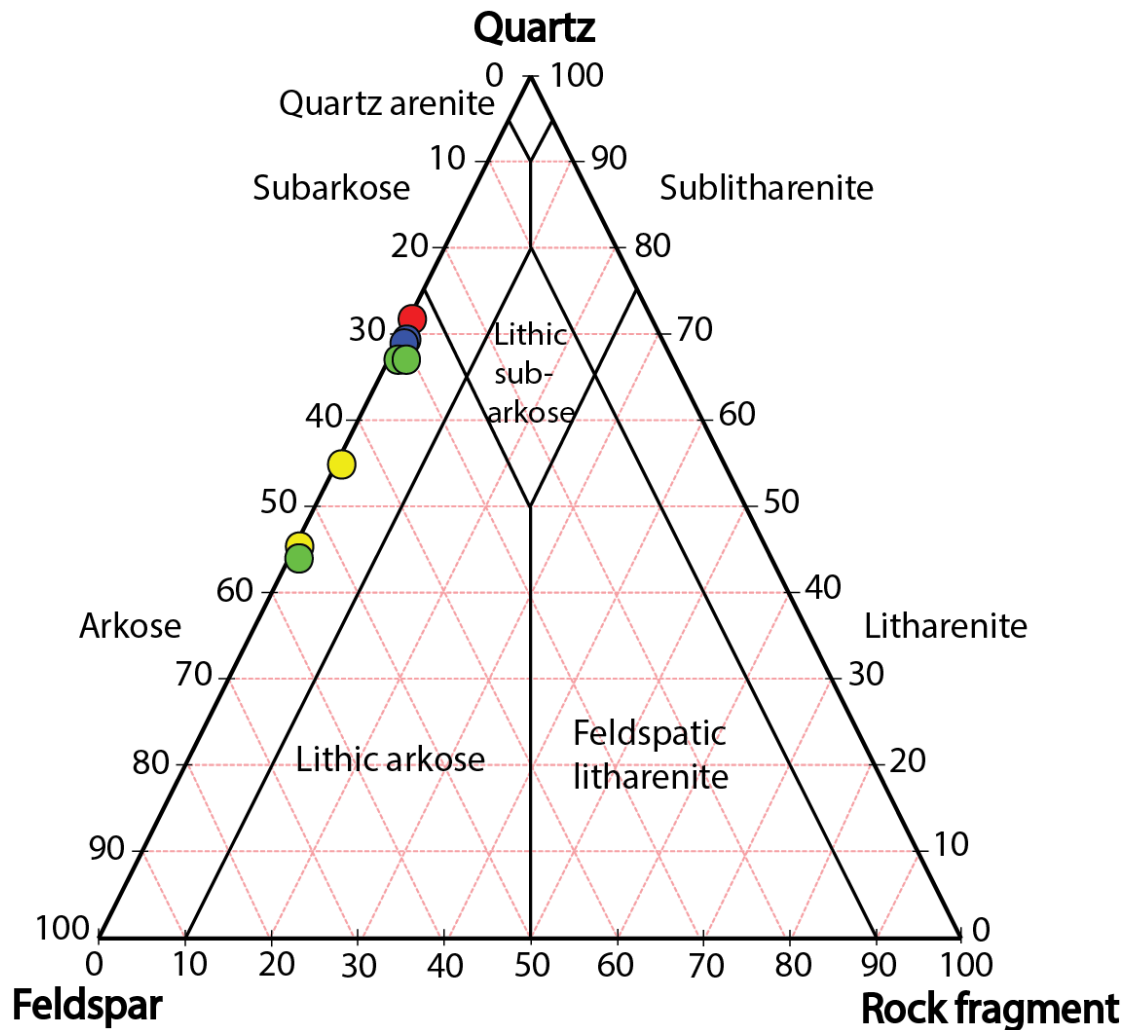
Stratigraphical unit	Sample	Clay matrix (%)	Classification
Makonde Fm.	WP62-1-14	10.3	Arkose
	WP62-2-14	7.5	Arkose
	MDW 09-08	0.0	Arkose
Kihuluhulu Fm.	MDW 10	0.0	Arkose
	MDW 62	0.0	Arkose
	WP222-2-14	0.0	Arkose
	N5-26-2-14	0.5	Arkose
	N5-27-1-14	0.0	Arkose